

Monitoring Dielectric Properties of Single MRC5 Cells and Oligomycin Treated Chinese Hamster Ovary Cells Using a Dielectrophoretic Cytometer

by

Bahareh Saboktakin Rizi

A Thesis submitted to the Faculty of Graduate Studies of
The University of Manitoba
in partial fulfilment of the requirements of the degree of

Master of Science

Department of Electrical and Computer Engineering
University of Manitoba
Winnipeg, Manitoba, Canada

Copyright ©2014 by Bahareh Saboktakin Rizi

To my wonderful parents

my terrific sister, Shekoofeh

and my role model, Bibi

Abstract

We have employed a differential detector combined with dielectrophoretic (DEP) translation in a microfluidic channel to monitor dielectric response of single cells and particularly to track phenomenon related to apoptosis. Two different cell lines were studied; Chinese hamster ovary cells (CHO) and MRC5 cells. Dielectric response was quantified by a factor called Force Index. Force Index was studied statistically to identify apoptotic subpopulations.

Another direction of this work was to monitor changes in the cytoplasm conductivity following inhibition of mitochondrial ATP production by Oligomycin. To make the DEP response mostly sensitive to the cytoplasm conductivity, medium conductivity and DEP frequency were adjusted such that Clausius Mossotti factor and hence DEP response become less sensitive to cell radius.

Chinese hamster ovary cells were used in this work and the impact of different concentrations of Oligomycin has been studied. We show that following exposure to Oligomycin at $8 \mu\text{g/ml}$, cytoplasm conductivity drops. The majority of the changes takes place within one hour of exposure to the drug. Furthermore, double shell models has been used to estimate cytoplasm conductivity in a medium with conductivity of 0.42 S/m and the drop in the cytoplasm conductivity following treatment with Oligomycin was estimated to be $\approx 0.16 \text{ S/m}$. The magnitude of the decrease in the cytoplasm conductivity is evidence that Glycolysis is active as an energy production pathway within the cell. This approach can be used to quantify Glycolysis versus mitochondria ATP production which has an application in Warburg effect in cancer cells and monitoring bioprocesses.

Acknowledgments

I would like to express the deepest appreciation to my advisor, Professor Douglas Thomson. I have had his constant support, invaluable guidance, and warm encouragement from the beginning in ups and downs of research. His easy going approach and patience made research an exciting journey for me. Also I would like to thank him for providing the opportunity to attend various workshops and conferences.

I am truly indebted to Professor Gregory Bridges for his meticulous comments and insightful suggestions. His door was always open to me with his exceptional sense of humor.

I would like to thank my colleagues; Marija Nikolic Jaric, Katrin Braasch, Elham Salimi, Ashlesha Bhide, Tim Cabel, Kaveh Mohammad, and Samaneh Afshar Delkhah. Katrin made enormous contribution to this work. She kindly prepared samples and she has made constructive suggestions during this work. I received invaluable help from Elham. I am particularly grateful for her help to familiarize me with tips and tricks of working with our setup and she was always open to debug problems with the experimental setup. I enjoyed working with Ash on the Semi-automated GUI program and I am thankful for her equal contribution. I would also like to express my appreciation for my MSc. external committee: Professor Malcolm Xing for evaluation of this work.

Last but not least, my heartfelt appreciation goes to my parents and my sister, Shekoofeh. It has been indeed impossible to take any step in life without them.

Contents

<i>Abstract</i>	ii
<i>Acknowledgments</i>	iii
<i>List of permissions obtained for the Copyrighted Material</i>	xii
1. Cytometry: Background and Motivation	1
1.1 Flow and Image Cytometry	2
1.2 Introduction to DEP Cytometry	3
1.3 Cell physiological changes and dielectric response	11
1.4 Contribution	25
2. Differential detection of cell DEP response	26
2.1 Forces in a microfluidic channel	27
2.2 Experimental setup	29
2.3 Data collection and analysis	33
3. Beyond the Force Index	37
3.1 non-viable cell Force Index and conductivity	38
3.2 Force Index distribution during apoptosis	40
4. DEP response to MRC5 cells	44
4.1 DEP response to Non-starved MRC5 cells	45
4.2 DEP response to 5 day starved MRC5 cells	53
5. DEP response to mitochondrial ATP inhibition	57
5.1 ATP: energy currency of the cell	58
5.2 Oligomycin and ATP	59
5.3 Oligomycin and ions	61
5.4 Cell preparation and experiment procedure	62
5.5 Results with medium conductivity of 0.17 S/m	63

5.6	Results with medium conductivity of 0.42 S/m	74
5.7	Estimating cytoplasm conductivity	86
5.8	Chapter conclusion	87
6.	<i>Conclusion and future work</i>	89

List of Tables

1.1	Typical intra/extracellular ion concentrations [1].	19
1.2	Limiting molar conductivity in water at 298° K [mSm^2mol^{-1}] [2]	20
1.3	$[K^+]_i$ before and during apoptosis	24
4.1	Percentage viability measured by different assays	46
4.2	Estimated dielectric properties of MRC5 cell	49
5.1	Percentage viability: Control compared to Oligomycin 0.5 μ g/ml	73
5.2	Percentage viability of the control samples.	86

List of Figures

1.1	A polarized cell in a non-uniform electric field experiences a net dielectric force.	4
1.2	Single shell model for calculating equivalent dielectric properties of a cell without large organelles. $\bar{\epsilon}_{cp}$ and $\bar{\epsilon}_m$ are the complex permittivity of cytoplasm and membrane respectively. R and d_m are cell radius and membrane thickness respectively.	6
1.3	Double shell model for calculating equivalent dielectric properties of a cell with a large nucleus. $\bar{\epsilon}_{np}$, $\bar{\epsilon}_n$, r_n , and r_n stand for complex permittivity of nucleoplasm and nucleus, nucleus radius and nucleus envelope thickness, respectively.	7
1.4	Clausius Mossotti factor spectrum calculated by: (a) single shell model and (b) double shell model medium conductivity=0.17 S/m, cytoplasm conductivity=0.15-0.45 S/m, viable cell radius = 5.5 μm . Other cell parameters are fixed as: nucleus radius=3.25 μm , membrane thickness=5 nm, nucleus envelope thickness= 40 nm, membrane permittivity= 6.8 ϵ_0 , cytoplasm permittivity= 60 ϵ_0 , nucleus envelope permittivity= 28 ϵ_0 , nucleus permittivity= 52 ϵ_0 , membrane conductivity= $3 * 10^{-3}$ S/m, nucleus envelope conductivity = $6 * 10^{-3}$ S/m, nucleus conductivity= 1.35 S/m [3, 4, 5].	8
1.5	Double shell model for K_{CM} spectrum for a viable cell while membrane permittivity is changing from 4.8 ϵ_0 to 8.8 ϵ_0 . Changing membrane conductance is not significant in MHz frequency range. Medium conductivity = 0.17 S/m and cytoplasm conductivity = 0.42 S/m, other parameters are fixed as Fig. 1.4	13

1.6	Cell dynamic response to a sudden shut down of $Na^+/K^+ATPase$ pump at $t=0$. Obtained from [6], Copyright (1980) American Journal of Physiology (with permission)	18
1.7	Cell dynamic response to a sudden shut down of $Na^+/K^+ATPase$ pump at $t=0$. Obtained from [7], Copyright (2003) National Academy of Sciences, U.S.A (with permission).	18
2.1	Particle in a microfluidic channel experiencing gravity, hydrodynamic lift and drag force. Below the center line lift and gravity can equate and particle reaches equilibrium.	27
2.2	Cell trajectory in microfluidic channel. Here, cell is experiencing an attractive DEP force. $P_2 > P_1$ and Force Index > 0	30
2.3	All possible DEP cytometer signatures, from left to right: negative DEP force (nDEP), no DEP force (no DEP), and positive DEP force (pDEP) . . .	31
2.4	DEP cytometer compartments. (a) microfluidic chip with 4 ports (b) top view of the microfluidic channel and the electrodes. (c) fluidic control system for adjusting pressure on each vial. (d) DAQ and graphical interfaces to control pressure, DAQ, and video recorder. (e) interferometer setup shielded in the cabinet. (f) anti-vibration cabinet including interferometer, microscope and video recorder, microfluidic chip.	34
2.5	Four second sample of the out put signal recorded by DAQ.	36
2.6	Sample histogram from an experiment on CHO cells in a medium with conductivity of 0.17 S/m.	36
3.1	Double shell model of K_{CM} for viable cell in a medium conductivity of 0.17 S/m. (a) cytoplasm conductivity is varying from 0.07-0.47 S/m, $\epsilon_{mem} = 6.8 \epsilon_0$ (b) ϵ_{mem} is varying from 4-8 ϵ_0 , cytoplasm conductivity= 0.42 S/m. (c) cell radius is varying from 4.5-8.5 μm . All other parameters are fixed as Fig. 1.4.	38
3.2	K_{CM} Double shell model of K_{CM} for viable and non-viable cell, medium conductivity = 0.17 S/m, other parameters are set as defined in the text. . . .	40
3.3	Gaussian fit to the Force Index histograms. More than one population arises as cells go into the apoptotic stage.	42

4.1	Histograms of no-DEP applied and velocity for the whole course of experiment and 6 MHz measurements at the beginning and end of the experiment.	46
4.2	Mean Force Index of the experiments performed by DEP voltage applied at different frequencies. Error bar are calculated from standard error of the mean.	46
4.3	Distribution of Force Index histograms in different frequencies of the applied DEP voltage.	47
4.4	Scaled FI to simulated K_{CM} by double shell model using optimized parameters for MRC5 cells	51
4.5	Averaged first peak magnitude for the course of experiment.	51
4.6	Averaged cell velocity calculated by two peaks.	52
4.7	Mean Force Index, FI has been corrected for each cell by velocity.	53
4.8	Histograms of no-DEP applied and velocity for the whole course of experiment and 6 MHz measurements at the beginning and end of the experiment.	54
4.9	Mean Force Index of starved MRC5 cells compared to non-starved cells.	55
4.10	Averaged cell velocity calculated by two peaks.	55
4.11	Force Index histogram distribution in different applied DEP voltage frequency.	56
5.1	a) medium b) cytoplasm: Glycolysis takes place in cytoplasm. Pyruvate produced in this process can either go into the Glycolysis pathway to produce ATP or into the mitochondria electron transport chain. c) mitochondria produces ATP by electron transport chain. Oligomycin inhibits electron transport chain by blocking proton channels in mitochondria membrane.	60
5.2	Force Index monitored in time. Purple dashed line represents overall mean FI for the control sample.	64
5.3	Force Index histograms of control and treated samples.	64
5.4	10 minute histograms of Force Index for different concentrations.	66
5.5	Force Index monitored in time. Purple dashed line represents overall mean FI for the control sample.	67

5.6	Force Index histograms of control and treated samples.	68
5.7	Force Index monitored in time. Purple dashed line represents overall mean FI for the control sample.	68
5.8	Force Index histograms of control and treated samples.	69
5.9	Force Index monitored in time. Purple dashed line represents overall mean FI for the control sample.	70
5.10	Force Index histograms of control and treated samples.	70
5.11	Force Index monitored in time. Purple dashed line represents overall mean FI for the control sample.	71
5.12	Force Index histograms of control and treated samples.	71
5.13	Force Index monitored in time. Purple dashed line represents overall mean FI for the control sample.	72
5.14	Force Index monitored in time. Purple dashed line represents overall mean FI for the control sample.	73
5.15	Force Index histograms for different medium conductivities.	76
5.16	Mean Force Index for 0.17-0.45 S/m medium conductivities. Solid circles stand for the case in which DEP is applied. Hallow circles stand for the case in which DEP is not applied.	77
5.17	K_{CM} sensitivity to cell radius in different medium conductivities simulated by a double shell model with a σ_{cyt} of 0.42 S/m.	77
5.18	K_{CM} sensitivity to cytoplasm conductivity in medium conductivity of 0.17 S/m and 0.42 S/m. For 1-4 σ_{cyt} is varying from 0.22-0.52 S/m in steps of 0.1 S/m.	78
5.19	Simulated K_{CM} using double shell model. σ_{cyt} =0.42 S/m, other parameters are set as defined in Chapter 1.	78
5.20	Force Index and velocity monitored in time. Purple dashed line represents overall mean FI for the control sample.	80
5.21	Force Index histogram over 120 minutes of experiment.	81

5.22	Force Index histogram after 60 minutes of experiment.	81
5.23	Force Index and velocity monitored in time. Purple dashed line represents overall mean FI for the control sample.	82
5.24	Force Index histogram over 120 minutes of experiment.	83
5.25	Force Index histogram after 60 minutes of experiment.	83
5.26	Force Index and velocity monitored in time. Purple dashed line represents overall mean FI for the control sample.	84
5.27	Force Index histogram after 120 minutes of experiment.	85
5.28	Force Index histogram over 60 minutes of experiment.	85
5.29	K_{CM} calculated by the double shell model versus cytoplasm conductivity with medium conductivity of 0.42 S/m, other parameters are fixed as presented in Chapter 1.	87

List of permissions obtained for the Copyrighted Material

- Figure 1.6 Cell dynamic response to a sudden shut down of Na^+/K^+ *ATPase* pump at $t=0$. Obtained from [6], Copyright (1980) American Journal of Physiology.
- Figure 1.7 Cell dynamic response to a sudden shut down of Na^+/K^+ *ATPase* pump at $t=0$. Obtained from [7], Copyright (2003) National Academy of Sciences, U.S.A.

Cytometry: Background and Motivation

Cytometry is the set of the biotechnological methods to gather and quantify information about cell parameters. Flow cytometry and image cytometry are two commonly used forms of cytometry. These methods are employed to evaluate cell growth status, proliferation, viability, morphology, DNA/RNA analysis, ion concentration measurements within the cell, presence and absence of specific proteins and many other applications. Recent advances in micro/nano scale technologies such as lab-on-chip, offer a diverse field of techniques in biological sciences especially cell analysis. Electrical measurement techniques based on dielectric properties of the cells have shown to be a powerful means to complement or substitute the traditional biological analysis devices in a non-invasive and reliable fashion. Among these methods, dielectrophoretic cell analysis and impedance measurement techniques are of growing interest. We briefly review two traditional cytometers; flow and image cytometry, and we provide an overview of dielectrophoretic cytometry.

1.1 Flow and Image Cytometry

Flow cytometry is based on passing the biological sample through a light beam in a sheath flow stream. Normally the sample is dyed with biological dyes such as fluorescent markers. One of the significant advantages of flow cytometry is the diversity of the fluorescent probes. A few examples of these commonly used probes are: membrane, mitochondria transmembrane potential and DNA content fluorescent probes. On the other hand, there are disadvantages of flow cytometry that demands emergence of other form of cytometry. Information obtained from flow cytometry is limited to the total fluorescent image of the cell not specific organelles within the cell and their morphology. Besides, there are limitations on bio compatibility of the dyes.

After technological advances in image capturing devices and digital cameras along with automation and image processing methods, image cytometry devices became a powerful means to capture and analyze images of cells and tissues. High resolution imaging, post processing automation by machine learning and tissue imaging are of the advantages of image cytometers. Image cytometry offers information about the interior organelles of a cell as well as a fluorescent imaging of the cell. Specific protein distribution before and after apoptosis can be captured by image cytometry. A few examples of limitation with image cytometry are: the need for highly trained operators to work with the devices, limitations associated with the speed of analysis, hidden cost and setup preparation time cost. Similar to flow cytometry, there are limitations with bio-compatibility of the fluorescent markers and dyes. Non-invasive and marker free methods of cytometry where the samples can be used later on for further analysis are of interest and preferred in laboratories.

1.2 Introduction to DEP Cytometry

1.2.1 Definition and History

Dielectrophoresis is defined as the phenomenon of moving and manipulating polarizable particles in a non-uniform electric field[8]. When a polarizable particle is placed in a non-uniform electric field, the force exerted due to the induced dipole moment of the particle results in a motion toward higher or lower density of the electric field.

Dielectrophoresis was not a well-known term when Pohl used it as an industrial means to remove carbon-black filler from samples of polyvinyl chloride. Pohl and Pethig had to change the title of one of their early papers on dielectrophoresis since dielectrophoresis was not even a word in one of the referees' opinion[9]. Pohl combined the Greek word *phorein* meaning *carry* and dielectric to infer the phenomenon of particles being carried dielectrically. The phenomena has the following characteristics [8]:

- The force is exerted on the particle only in a non-uniform electric field.
- Dielectrophoretic force is observed in AC as well as DC electric field.
- Dielectric force is attractive if the permittivity of the particle is larger than the suspension medium. In this case particle moves to the region with higher electric field density.
- Dielectric force is repulsive if the permittivity of the particle is less than the suspension medium. In this case particle moves to the region with lower electric field density.
- DEP phenomenon is mostly easily observed with particle sizes in the range of 1 to 1000 microns.

1.2.2 Theory

As previously mentioned, a cell surrounded by a medium in a non-uniform electric field will be polarized into non-homogenous positively and negatively charged regions, as shown in Fig. 1.1.

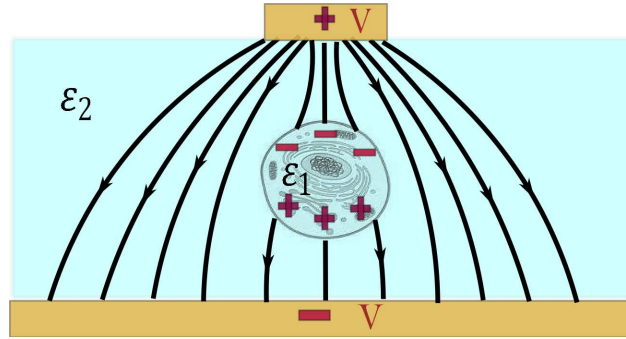


Fig. 1.1: A polarized cell in a non-uniform electric field experiences a net dielectric force.

T. B. Jones, in *Electromechanics of Particles* has discussed in detail different cases in terms of particle loss, *i.e.*, lossy/lossless particles in a uniform/non-uniform electric field. Biological cells are considered as dielectric particles with loss. The dielectric force on a particle can be translated as the dielectric force on the equivalent system of multi-poles for the polarized particle. Here, we assume particle size is small enough to ignore field non-uniformities to be able to use dipole approximation of the DEP force.

A first order approximation of the time averaged DEP force on a spherical particle can be expressed as:

$$F_{DEP} = \langle \bar{F}_{DEP}(t) \rangle = 2\pi\epsilon_1' r^3 \frac{\bar{\epsilon}_1 - \bar{\epsilon}_2}{\bar{\epsilon}_1 + 2\bar{\epsilon}_2} \nabla E_{0,rms}^3 \quad (1.1)$$

where, $\bar{\epsilon}_i$ is the complex permittivity of the cell or the medium defined as:

$$\bar{\epsilon}_i = \epsilon_i' - j \frac{\sigma_i}{\omega}, \text{ assuming } \epsilon_i'' = 0 \quad (1.2)$$

In Equation 1.1, the fraction $\frac{\bar{\epsilon}_1 - \bar{\epsilon}_2}{\bar{\epsilon}_1 + 2\bar{\epsilon}_2}$, known as the Clausius Mossotti factor, can be found by the boundary condition satisfaction on the surface of the spherical particle when solving for electrostatic potential function. Consequently it appears in the effective polarization of the particle and DEP force exerted on the particle. The Clausius Mossotti factor is a measure of effective polarization of a particle relative to the surrounding medium. In this thesis we refer to Clausius Mossotti factor as K_{CM} . The frequency dependent behavior of K_{CM} is inherited from the frequency dependent nature of the complex permittivity of materials.

A biological cell, specifically a mammalian cell which is of interest in this thesis, is composed of different organelles and their membranes, all surrounded in the cytosol and cell membrane. These compartments don't have identical dielectric properties. Consequently, to predict dielectric response, it is beneficial to model a cell as a lossy dielectric sphere with multi-layers of dielectric properties. There are two main methods to model a cell as a multi-layer dielectric sphere; the single shell model and the double shell model. In the K_{CM} spectrum, the permittivity of the whole cell is compared to the medium. Therefore, the goal in the single/double shell model is to calculate the equivalent complex permittivity of the whole cell with its compartments[3].

Single Shell Model: In the single shell model, biological cells are modeled as a homogeneous electrolyte covered with an isolating membrane. When using single shell model, large organelles within the cytosol are ignored as a separate dielectric material. For example, non-nucleated erythrocytes can be modeled by a single shell model since they don't have nucleus or any other significantly large organelle in their cytoplasm [3, 10]. As shown in Fig. 1.2

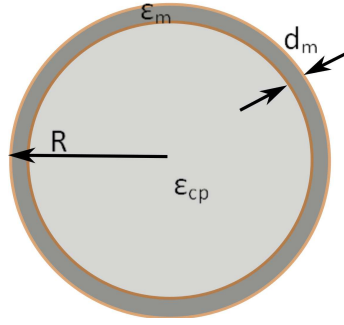


Fig. 1.2: Single shell model for calculating equivalent dielectric properties of a cell without large organelles. $\bar{\epsilon}_{cp}$ and $\bar{\epsilon}_m$ are the complex permittivity of cytoplasm and membrane respectively. R and d_m are cell radius and membrane thickness respectively.

The equivalent permittivity of the cell can be obtained from the following set of equations 1.3.

$$\bar{\epsilon}_c = \bar{\epsilon}_m \frac{2(1 - r_1) + (1 + 2r_1)E}{(2 + r_1) + (1 - r_1)E} \quad (1.3a)$$

where E and r_1 are defined as:

$$E = \frac{\bar{\epsilon}_{cp}}{\bar{\epsilon}_m} \quad (1.3b)$$

and

$$r_1 = \left(1 - \frac{d_m}{R}\right)^3 \quad (1.3c)$$

There are several limitations for single shell model. It is an over simplified dielectric model and ignores the impact of the organelles inside the cytoplasm. Cells with large nucleus such as lymphocytes, unlike erythrocytes can not be accurately modeled as one electrolyte and one membrane. These cells show high frequency dielectric behavior in their spectrum measurement which cannot be explained by single shell model. For example, erythrocytes show a single dielectric dispersion which is dominated by the Maxwell-Wagner dispersion of the cytoplasm and the membrane; however, lymphocytes have two sub-dispersions which cannot be explained in theory by single shell model. Therefore, there is a need to model large sub-organelles as a distinct dielectric material.

Double Shell Model: In the double shell model, nucleus and its membrane are added to the single shell model, shown in Fig. 1.3. Mitochondria and other organelles with small volume fraction are ignored in this model. Equation set 1.4 shows how to calculate the equivalent permittivity of a cell by the double shell model.

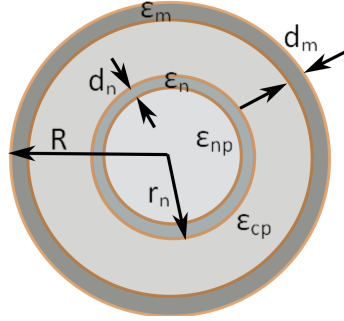


Fig. 1.3: Double shell model for calculating equivalent dielectric properties of a cell with a large nucleus. $\bar{\epsilon}_{np}$, $\bar{\epsilon}_n$, r_n , and r_n stand for complex permittivity of nucleoplasm and nucleus, nucleus radius and nucleus envelope thickness, respectively.

$$\bar{\epsilon}_c = \bar{\epsilon}_m \frac{2(1 - r_1) + (1 + 2r_1)E_1}{(2 + r_1) + (1 - r_1)E_1} \quad (1.4a)$$

$$\text{where } r_1 = \left(1 - \frac{d_m}{R}\right)^3 \quad (1.4b)$$

$$E_1 = \frac{\bar{\epsilon}_{cp} 2(1 - r_2) + (1 + 2r_2)E_2}{\bar{\epsilon}_m (2 + r_2) + (1 - r_2)E_2} \quad (1.4c)$$

$$\text{where } r_2 = \left(\frac{r_n}{R - d_m}\right)^3 \quad (1.4d)$$

$$\text{,and } E_2 = \frac{\bar{\epsilon}_{np} 2(1 - r_3) + (1 + 2r_3)E_3}{\bar{\epsilon}_n (2 + r_3) + (1 - r_3)E_3} \quad (1.4e)$$

$$\text{where } r_3 = \left(1 - \frac{d_n}{r_n}\right)^3 \quad (1.4f)$$

$$E_3 = \frac{\bar{\epsilon}_{np}}{\bar{\epsilon}_n} \quad (1.4g)$$

Fig. 1.4 shows the Clausius Mossotti factor spectrum simulated by single and double shell models. Adding nuclear as a distinct dielectric material in the double shell model affects the spectrum mostly in the MHz frequency range.

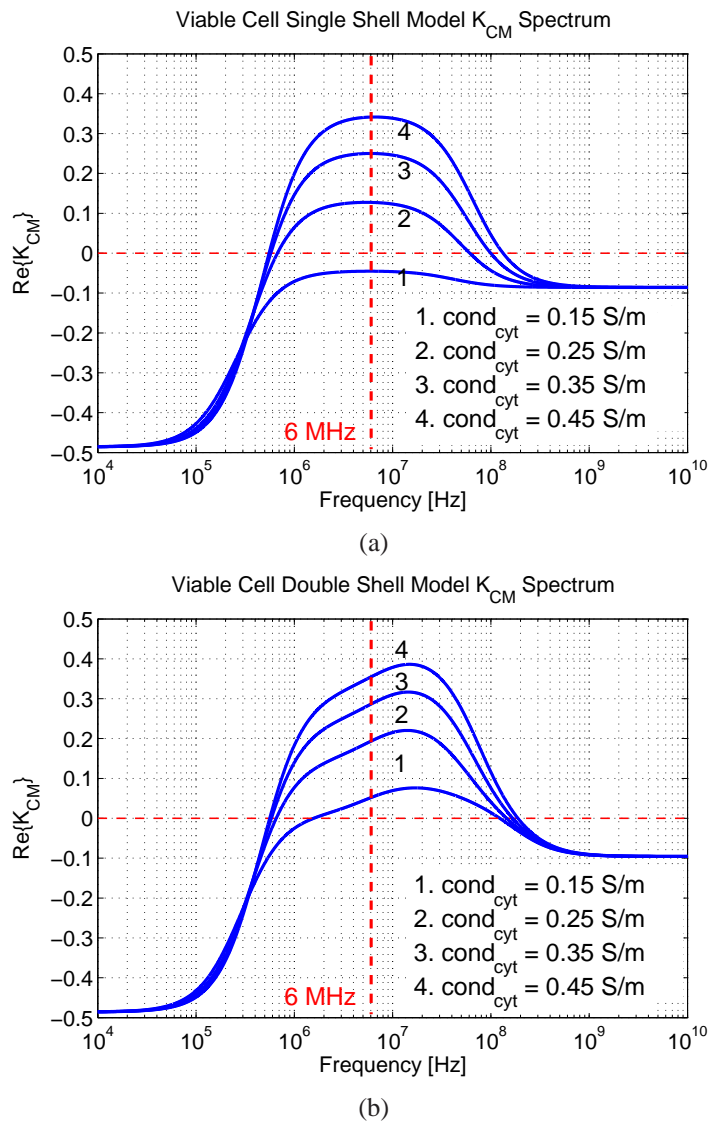


Fig. 1.4: Clausius Mossotti factor spectrum calculated by: (a) single shell model and (b) double shell model medium conductivity=0.17 S/m, cytoplasm conductivity=0.15-0.45 S/m, viable cell radius = 5.5 μm . Other cell parameters are fixed as: nucleus radius=3.25 μm , membrane thickness=5 nm, nucleus envelope thickness= 40 nm, membrane permittivity= 6.8 ϵ_0 , cytoplasm permittivity= 60 ϵ_0 , nucleus envelope permittivity= 28 ϵ_0 , nucleus permittivity= 52 ϵ_0 , membrane conductivity= 3×10^{-3} S/m, nucleus envelope conductivity = 6×10^{-3} S/m, nucleus conductivity= 1.35 S/m [3, 4, 5].

1.2.3 Techniques and Applications of Dielectrophoresis

In modern technology, the need to analyze small sized particles demands a means to manipulate, sort, trap and isolate micron sized particles [11]. Tools such as optical tweezers and acoustic forces have been employed for trapping and isolating particles however electrical forces such as dielectrophoresis offer a more powerful tool not only to remotely manipulate small sized single particles but also jointly with detection techniques can be used as a particle analyzer. In addition, biological particles are a good candidate for dielectrophoresis analysis since they are dielectric particles with micron scale size. Consequently, there is a growing interest in biotechnology, bioengineering, biochemistry and biophysics to employ DEP phenomenon in many applications. In the recent decade the total number of publication on dielectrophoresis theory, technique and application has been significantly increasing. However recent papers mostly cover the application prospective rather than the theory which was covered in previous decades [9].

DEP trapping, separating and transport of particles, electrorotation and traveling wave technique are the major applications of dielectrophoresis that we briefly review here.

1.2.3.1 DEP trap, sort and transport of particles

Cells can be trapped, moved or sorted in their surrounded medium based on their polarizability. Polarizability differences of subpopulations is expressed by their Clausius Mossotti factor or K_{CM} . Non-identical K_{CM} either caused by frequency dependent behavior of Clausius Mossotti factor or subpopulations showing K_{CM} with different signs (positive/negative) or different magnitudes are used to manipulate certain cell subpopulations. Since K_{CM} is frequency dependent, choosing the electric field frequency such that K_{CM} is positive for a subpopulation and negative for the other, cell populations can be differentiated. For in-

stance, differentiating viable from nonviable cells, cancerous cells from healthy white and red blood cells, and stem cell enrichment are a few examples of sorting based on the sign of K_{CM} [12, 13, 14]. One limitation with this technique is small magnitudes of K_{CM} when operating near the zero K_{CM} crossover frequency.

In equation 1.1, DEP force is proportional to the volume of the cell as well as K_{CM} . Consequently, in DEP sorting, one should make sure that size variation effects can be accounted for sorting subpopulations. One of the techniques that successfully sorts subpopulations considering size variations as well as K_{CM} , is *DEP Field-Flow Fractionation (FFF)*. In this technique, cell subpopulations levitate in different heights in the microfluidic channel based on the balance between DEP force, lift and gravitational forces on the particle. The equilibrium height in the channel is a function of frequency, voltage, flow velocity and electrical properties. Setting frequency and velocity such that subpopulations levitate in distinguishable heights is the basis of *FFF* [15]. Field-Flow Fractionation has been employed to separate Breast Cancer Cells from $CD34+$ Hematopoietic stem cells and separation of Leukocyte subpopulations by Gascoyne *et al.* [16].

1.2.3.2 Electrorotation

A polarizable particle in a rotating electric field experiences a torque which is proportional to the imaginary part of the Clausius Mossotti factor. The time averaged torque is defined by 1.5.

$$\langle \bar{T}(t) \rangle = -\pi\epsilon_1 r^3 \text{Im}[K_{CM}] \bar{E}^2 \quad (1.5)$$

Cell rotation rate spectra obtained from ROT is used to estimate cell dielectric properties such as cytoplasm conductivity and membrane permittivity. This is done by modeling the rotating cell by single or double shell model and characteristic (crossover) frequency of ROT spectra [17, 18]. Optical tweezers or DEP commonly used to levitate the cell in a specific

position in the rotating electric field [19].

1.2.3.3 Travelling wave:

Applying a polyphase AC voltage to a series of interdigitated electrodes can produce a travelling wave electric field. The time averaged DEP forces on the polarized particle is a function of real and imaginary parts of the Clausius Mossotti factor and in perpendicular directions; translational and vertical DEP forces. The two dimensional nature of DEP forces in travelling wave DEP opens up a broad variety of applications in biotechnology and biological analysis [20, 21, 22].

1.3 Cell physiological changes and dielectric response

The dielectric response of a cell is determined by cell dielectric properties. Cell physiological events that result in a change in dielectric properties are of interest in dielectric cytometers. Specifically, dielectric response by a dielectrophoretic (DEP) cytometer is affected by cell polarizability. Not every physiological process results in a change in dielectric properties nor is every dielectric cytometer sensitive to all the dielectric modulations. Cytoplasm, cell membrane, nucleus and nucleus membrane dielectric properties such as permittivity and conductivity are the dominant factors considered in cell modeling and dielectric response. However, a revision in the double shell model is needed when cells have a large volume fraction of other organelles such as mitochondria. In this chapter we focus on dielectric properties used in a double shell model with cell types refined to mammalian cells with a more interest on Chinese Hamster Ovary cells.

1.3.1 Cytoplasmic membrane

Two layers of lipid molecules form most of the biological membranes such as cytoplasm and nucleus membrane. Therefore membrane thickness is just two lipid molecules length or a few nanometers. These molecules have two hydrophobic tail and one hydrophilic tail. Hydrophobic tails face each other and form the double layer lipid membrane. The hydrophobic tail which is not exposed to the membrane surface is composed of phospholipids such as Phosphatidylserines (PS). When cell undergoes apoptotic or cell death, which we talk in more detail in following sections, phospholipid tails flip outside and get exposed to the outer surface of the cell membrane. Specific dyes that bind to the phospholipids, such as Nexin, are commonly used as a viability measurement assay.

The cell membrane is an insulating layer separating the cytoplasm (i.e. electrolyte) from the outer media. Therefore, it behaves like a capacitor. However, the cell membrane is not a smooth structure. Folds, ruffles and microvillus define the actual surface area of the membrane. Relative membrane permittivity, thickness, morphology and surface area modulate membrane capacitance [17, 23]. Membrane capacitance differences have been widely used to discriminate cell types and their growth stage using crossover frequency by ROT and DEP techniques. Separation of trophoblast cells from peripheral blood mononuclear cells [24], stimulated and unstimulated lymphocytes [25, 26] and differentiating normal and malignant white blood cells [4] are a few examples of cell differentiation based on capacitance change resulted from surface complexity alteration. Fig. 1.5 shows how K_{CM} changes with membrane permittivity modulation.

The cell membrane also consists of thousands of channels, pumps, and carriers responsible for ion transport inside and outside of the cell. This ability to flow current via membrane is expressed by membrane conductivity. DEP and ROT provide a means to estimate membrane conductance as well as membrane capacitance [27, 24].

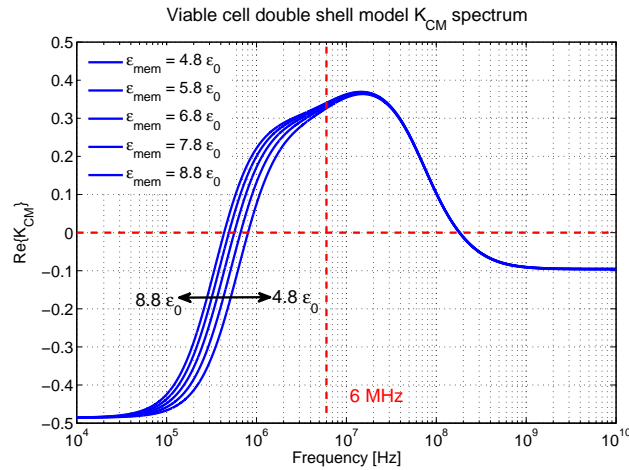


Fig. 1.5: Double shell model for K_{CM} spectrum for a viable cell while membrane permittivity is changing from $4.8 \epsilon_0$ to $8.8 \epsilon_0$. Changing membrane conductance is not significant in MHz frequency range. Medium conductivity = 0.17 S/m and cytoplasm conductivity = 0.42 S/m , other parameters are fixed as Fig. 1.4

Furthermore, membrane permeability to certain ions via proteins forming channels, pumps and carries is important in determining ion concentrations and electrical properties of cytoplasm and inner organelles. Understanding membrane dynamic regulations and cell homeostasis helps to better interpret cell dielectric response and improve dielectric models of the cell. Here, these three ion traffic controllers are briefly described [28, 1].

1.3.1.1 channels

Channels are membrane proteins which are selectively permeable to ions and small molecules. Depending on the ion concentrations in their open state, they can transport ions down the concentration gradient within or outside the cytoplasm. Their ion transport rate or diffusion rate is considerably higher than carriers and pumps. Transporting ions via channels is an important part of regulating transmembrane potential. Membrane potential pulses produced by channel toggling between open and closed state, provides a communication means for excitable cells such as muscle and neurons. Flick's first law of diffusion expresses the number

of molecules crossing a unit area per unit time or J_{ion} , as shown in Eq. 1.6 [1].

$$J_{ion} \approx -D \frac{\partial C}{\partial x} \quad (1.6)$$

where, D is the diffusion constant and C is the concentration. Assuming channels are cylindrical with diameter of 0.5 nm, length of 5 nm, D of 3000 $\mu m^2/s$ and typical concentration difference (ΔC) of 100 mM or $6 * 10^{-2}$ molecules/ nm^3 results in $J_{ion} \approx 3 * 10^7 m^{-2}s^{-1}$ [1].

1.3.1.2 carriers

Carriers are enzyme like proteins that bind to the specific ion or small molecule on one side of membrane and release it from the other side of the membrane. They can transport ions down the concentration gradient (passive transport) or consume energy and transport up the concentration gradient. Unlike pumps and channels, carrier proteins move across the membrane to transport ions and compared to channels are very slow.

1.3.1.3 Pumps

Pumps are enzymes that consume ATP energy to transport ions up the concentration gradient. Pumps are slower compared to channels. They move an order of 100 ions per second, however, channels are able to transport 10-100 million ions per second. ATPase pumps can be found in plasma membranes and mitochondria. There are a few types of ATP driven pumps but we focus on $Na^+/K^+ATPase$ pumps on the plasma membrane. ATP dependent pumps, unlike channels, require at least two gates to transport ions. For example, $Na^+/K^+ATPase$ requires one gate for Na^+ and one for K^+ , so at the expense of one ATP

molecule, 3 Na^+ and 2 K^+ are moved out and into the plasma, respectively. Ions constantly leak down their gradient via channels. Therefore, pumps are constantly utilizing energy to maintain the balance and membrane potential.

$Na^+/K^+ATPase$ pumps play a significant role in regulating cell volume. Cell volume is determined by osmolarity meaning water moving down its gradient into or out of the cell. $Na^+/K^+ATPase$ regulate ion concentrations and hence osmolarity by pumping ions in and out. It has been studied that Ouabain which is a $Na^+/K^+ATPase$ pump blocker results in cell swell and burst [29]. Also it has been shown that inhibition of $Na^+/K^+ATPase$ pumps can initiate apoptosis [30]. In the next section, the impact of inhibition of $Na^+/K^+ATPase$ pumps on ion concentrations are shown by the existing computational models for dynamic cell regulations.

1.3.1.4 Computational models for cell dynamic regulations

One of the first and most powerful computational models for action potential of excitable cells has been suggested by Hodgkin and Huxley in 1952 [31]. The next generations of these equations can be generalized to non-excitable cells as well [32]. These equations are based on cell volume, membrane voltage and ion concentrations inside and outside of the cell expressing cell dynamics in steady state [33, 7, 6, 34, 35, 36, 37]. Ion concentrations are based on channel leakage down the concentration gradient and $Na^+/K^+ATPase$ activity to maintain cell volume and osmolarity. Modelling cell regulations following a pump shut down or a sudden change in a specific ion concentration in cytoplasm or medium has been studied extensively by these models and verified experimentally [38].

Here we discuss Jacobsson's approach through cell dynamic regulations which is one of the first approaches to solve cell volume, membrane potential and ion flux equations simultaneously. In steady state the total flux of ions in and out of the cell is zero. In other words,

osmolarity inside and outside of the cell are equal. The total flux includes ions moving down the gradient via channels as well as ions transported by pumps. The dominant ions in the equations are Na^+ and K^+ which move down their concentration gradient inside and outside of the cell as well as actively pumped by $Na^+/K^+ATPase$ in the reverse direction. The anion keeping the balance is Cl^- which is transported by channels (pores) and not by the active transport.

The passive ion flux via channels is expressed by equation 1.7.

$$\frac{P_{Na^+} \Delta\phi ([Na^+]_o - [Na^+]_i \exp(\Delta\phi))}{\exp(\Delta\phi) - 1} \quad (1.7)$$

where $[Na^+]_o$ is the external sodium concentration, $[Na^+]_i$ is the internal sodium concentration, P_{Na^+} is the permeability to sodium ions and $\Delta\phi$ is the membrane potential and ϕ is defined as:

$$\phi = \frac{F * V}{R * T} \quad (1.8)$$

and V is the electrical potential as a function of x (across membrane) and $\frac{R*T}{F}$ is 26.7 mV at body temperature of mammals.

P_{Na^+} is calculated as the number of [pores/cm²] times the permeability of a single pore [cm³/sec * pore] times Faraday's constant [C/mol] by Armstrong (2003)[7]. Number of pores crucially defines the time constant to reach steady state following a sudden change such as blocking pumps. The same equation with appropriate sign is valid for K^+ and Cl^- ions moving down their concentration gradient.

Armstrong (2003) calculates $Na^+/K^+ATPase$ pump flux of Na^+ ions as:

$$J_{Na^+} = 2.17 \frac{[ATP]}{(1 + \frac{[Na^+]_c}{[Na^+]_i})^3} \quad (1.9)$$

where [ATP] is internal ATP concentration and $[Na^+]_c$ is the concentration of sodium ions for half maximal occupation of Na^+ binding sites in the pump. For low concentrations it can

be assumed that only [ATP] and third power of $[Na^+]_i$ play a significant role in ion fluxes. 2.17 is the pump rate coefficient which was calculated empirically by Armstrong (2003). Finally, J_{Na^+} is expressed in $mol.cm^{-1}.sec^{-1}$.

Cell volume comes into the equations by osmolarity equilibrium at the steady state. For a sudden change in homeostasis, the set of equations for ion flux, volume and membrane potential are solved simultaneously to reach steady state.

These models offer a reliable means to simulate ion concentrations and cell volume following a disturbance in channels or blocking the pumps. Having the ion concentrations as a function of time enables us to calculate cytoplasm conductivity and hence cell dielectric response as presented in the next section. Figures 1.6 and 1.7 show simulated cell dynamics after blocking $Na^+/K^+ATPase$ pumps modeled by Armstrong (2003) and Jacobsson (1980). According to this model, after shutting down the pump the cell is no longer able to compensate for the ion leakage down their gradient through channels. Therefore, membrane voltage magnitude decreases and ion concentrations approach their background (medium) values; $[Na^+]_i$ increases and $[K^+]_i$ decreases. The time reported to reach equilibrium is within 20-60 minutes however it is highly dependent on the number of pores in the membrane.

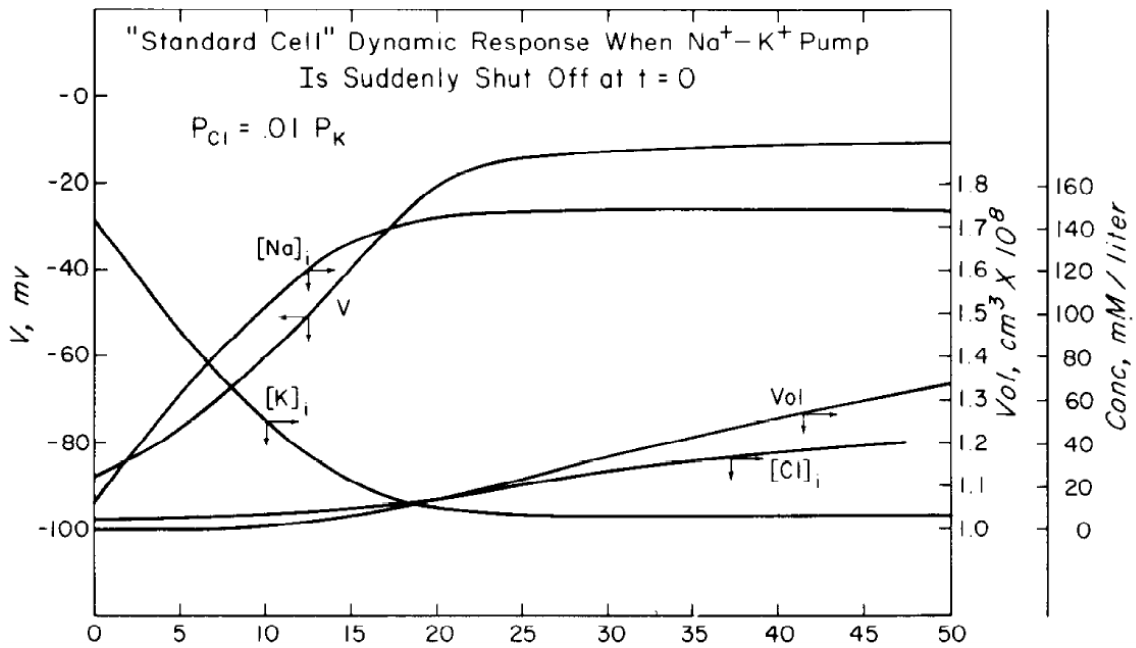


Fig. 1.6: Cell dynamic response to a sudden shut down of Na^+ / K^+ *ATPase* pump at $t=0$. Obtained from [6], Copyright (1980) American Journal of Physiology (with permission)

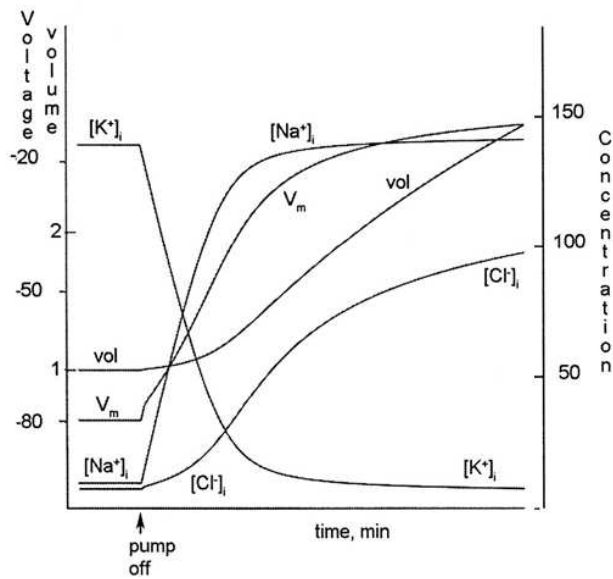


Fig. 1.7: Cell dynamic response to a sudden shut down of Na^+ / K^+ *ATPase* pump at $t=0$. Obtained from [7], Copyright (2003) National Academy of Sciences, U.S.A (with permission).

1.3.2 Cytoplasm

The cytoplasm consists of cytosol and organelles confined within the cell membrane. Cytosol is the medium (mostly water) between organelles where ions and organic molecules can be found in dissolved or suspended form. Besides these small molecules, cytoskeleton, proteins, ribosomes and other big structures are found in the cytoplasm. Presence of such crowded structure causes an effect called *macromolecular crowding* prohibiting cytosol from behaving like an ideal solution. Therefore, ions are not able to reach the mobility found in an ideal solution. We will show in the next chapters that reduced mobility of the ions within the cytoplasm reduces expected conductivity and influences dielectric response [39].

Internal and external ion concentrations reported for a typical cell is presented in Table 1.1. As shown previously, computational models enables us to estimate ion concentration within the cell following a sudden change such as blocking ATP dependent pumps or a change in medium ion concentration. In order to calculate internal conductivity from ion concentrations, *Kohlrausch's law* is used as defined in Equation 1.10:

$$\Lambda_m = \Lambda_m^0 - K\sqrt{c} \quad (1.10)$$

where Λ_m is the molar conductivity, Λ_m^0 is the limiting molar conductivity, K is an empirical constant, and c is the electrolyte concentration. For low enough concentrations we can ignore the second term and calculate conductivity by the limiting molar conductivity as defined in

Tab. 1.1: Typical intra/extracellular ion concentrations [1].

Ion species	Intracellular [mM/liter]	Extracellular [mM/liter]
K^+	155	4
Na^+	12	145
Ca^{2+}	10^{-4}	1.5
Cl^-	4	120

Equation 1.11

$$\Lambda_m^0 = \nu_+ \lambda_+^0 + \nu_- \lambda_-^0 \quad (1.11)$$

ν_+ is the cation concentration, ν_- is the anion concentration and λ_i is the limiting molar conductivity of the individual ions in water reported in Table 1.2. Then cytoplasm conductivity can be rewritten as Equation 1.12 [2]:

$$\sigma_{cytoplasm} = [Na_+]_i \lambda_{Na}^0 + [K_+]_i \lambda_K^0 + [Cl^-]_i \lambda_{Cl}^0 \quad (1.12)$$

Substituting typical interacellular concentration reported in Table 1.1 into Equation 1.12 results in a cytoplasm conductivity of 1.23 S/m which is an order of three higher than measured in mammalian cells. This can be attributed to the lower mobility in cytosol and macromolecular effect as mentioned before. Furthermore, ions locked up in organelles and proteins appear in dry weigh ion measurements and values commonly reported for intracellular ion concentration. However, these ions cannot contribute to conductivity. In addition, in a cytoplasm crowded with proteins and big molecules, ions have limited space to scatter and move. Therefore, expected mobility and conductivity are less than what is calculated and measured in water or other ideal solvents by a factor of $\approx 2-3$. Gimsa *et al.* (1996) by Dielectric Spectroscopy and Huang *et al.* (1995) by Electro-rotation have reported similar mismatch in expected cytoplasm conductivity previously [40, 41, 39].

Tab. 1.2: Limiting molar conductivity in water at 298° K [mSm^2mol^{-1}] [2]

Ion species	Na^+	K^+	Cl^-
λ_i^0	5.011	7.350	7.634

1.3.3 Apoptosis

The term *apoptosis* for programmed cell death first was used by Kerr *et al.* (1972) [42]. Apoptosis is a part of the developing cycle of cells and organisms. For example, cells between fingers and toes go under apoptosis in developing stage of embryo and allows fingers to separate. In the human body, 10 million cells are generated every day to compensate for the apoptotic cells. They may go under apoptosis as a result of healthy growth cycle, defense mechanism against a disease, mild injury or drug exposure. Diseases such as cancer, HIV, Parkinson and Alzheimer can be correlated with abnormalities in specific type of cell apoptosis such as excessive or inefficient apoptosis [43, 44].

The alternative changes following apoptosis is referred to as necrosis [45]. Kanduc (2002) *et al.* refer to necrosis as the post-mortem events in the apoptotic cell and call it unjustified to compare necrosis to apoptosis since they are not two distinct pathways of cell death. There are substantial differences in the apoptosis and necrosis processes. Apoptosis is highly energy dependent and happens within determined pathways and triggers. Whereas necrosis happens as a result of severe energy depletion or severe membrane injury and does not have a determined pathway. Cell shrinkage is an element of apoptosis which is a result of chromatin condensation and ion regulations. In necrosis, cell goes through swelling, membrane disruption and ultimately cell lysis. Cells may go through the necrosis process after apoptosis; however, it is possible to maintain viability in apoptosis which is hard to maintain in necrosis. Furthermore, the possibility of reversing apoptosis is under research whereas necrosis is an absolutely irreversible process [43].

Many of the biological assays are sensitive to the post-mortem changes of the cell. They are sensitive to different biochemical or morphological events in the cell such as membrane surface area changes (microvilli, blebs and folds screened by SEM), transmembrane potential of mitochondria alteration (TMRE assay), membrane permeability to dyes (Trypan blue exclusion assay), and phosphatidylserine (PS) externalization (Annexin V assay) [46]. The

need for a means to predict the onset of apoptosis is beyond all doubt and dielectric cytometers such as the DEP cytometer can be sensitive to apoptosis and post-mortem events in the cell [47]. Cell radius, membrane capacitance and conductivity, and cytoplasm conductivity modulations are of dominant factors that can be monitored by DEP cytometers.

Dielectrophoresis has been used in tracking apoptosis and identifying sub-populations by Labeed *et al.* (2006) [48]. In their study apoptosis is induced by Staurosporine in the human Leukemic (K562) cell line. Cell shrinkage is reported during apoptosis. Furthermore, membrane capacitance increased from 9.7 to 19.9 mF/m^2 which is a result of increased membrane folds and cell shrinkage. Following 4 hours of treatment, an increase in the cytoplasm conductivity was observed and maintained until 12 hours of treatment. It is known that during apoptosis, a cell experiences efflux of K^+ and Cl^- ions and influx of Na^+ ions [44, 30, 49, 50]. For osmolarity balance, water moves outside of the cell which causes cell shrinkage. The rise in the cytoplasm conductivity is mainly due to cell volume decrease. Interestingly, after 24 hours of treatment 3 sub-populations were detected: a) Increased cytoplasm conductivity sub-population associated with pre-apoptotic cells, b) decreased cytoplasm conductivity associated with cell undergoing apoptosis but still maintaining cytoplasm conductivity higher than the medium, and c) cells undergoing necrosis with cytoplasm conductivity less than the medium. This quantification is then used in differentiating multi drug resistant counterpart of the cell line studied (K562AR). A higher cytoplasm conductivity has been observed by Labeed *et al.* (2003) after treatment of K562AR (MDR counterpart of K562) by XR9576 [51].

Different cell lines and growth stages may respond to apoptosis differently. Pethig *et al.* (2007), studied the impact of induced apoptosis on membrane capacitance in Jurkat cells treated by etoposide (anti cancer drug). In contrary to Labeed *et al.* , they have observed a decrease in membrane capacitance from 13.34 to 10.49 mF/m^2 during apoptosis . Membrane smoothing and loss of microvilli and blebs are observed by SEM microscope during

apoptosis which is an evidence for decrease in membrane capacitance [52]. The decrease in membrane capacitance is consistent with what Wang *et al.* (2002) reported for human promyelocytic HL-60 cells treated with Genistein decreasing from 17.6 to 9.1 mF/m^2 during apoptosis [53]. In another study by Ratanachoo *et al.* (2002), a decrease in the membrane capacitance and increase in the membrane conductance has been observed while treating the cells by different apoptosis inducers. The dielectric change caused by apoptosis was detected within 15 minutes of treatment for the cases that inducers caused a direct alteration to membrane and within 30 minutes for the cases that inducers caused an alteration to cytoplasmic organelles [54]. Membrane capacitance decrease has been also reported by Lv *et al.* in NB4 cells following 2 hours of treatment by Ara-C [55].

During apoptosis cytoplasm conductivity is mainly determined by ion concentrations and ion flux rates inside and outside of the cytoplasm. As mentioned previously malfunction in the channels (pores) and pumps results in a change in ion flux rates, ion concentrations, osmolarity and cell volume. Cytoplasm ion concentrations during apoptosis has been studied extensively. Among all the ions being transported via the cell membrane, K^+ , Na^+ , Cl^- , and Ca^{2+} are of interest. K^+ and Na^+ play a significant role in calculating conductivity due to their high mobility. However, Na^+ concentration inside the cell is negligible so as to account for conductivity. Cl^- plays an important role in osmolarity balance and cell volume regulation. It is thought that Ca^{2+} and K^+ can be important in triggering biological events within the cell such as mediating apoptosis [49, 56, 57]. Ion concentrations are measured by dry weight and fluorescent dye evaluation measured by plasma/mass spectrometry (dry weight) and flow cytometry, respectively.

Hughes *et al.* (1997) reported decrease in internal K^+ concentration in Thymocytes during DEX-induced apoptosis from $\approx 140mM$ to $\approx 60mM$ in 8 hours of exposure to the drug whereas Trypan Blue exclusion did not determine any significant changes in cell viability during these 8 hours [58]. Cell shrinkage and internal K^+ concentration drop has been re-

ported by other groups as well, summarized in Table 1.3. Besides these studies Yu (2003) has done a valuable review on intracellular K^+ concentration [57].

Tab. 1.3: $[K^+]_i$ before and during apoptosis

Reference	Cell line	Inducer	\approx before[mM]	\approx after[mM]
McCarthy <i>et al.</i> (1997) [59]	HL-60	UV-irradiation (2 hours)	120	60
Hughes <i>et al.</i> (1997) [58]	Thymocytes	DEX (8 hours)	140	60
Xiao <i>et al.</i> (2002) [60]	glial cells	Ouabain (10-15 hours)	100	20
Barbiero <i>et al.</i> (1995)[61]	fibroblast	VP-16	150	50

1.4 Contribution

- In this work, the DEP response of Chinese hamster ovary (CHO) cells has been quantified and studied statistically in order to identify the pre-apoptotic phase of a population. Statistical analysis and curve fitting tools are employed to aid in better understanding of the dielectric response of a cell population and identify apoptotic sub-populations.
- Dielectric properties of MRC5 cells have been estimated by optimizing parameters in the double shell model to match the experimental and simulated cross over frequencies. Furthermore, dielectric response for this cell line is studied in starved and healthy samples.
- To study dielectric response of the cell to controlled changes in its biochemistry, we have used Oligomycin to inhibit the mitochondrial ATP production in a cell population. Medium conductivity and DEP frequency have been adjusted to improve the DEP cytometer sensitivity to changes in the cytoplasm conductivity. The maintenance of homeostasis through the Na^+/K^+ ATPase pump is a fundamental process in mammalian cells and this study aids in the understanding of its impact on the cytoplasm conductivity.

This study is focused on time course measurements within the first two hours of mitochondrial ATP synthase inhibition. Results are in agreement with computational models of ion regulations within the cell following inhibition of ATPase pumps. Monitoring the cell response within the first hours of the treatment with Oligomycin reveals important information on ion regulation.

Differential detection of cell DEP response

Analyzing micrometer sized particles such as single cells requires small enough tools to manipulate, trap, actuate and sense the cells. Micromachining and microfabrication offer micron size structures to analyze and study single cells. Specifically, microfluidics technology have become an attractive candidate for cell analysis. They provide high throughput, small required sample volume, marker free detection, compatibility with electronic sensors and biological assays, and ability to be implanted in vivo.

In this chapter we briefly review the forces on a particle in a microfluidic channel with embedded detection and DEP electrodes. Furthermore, we present the DEP actuation and detection setup used for the experiments. Finally, the DEP response is quantified by a factor called Force Index.

2.1 Forces in a microfluidic channel

When a particle (in our case a single cell) is flowing in a microfluidic channel, it experiences hydrodynamic forces. Cell trajectory in the channel and hence cell elevation with respect to the non-uniform electric field is influenced by the net force exerted on the cell. Therefore, to predict and interpret dielectric response it is important to study hydrodynamic forces. Drag force, lift force and gravitational forces are briefly reviewed here. More details on cell trajectory and forces can be found in previous theses by Tim Cabel [62].

Fig 2.1 shows lift, drag and gravitational forces acting on a particle flowing in a microfluidic channel. Reynolds number in a microfluidic channel is less than one meaning flow is laminar and velocity profile across the channel is parabolic as shown in Fig 2.1.

Drag force is a friction force acting in the opposite direction of the particle motion within a fluid. Its magnitude is a function of relative velocity of the particle (\bar{v}_p) in respect to the flowing medium (\bar{v}_m), radius of the particle (R), and viscosity of the medium (η) expressed by Equation (typically for water) 2.1 [63].

$$F_{drag} = 6\pi\eta R(\bar{v}_p - \bar{v}_m) \quad (2.1)$$

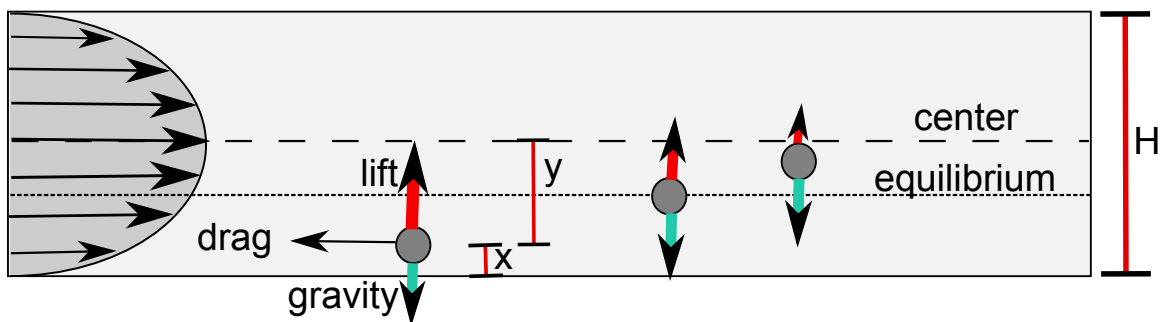


Fig. 2.1: Particle in a microfluidic channel experiencing gravity, hydrodynamic lift and drag force. Below the center line lift and gravity can equate and particle reaches equilibrium.

Lift forces are repulsive forces from the walls. In a parabolic velocity profile defined by Equation 2.2,

$$v_p = 6 \langle v \rangle \left(\frac{x}{H} \right) \left(1 - \frac{x}{H} \right) \quad (2.2)$$

where $\langle v \rangle$ is the mean fluid velocity, x is the distance of the center of the particle to the bottom of the channel, H is the channel height and y is the distance of the center of the channel to the center of the particle, when the particle is passing close to the walls of the channel, two sides of the particle experience different velocities. The velocity lag on the side close to the wall causes extra pressure on this side and consequently pushes the particle away from the wall. Furthermore, as a particle approaches the wall, flow streamlines change around the particle. The new asymmetric streamlines cause an extra pressure on the side of the particle close to the wall and consequent lift force against the wall [64]. Lift force is calculated by Equation 2.3. The empirical constant C is calculated as 0.172 by Williams *et al.* (1992) [65, 15].

$$F_{lift} = -C \frac{6\eta R^3 \langle v \rangle y}{H(H/2 - |y| - R)} \quad (2.3)$$

Lift force pushes the particle away from the wall. This causes the particle to rise in the channel. At some point gravitational force becomes equal to lift force. This is possible in the bottom area of the center line where lift force and gravity are in the opposite direction. C can be estimated from the equilibrium height in the channel which can be measured by experiment.

Gravity force is determined by Equation 2.4 as:

$$F_{gravity} = -\frac{4}{3}\pi R^3 g(\rho_p - \rho_m) \quad (2.4)$$

where, ρ_p and ρ_m are particle and medium densities respectively and g is the acceleration due to gravity. In water, a typical cell has a density of $\approx 1.05 \rho_{water}$.

2.2 Experimental setup

2.2.1 DEP actuation and detection

To apply the DEP voltage and sense the dielectric response of the cell a set of coplanar electrodes are deposited on the bottom of the microfluidic channel. More details on the fabrication process, design protocol, and COMSOL simulations of the electric fields can be found in previous theses ([66, 62]). A 2D representation of the electrodes are shown in Fig. 2.2. A DEP voltage is applied to the center coplanar electrode, providing a non-uniform electric field between the center electrodes and the ground electrodes on each side. This applied voltage is sinusoidal, set to $8 V_{P-P}$ to provide electric field density for actuation with electrode dimensions in hand. Commonly the DEP frequencies is set at 6 MHz. At this frequency, the $Re(K_{CM})$ spectrum contrast between a viable and non-viable cells is relatively large and K_{CM} magnitude is sensitive to cytoplasm conductivity. This will be discussed in Chapter 3. Maximizing contrast improves differentiating viable and non-viable cells in a cell population.

Sensing takes place by the detection electrodes on each side connected to low voltage amplitude ($\approx 300mV_{P-P}$) and high enough frequencies ($\approx 1.45GHz$) for simultaneous actuation and detection without significant coupling, as shown in Fig. 2.2. A microwave interferometer approach is employed to detect the capacitance changes while a cell passes along the electrodes. Capacitance changes are a function of K_{CM} and hence dielectric properties of the cell. A resonator is coupled with the microfluidic channel so as the change in the capacitance changes the resonance frequency and output voltage of a Lock-in-Amplifier [67].

The DEP cytometer is based on a differential detection of single cells before and after DEP actuation in a microfluidic channel and has been described in detail by other colleagues [67, 62]. Briefly, the cell first passes over the first pair of detection electrodes, and produces

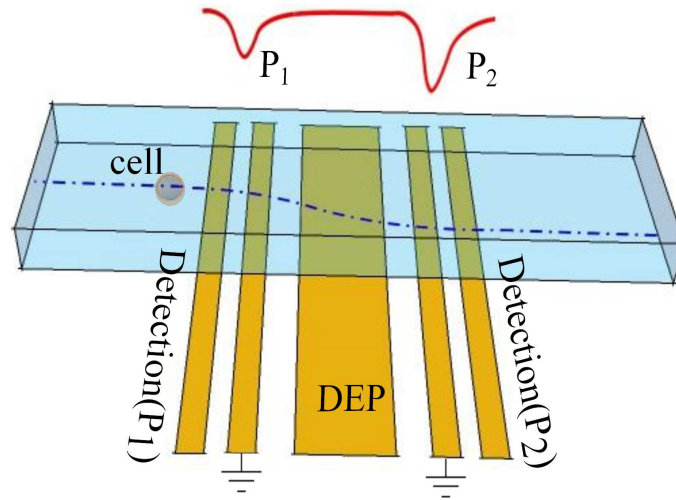


Fig. 2.2: Cell trajectory in microfluidic channel. Here, cell is experiencing an attractive DEP force. $P_2 > P_1$ and Force Index > 0 .

a signal with a voltage value of P_1 shown in Fig. 2.2. The DEP field produced between the DEP electrode and ground then actuates the cell. After passing the first detection electrode and experiencing the non-uniform electric field by DEP electrodes, the cell then passes over the second pair of detection electrodes, and produces a signal with a voltage value of P_2 .

When the DEP voltage is applied, cell experiences a DEP force with the same sign as K_{CM} (described in previous chapter). Depending on the magnitude and sign of the Clausius Mossotti factor, the cell will be attracted or repelled from the higher density electric field region. For example, as described in Chapter 1 if K_{CM} is positive then the flowing cell is more polarizable than the medium and DEP forces will be positive too; meaning cell experiences an attractive DEP force towards the electrodes and higher electric field density. Therefore, the second peak would be larger than the first peak. This signature is called positive DEP or pDEP. The two peaks form the detection signature profile for each cell. For a negative value of K_{CM} the signature is called nDEP. When no actuation voltage is applied, cell will continue the height it entered the channel while passing two detection electrodes and two peaks will be equal. All three possible signatures are presented in Fig. 2.3.

We quantify each cell signature using a normalized differential response called the *Force*

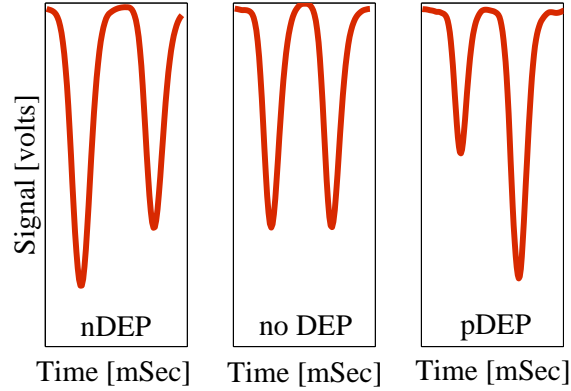


Fig. 2.3: All possible DEP cytometer signatures, from left to right: negative DEP force (nDEP), no DEP force (no DEP), and positive DEP force (pDEP)

Index defined by Equation 2.5:

$$\text{Force Index or FI} = \frac{P_2 - P_1}{P_2 + P_1} \quad (2.5)$$

Where P_2 and P_1 are the leading and trailing peaks illustrated in Fig. 2.2. Force Index depends on $Re(K_{CM})$ and the height at which the cell enters the analysis region, cell horizontal velocity and cell radius. For each cell a Force Index is measured and histograms of Force Index are used to monitor the evolution of the dielectric response of the cells which will be described in the next chapters.

Using a FEM model in COMSOL multiphysics, particle trajectories can be simulated for different heights in which cell enters the channel. Therefore, in theory height, velocity, and size impact on Force Index could be quantified. More information can be found in the previous theses [62].

Viable and non-viable cells have different dielectric properties. Therefore, K_{CM} , DEP force, and Force Index alter from viable state to non-viable. By determining a threshold in Force Index where viable and non-viable cells can be differentiated, viability can be measured. Since each viability assay is sensitive to a different physiological event in the cell, this

threshold can be arbitrary to some extent. Annexin V readings of viability is known as an early indication of apoptosis and is used to determine the Force Index threshold here. Zero Force Index threshold matches the best with Annexin V assay; meaning cells showing a pDEP signature are marked as viable and cells showing a nDEP signature are marked as non-viable (at 6 MHz and medium conductivity of 0.17 S/m). Consequently, In this thesis viability measured by the DEP cytometer is defined as Equation 2.6:

$$Viability = \frac{\text{number of pDEP}}{\text{total number of cells}} \quad (2.6)$$

Previous experiments has shown that DEP percentage viability almost matches percentage viability measured by the Annexin V assay rather than other biological assays [12].

2.2.2 Microfluidic chip

The microfluidic chip used in this thesis is designed to have two inlets and two outlets, presented in Fig. 2.4 (a). Pressure applied on the inlets and outlets are adjusted by a fluidic control system shown in Fig 2.4 (c). Inlet #1 is connected to a loaded vial while other vials are empty. Pressure difference between inlets and outlets leads the fluid flow from inlet #1 to the others. In this manner, most of the fluid fills vials #2 and the rest enters vials #3 and #4 with more fluid in vial #3. The channel interconnecting inlets and outlets (H-channel) is designed to have a smaller width (120 μm) compared to the side channels (250 μm). Smaller width of the channel increases fluid resistance and helps controlling velocity in the analysis volume by achieving smaller pressure difference for larger pressure difference between vials. The electrode array is fabricated on the bottom of the smaller channel. The top view of the electrodes are shown in Fig. 2.4 (b) with lighter colors as the electrodes.

2.2.3 Flow control

Flow control is provided by *Fluigent* device and corresponding MFCS software. By adjusting the pressures on each vial in the MFCS graphical interface, particle velocity is adjusted. For experiments in this thesis, the velocity of about 2000 – 3000 micrometer per sec is acquired by setting pressures on vials #1 to #4 to 20, 21, 19, and 19 mbars. With a slight change in the pressure the desired velocity can be achieved. Velocity of the cell is frequently checked on an oscilloscope by dividing the effective length of the detection electrode to the time between two peaks; in other words, dividing the distance between high electric field density provided by the detection electrode (210 μm) to the time required to travel between them.

Every 10 minutes, the fluid is purged through the system to keep the cell density constant and prevent or resolve clogging problems. Larger cells tend to sediment in four tubes connecting vials to the ports and cell density decreases over time. After the purge is stopped, it takes about 60 seconds to get the fresh cells from the vials into the analysis volume where the signals can be detected.

2.3 Data collection and analysis

The data recorded in each experiments consists of videos and excel files containing output signal of the detection system in time. The videos are recorded by a digital video camera equipped with a microscope and capable of recording 15 frames per second. Fig. 2.4 (b) is a sample screen capture of the video.

The output voltage is recorded by PCI data acquisition aided by a Matlab graphical user interface(GUI) written by Tim Cabel. In post processing, the meaningful signatures are scrutinized and collected by another Matlab GUI in a manual, semi-automated, or auto-

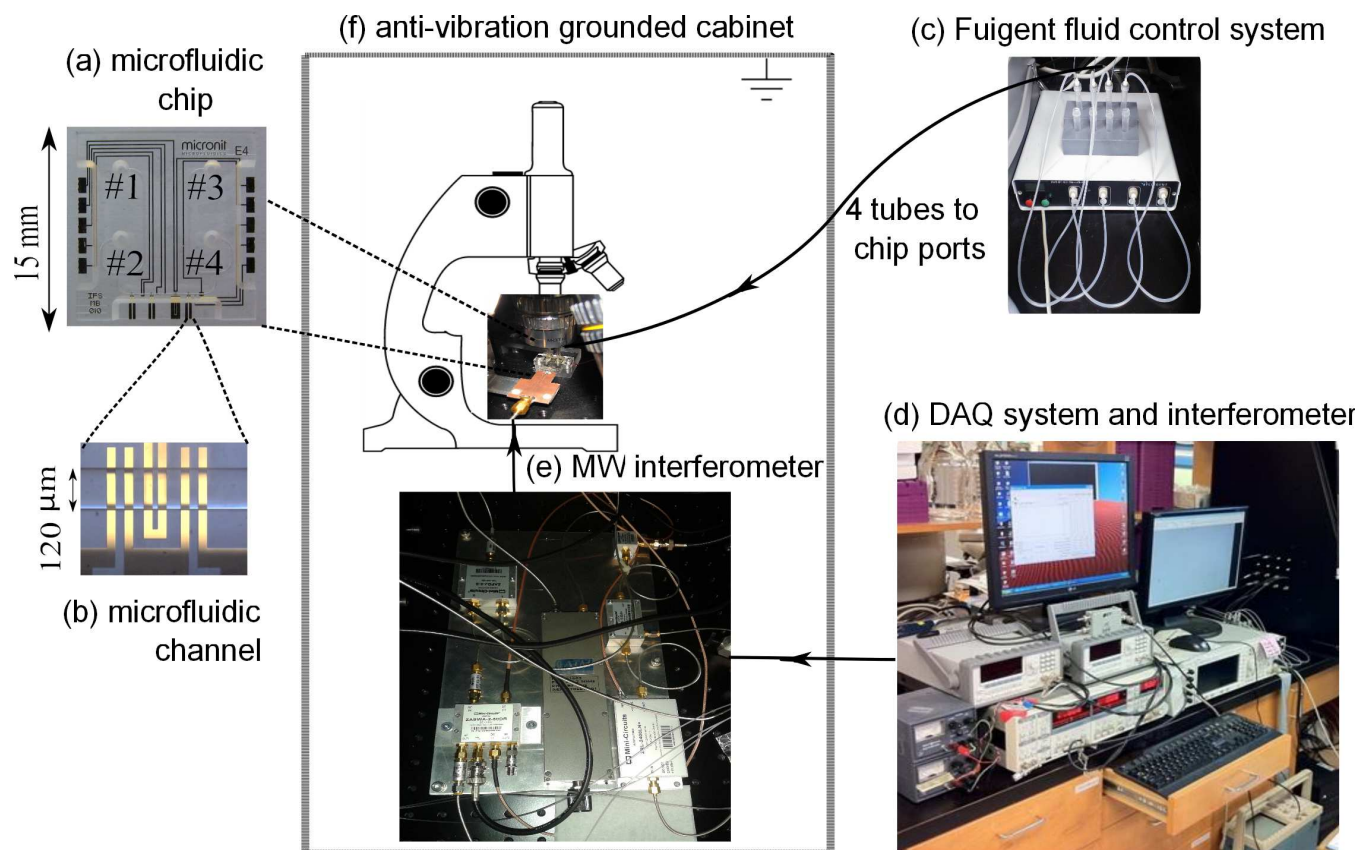


Fig. 2.4: DEP cytometer compartments. (a) microfluidic chip with 4 ports (b) top view of the microfluidic channel and the electrodes. (c) fluidic control system for adjusting pressure on each vial. (d) DAQ and graphical interfaces to control pressure, DAQ, and video recorder. (e) interferometer setup shielded in the cabinet. (f) anti-vibration cabinet including interferometer, microscope and video recorder, microfluidic chip.

mated approach¹. The data acquisition platform is shown in Fig. 2.4 (d).

For each cell or group of cells passing through the detection electrodes a signature is recorded. The meaningful signals should be collected from all the recorded signals for the post-processing. Signals that are not acceptable are multiple cells passing through the electrodes simultaneously, cells stuck together or a cell stuck to the electrodes and noisy signals. In the collection process, event information such as P_1 and P_2 values, time and Force Index is exported in an excel file. Normally a histogram is used to represent Force Index of a popu-

¹Manual collection GUI by Tim Cabel [62], Semi-automated collection by Bahareh Saboktakin Rizi and Ashlesha Bhide, and automated collection GUI by Ashlesha Bhide [68] may be used depending on the system noise, number of the required analyzed and total cells, and purpose of the Force Index collection.

lation. To study Force Index modulations in time, raw Force Index values or averaged Force Index may be used.

Fig. 2.5 shows a three second sample of signals taken from the DEP cytometer. The meaningful signals are collected and used to calculate Force Index. Accepted signals are one of the signatures (nDEP, noDEP, pDEP) shown previously in Fig. 2.3. Any other signature would be rejected. Multiple cells flowing simultaneously above the detection electrodes and cells stuck together are examples of the rejected signals.

When DEP voltage is applied, flowing cell gets attracted (positive FI) or repelled (negative FI) from the set of electrodes. However when DEP voltage is not applied, cell passes both of the detection electrodes with the same height as it entered the channel. When DEP voltage is not applied, the force Index might have a slight discrepancy from expected zero value which might be a result of asymmetries in the electrodes. Also non-spherical cells have a more complicated motion in a flow since shear forces make them wobble and rotate as they are passing the electrodes. This can cause a slight difference in the height in which cell passes the first electrode compared to the second electrode. Another colleague Marija Nikolic-Jaric *et al.* (2011) has studied this effect previously [69].

Histograms are used to illustrate and compare Force Index values as cell physiological state varies. Since Force Index is an analogue value, transform of histograms from right hand side (positive) to left (negative) can be used as a monitoring means for physiological events in the cell causing a change in dielectric response. Fig. 2.6 shows a sample Force Index histograms for a CHO population with an initial viability of 95.9 % measured by DEP. After 5 days, viability dropped to 25.9 % and Force Index distribution has been changed as well. Furthermore, they illustrate the existence and distribution of sub-populations which is presented in the next chapter.

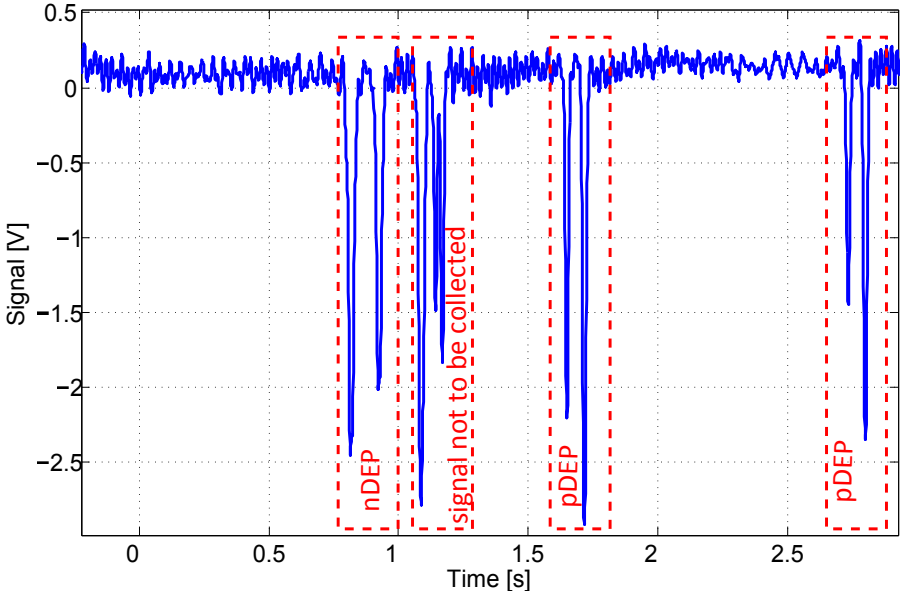


Fig. 2.5: Four second sample of the out put signal recorded by DAQ.

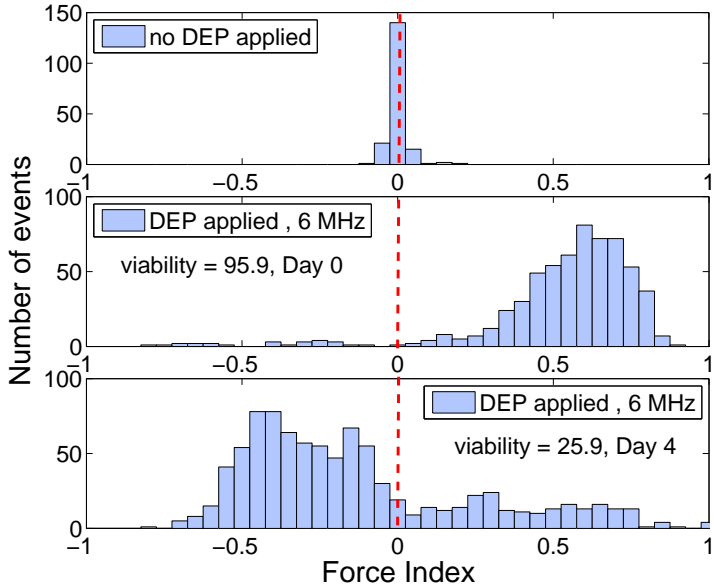


Fig. 2.6: Sample histogram from an experiment on CHO cells in a medium with conductivity of 0.17 S/m.

Beyond the Force Index

In this chapter, we study Force Index beyond a binary factor and viability. The K_{CM} spectrum of a viable and non-viable cell population are compared and the impact of the cytoplasm conductivity, mobility and Force Index are shown. Furthermore, we have tried to extract more information from FI histograms by fitting known statistical distributions and identify apoptotic sub-populations.

3.1 non-viable cell Force Index and conductivity

In Chapter 1, we presented several physiological events during apoptosis which impact the dielectric response of the cell. Monitoring the Force Index in time can be a means to track these events during apoptosis. As shown in Chapter 1 and Fig. 3.1 at 6MHz K_{CM} is dominated by cytoplasm conductivity and changing other parameters such as size and membrane properties would not impact DEP response significantly. Consequently, DEP force and Force Index are dominated by cytoplasm conductivity.

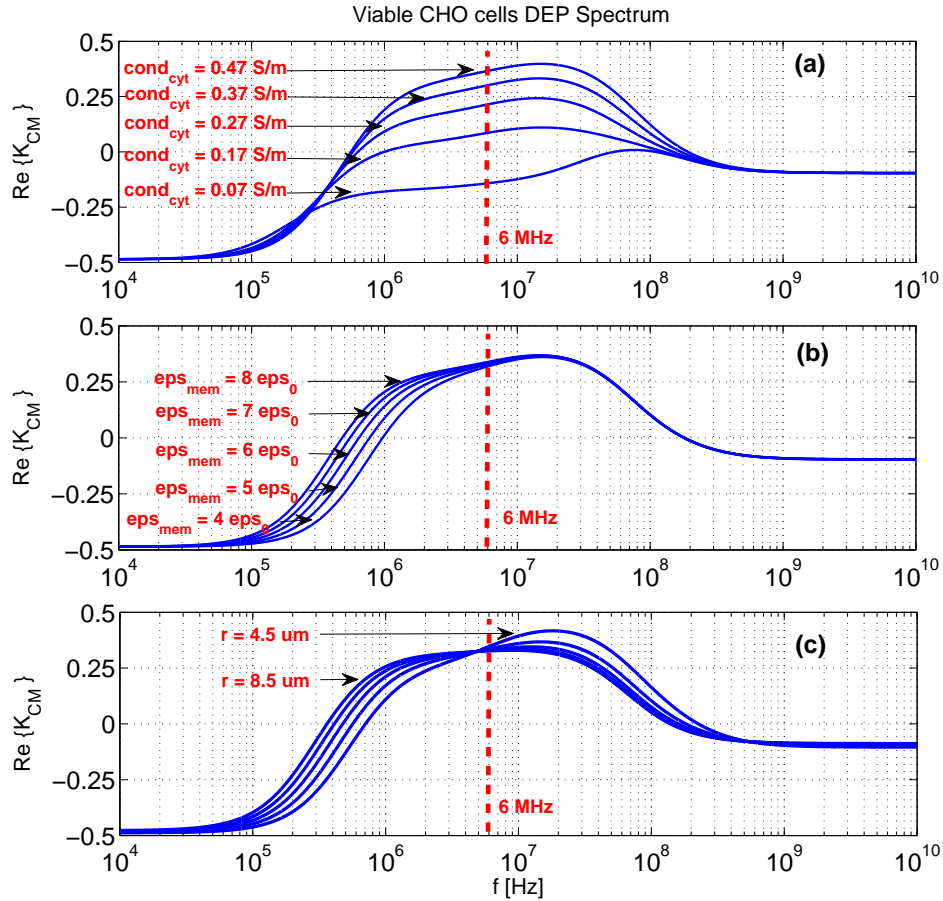


Fig. 3.1: Double shell model of K_{CM} for viable cell in a medium conductivity of 0.17 S/m. (a) cytoplasm conductivity is varying from 0.07-0.47 S/m, $\epsilon_{\text{mem}} = 6.8 \epsilon_0$ (b) ϵ_{mem} is varying from 4-8 ϵ_0 , cytoplasm conductivity= 0.42 S/m. (c) cell radius is varying from 4.5-8.5 μm . All other parameters are fixed as Fig. 1.4.

In Chapter 2, we defined viability as the number of pDEP cells to the total number of the cells with respect to the fact that non-viable cells have a negative K_{CM} , hence negative DEP signature (nDEP) and negative Force Index in a medium conductivity of 0.17 S/m. Here we show that the double shell model of K_{CM} at 6 MHz for a viable cell is positive with a larger cytoplasm conductivity than the medium conductivity. Interestingly, for a non-viable cell K_{CM} at 6 MHz only gets negative if the cytoplasm conductivity is decreased below the medium conductivity. In fact with perturbation in the active mechanisms such as pumps in the cell membrane during apoptosis, cytoplasm ion concentrations would drop but it would not drop to less than the medium ion concentrations. In an apoptotic cell, membrane pumps and channels do not function properly. Therefore, ion concentrations inside the cell approach their value in the medium and reach the equilibrium. But the mobility of ions in cytosol which is crowded by large molecules is lower than in the medium and hence effective conductivity would be less than the expected value.

Fig. 3.2 shows double shell simulation of the K_{CM} for a medium conductivity of 0.17 S/m, viable cytoplasm conductivity of 0.42 S/m, and different non-viable cytoplasm conductivities. The cytoplasm conductivity is a fraction of medium conductivity by a factor of 2 or 3 resulted from the reduced mobility in the cytosol. Detailed parameters are:

Viable cell parameters: cytoplasm conductivity=0.42 S/m, medium conductivity=0.17 S/m, viable cell radius = 5.5 μm . Other cell parameters are fixed as: nucleus radius=3.25 μm , membrane thickness=5 nm, nucleus envelope thickness= 40 nm, membrane permittivity= 6.8 ϵ_0 , cytoplasm permittivity= 60 ϵ_0 , nucleus envelope permittivity= 28 ϵ_0 , nucleus permittivity= 52 ϵ_0 , membrane conductivity= $3 * 10^{-3}$ S/m, nucleus envelope conductivity = $6 * 10^{-3}$ S/m, nucleus conductivity= 1.35 S/m [3, 4, 5]

Non-viable cell parameters: cytoplasm conductivity= 0.17 S/m and (1/2) * 0.17 and (1/3) * 0.17 S/m, medium conductivity=0.17 S/m, non-viable cell radius = 5 μm . Other cell parameters are fixed as: nucleus radius=3.25 μm , membrane thickness=4.25 nm, nu-

cleus envelope thickness= 40 nm, membrane permittivity= $6.8 \epsilon_0$, cytoplasm permittivity= $60 \epsilon_0$, nucleus envelope permittivity= $28 \epsilon_0$, nucleus permittivity= $52 \epsilon_0$, membrane conductivity= $15 * 10^{-3}$ S/m, nucleus envelope conductivity = $30 * 10^{-3}$ S/m, nucleus conductivity= cytoplasm conductivity [3, 4, 5].

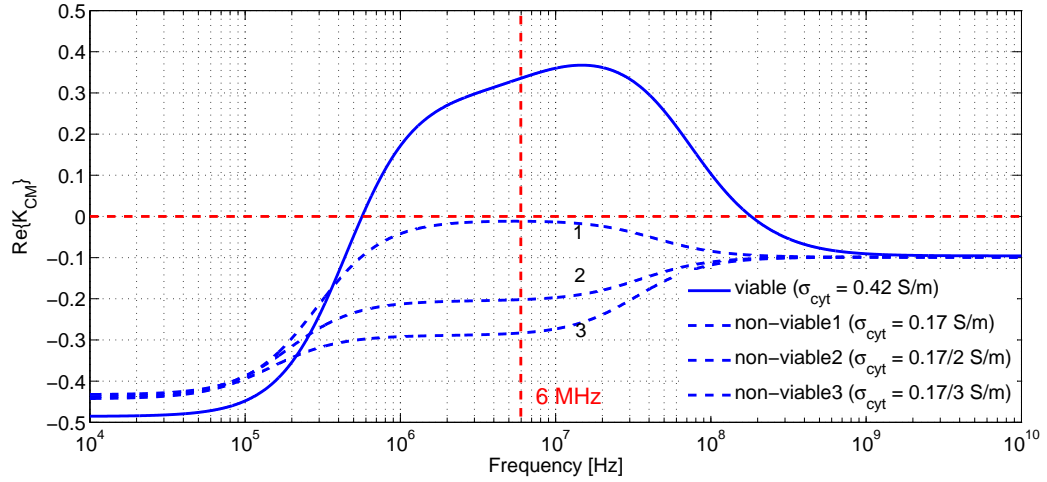


Fig. 3.2: K_{CM} Double shell model of K_{CM} for viable and non-viable cell, medium conductivity = 0.17 S/m, other parameters are set as defined in the text.

3.2 Force Index distribution during apoptosis

In this section, we study Force Index distribution during apoptosis by fitting known statistical distributions on a time course measurement of the DEP responses of CHO cells ¹. In this chapter we define Force Index with a factor of 2 which was eliminated in the next generation of data collection user interface programs.

$$\text{Force Index} = 2 * \frac{P_2 - P_1}{P_2 + P_1} \quad (3.1)$$

¹This set of experiment is performed by other colleagues on December 2011 and is published by Braasch *et al.* [70].

3.2.1 Cell preparation

Chinese Hamster Ovary (CHO) cells expressing a human llama chimeric antibody (EG2) were used for this work. Yves Durocher of the NRC, Canada kindly provided the cell line (CHODG44-EG2-hFc/clone 1A7) [71]. The cells were cultured in a 3 l glass bench-top bioreactor (Applikon, Foster City, CA) at 200 rpm in an incubator at ($37^{\circ}C$) with 40% CO_2 overlay. The cells were grown in BioGro-CHO serum-free medium (BioGro Technologies, Winnipeg, MB) supplemented with 0.5 g/L yeast extract (BD, Sparks, MD), 1 mM glutamine (Sigma, St. Louis, MO), and 4 mM GlutaMax I (Invitrogen, Grand Island, NY). This experiment has been done in five days with measurements every 24 hours for the first four days and every 6 hours for the last day.

3.2.2 Gaussian fit

In this section we have fitted Gaussian distributions to the Force Index histograms during apoptosis to identify sub-populations of Force Index and cytoplasm conductivity during various as a culture ages.

As shown in the histograms of figure 3.3, when cells undergo apoptosis stage Force Index decreases and Force Index histograms shift from positive side of the axes to negative values. Since K_{CM} is dominated by cytoplasm conductivity at 6 MHz, the decrease in the Force Index is evidence for a drop in the cytoplasm conductivity. This is in agreement with reported observations on cytoplasm conductivity during apoptosis [48]. Matlab² curve fitting tool has been used to fit different distributions to the histograms. The best distribution is seen by fitting Gaussian to the pDEP and nDEP populations separately. However, in some cases more than one Gaussian can be fitted to the data.

²Matlab R2012a, Curve fitting toolbox-Gaussian distribution-center and scale:off

Maximum possible number of Gaussian has been fitted to data with reasonable histogram bin width. The bin width has been changed several times to make sure the Gaussian curves fitted to data remains consistent. Furthermore, Gaussian curve fits has been repeated for 2/3 of the data chosen randomly to make sure that Gaussian curves remain consistent (number of Gaussians and mean value).

The Gaussian curve used is expressed by 3.2.

$$y = a * \exp(-((x - b)/c)^2) \quad (3.2)$$

where b is the mean Force Index and c is $\sqrt{2}$ times standard deviation.

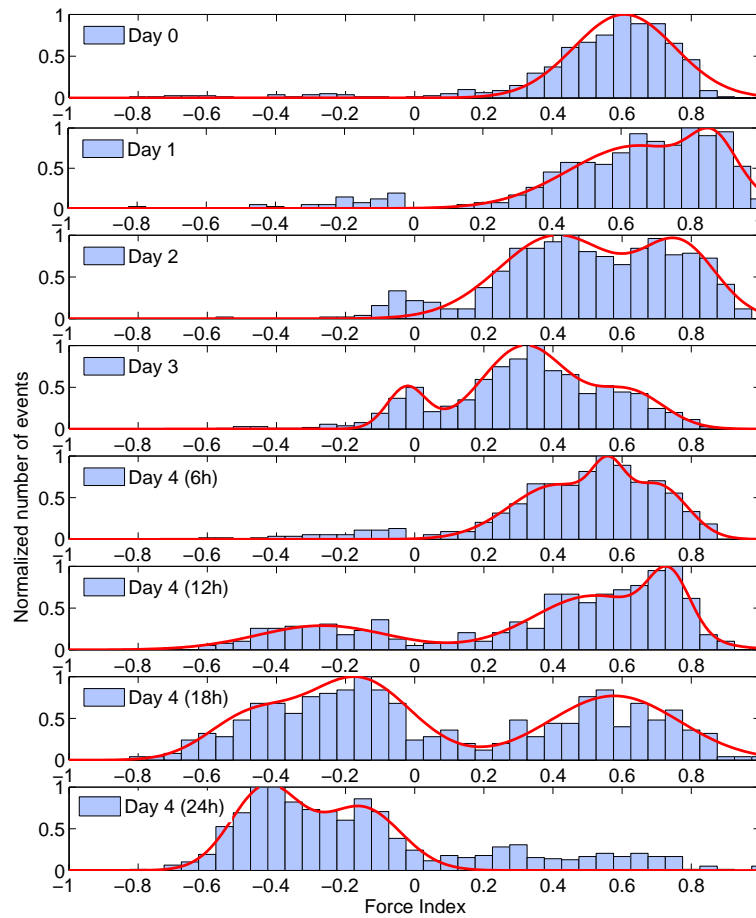


Fig. 3.3: Gaussian fit to the Force Index histograms. More than one population arises as cells go into the apoptotic stage.

It is clear from Fig. 3.3 that more than one population with positive Force Index exists as cells goes under apoptosis. On the other hand, when majority of the cells become apoptotic with negative Force Index, more than one population arises on the left hand side of the histogram (nDEP) as well.

The increase in the Force Index in the pre-apoptotic cells can be a potential means to predict apoptosis. This have an application in pharmaceutical productions and bioprocess monitoring in which there is a need to detect apoptosis before conventional late indicators.

We hypothesize that the extra higher Force Index populations may be due to a pre-apoptotic population which have a higher cytoplasm conductivity. Labeed *et al.* (2006) reported a rise in cytoplasm conductivity previously for pre-apoptotic cells undergoing apoptosis by Staurosporine [48].

DEP response to MRC5 cells

Different cell lines have distinct dielectric properties and hence DEP response. In this chapter, we estimate the cross over frequency of K_{CM} experimentally by a frequency spectrum for non-starved cells as well as five day starved MRC5 cells. Having the experimental cross over frequency, the double shell model parameters has been optimized to match the simulated and experimental cross over frequency and hence dielectric parameters for MRC5 cells has been estimated. Furthermore, K_{CM} for MRC5 cells has been speculated from the mean Force Index spectrum by a linear scale of mean Force Index to K_{CM} and disagreements are explained. Size and velocity impact on the scaled Force Index has been presented as well.

MRC5 cells are fibroblast cell line obtained from lung tissue of human fetus. This cell line has been grown in laboratories for more than 35 years and particularly are of interest for vaccine production. Since viruses cannot reproduce solely, they need a cell culture as a host. Human cell cultures are proven to be a safe host for vaccine production. MRC5 cell line is one of the a few options of human cell line for vaccine production since cells obtained from animals might carry viruses which are harmful for human.

For our experiments cells were cultured in shaker flask and compared to Chinese hamster ovary cells were elongated with average diameter of $\approx 13.5 \mu\text{m}$. All experiment were performed with a medium conductivity of 0.17 S/m.

4.1 DEP response to Non-starved MRC5 cells

4.1.1 Viability and Force Index

The frequency spectrum has been done starting from 50 KHz, increasing to 20 MHz. Two measurements at 6 MHz has been done as well. One at the beginning and one at the end of the experiment (5 hours long) to compare viability. At each frequency about 500 cells have been analyzed. As before the DEP cytometer, viability is calculated by dividing the number of pDEP cells to total number of the cells analyzed at 6 MHz. Percentage viability reported in Table 4.1 by DEP cytometer is the average value of beginning (78.96 %) and the end (82.46 %) of experiment which are in agreement with Nexin assay. Previously it has been shown that Nexin is the best viability match with DEP cytometer for Chinese hamster ovary cells [12]. As shown in Fig. 4.1, in the second measurement at 6 MHz (after 5 hours) another population with higher Force Index arises in the histograms which we hypothesize for cells experiencing pre-apoptotic stage. However, viability is not affected significantly. Comparing Cedex and Nexin results reported in Table 4.1, DEP measurements of viability is close to Nexin results. Cedex viability assay is based on penetration of Trypan blue dye via membrane into cytoplasm. Since cell membrane should get perforated and exposed to dye in order to be excluded by this assay, Trypan blue is a late apoptosis indicator. However, Nexin is sensitive to Phosphatidylserines (PS) molecules exposed to the outer surface of the membrane which is an early indicator of apoptosis. Therefore, DEP cytometer can be a means of indicating apoptosis in early stages for MRC5 cells as well as previously observed in CHO cells.

The cross over frequency is defined as the frequency where K_{CM} is zero resulting in zero Force Index. As shown in Fig. 4.2, cross over frequency takes place between 300 KHz and 400 KHz (close to 400 KHz).

As we expect from the frequency dependent behavior of K_{CM} , distribution of the Force Index histogram changes by changing the applied DEP frequency presented in Fig. 4.3.

Tab. 4.1: Percentage viability measured by different assays

Assay	DEP	Nexin	Viacount	Cedex
Percentage viability	80.7	81.3	86.46	93.5

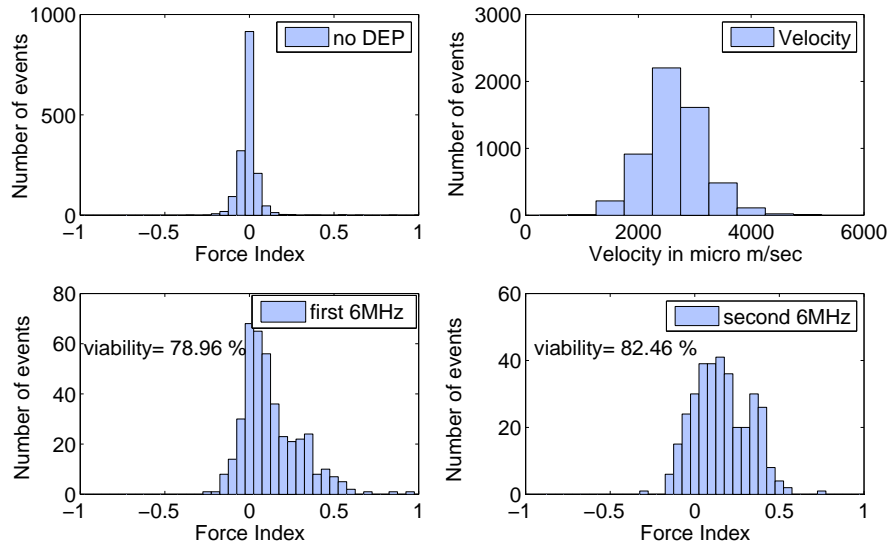


Fig. 4.1: Histograms of no-DEP applied and velocity for the whole course of experiment and 6 MHz measurements at the beginning and end of the experiment.

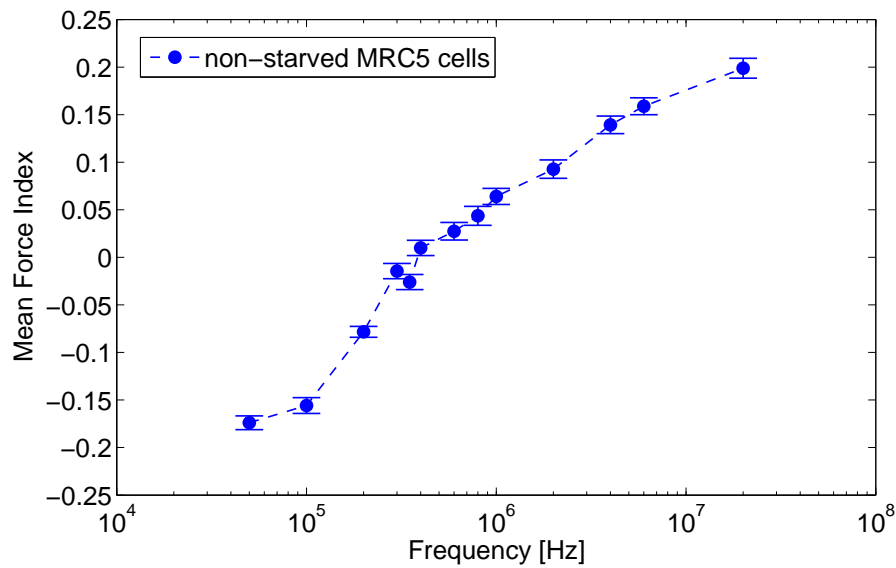


Fig. 4.2: Mean Force Index of the experiments performed by DEP voltage applied at different frequencies. Error bar are calculated from standard error of the mean.

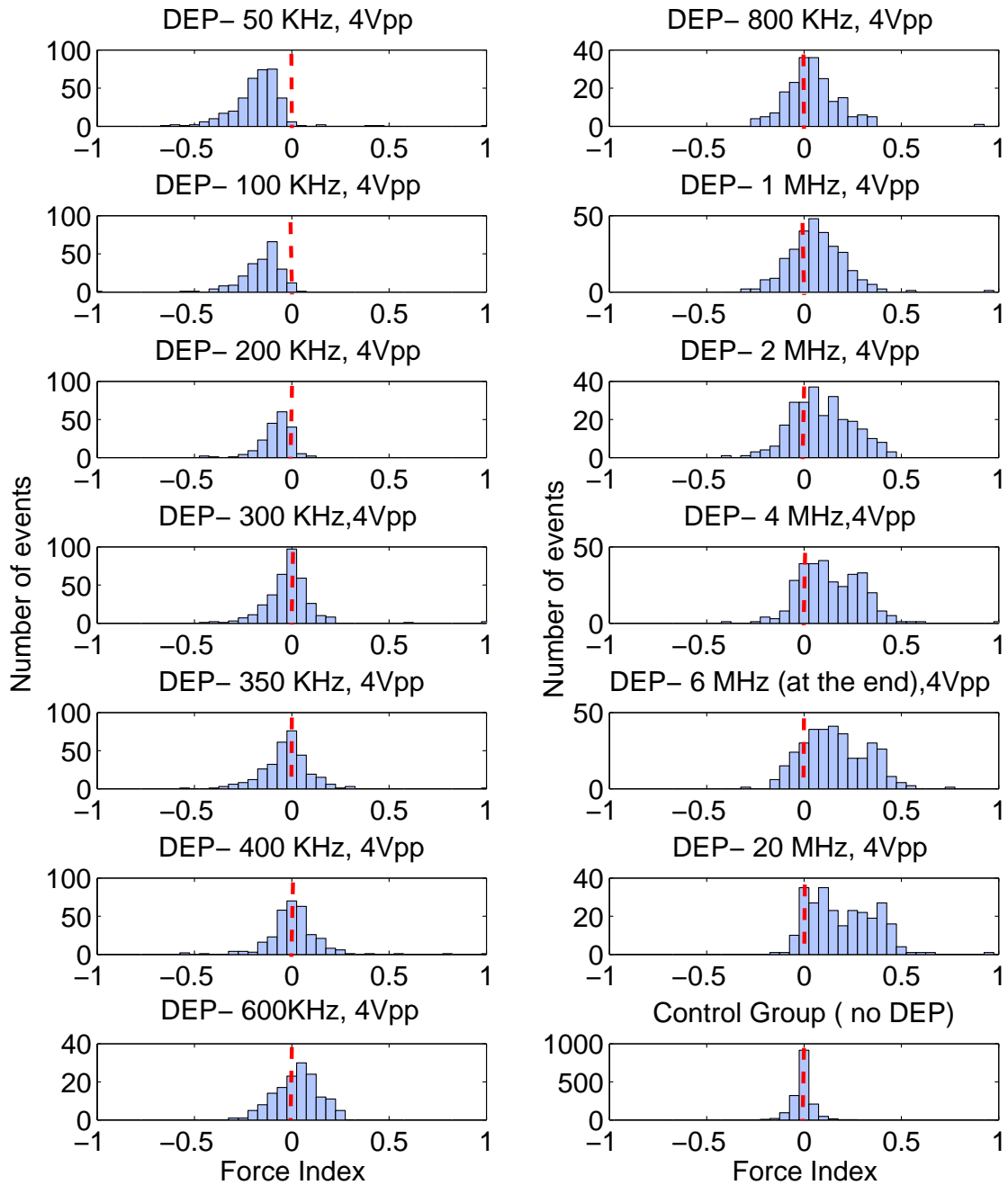


Fig. 4.3: Distribution of Force Index histograms in different frequencies of the applied DEP voltage.

4.1.2 Estimating cell parameters by K_{CM}

To our knowledge, no measurements on MRC5 cells dielectric properties has been presented in the literature to date except for membrane capacitance of $11.5 \text{ mF}/\text{m}^2$ by Muratore *et al.* (2012). They have employed DEP to differentiate Myoblasts from MRC5 cells [72]. They have used cross over frequency of 500 KHz to separate different cell populations co-cultured with MRC5 cells in a medium with conductivity of 0.12 S/m. However, other dielectric properties have not been estimated for this cell line.

Membrane capacitance can be estimated by the cross over frequency from Equation 4.1 as follows [72]:

$$f_{co} = \frac{\sqrt{2}\sigma_m}{2\pi r C_m} \quad (4.1)$$

where, f_{co} is the cross over frequency, σ_m is the medium conductivity, r is the cell radius, and C_m is the membrane capacitance. Substituting our values with the cross over frequency of 350 KHz in the equation results in the membrane capacitance of $16.2 \text{ mF}/\text{m}^2$ which is in agreement with $11.5 \text{ mF}/\text{m}^2$ that Muratore *et al.* have reported for MRC5 cells.

To estimated MRC5 dielectric properties, the double shell model parameters have been optimized to match the cross over frequency obtained experimentally by Force Index spectrum (presented in the previous section) to the simulated cross over frequency calculated by double shell model. Unconstrained Nelder-Mead simplex direct search has been used as the optimization algorithm by Matlab.

After 144 iteration the optimized cross over frequency of $350 \text{ KHz} \pm 54 \text{ Hz}$ was achieved with the parameters reported in Table 4.2. In optimization, medium dielectric properties and cell radius were fixed as well as membrane permittivity. In fact, we can account for the impact of membrane permittivity in membrane capacitance solely by changing membrane thickness.

To achieve membrane capacitance of $16.2 \text{ mF}/\text{m}^2$, the membrane relative permittivity was fixed at 4.9. Cell radius was fixed at: $6.75 \text{ }\mu\text{m}$, medium conductivity: 0.17 S/m , and medium relative permittivity: 78. CHO dielectric parameters have been used as the starting point for the optimization.

The optimization has been done with constrained variables as well¹. The problem does not converge for membrane thicknesses of less than 3. Dependency on the initial guess was studied by changing the initial values. Solution is highly dependent on the membrane thickness and it is fairly independent of other parameters.

The real part of K_{CM} spectrum at the cross over frequency is dominated by the membrane dielectric parameters. Therefore, estimating other dielectric parameters solely by cross over frequency would not be possible.

Tab. 4.2: Estimated dielectric properties of MRC5 cell

Parameter	Optimized
'Membrane Thickness [nm]	2.7
'Nuclear membrane Thickness [nm]	46.4
'Cytoplasm Conductivity [S/m]	0.34
'Membrane Conductivity [S/m]	3.2E-07
'Nucleus Conductivity [S/m]	1.4
'Nuclear Membrane Conductivity [S/m]	6.7E-06
'Cytoplasm Relative Permittivity	65
'Nucleus Relative Permittivity	50.7
'Nuclear Membrane Relative Permittivity	4.7
'Nuclear Radius/Total Cell Radius	0.1

¹Matlab function used: `fminsearchbnd`, available online. Copyright (c) 2006, John D'Errico

4.1.3 Fitting Force Index spectrum to K_{CM}

Here we scale the experimental mean Force Index to the simulated K_{CM} spectrum using double shell model and optimized parameters is Table 4.2. A linear scale at low frequencies has been used since the non-uniformity of the electric field can be ignored in negative DEP. As compared in Fig. 4.4, linear scale of mean Force Index shows significant disagreement with simulated K_{CM} at high frequencies. The 20 MHz data would not be valid. The cable resistance and capacitance in high frequencies would decrease the $4v_{p-p}$ applied voltage. Therefore, the DEP voltage at 20 MHz was less than the value set on $4v_{p-p}$

The impact of size and velocity alteration during 5 hours course of measurement has been speculated to explain this disagreement. The change in size and velocity are presented in Figures 4.5 and 4.6. As cell diameter gets larger, lift force increases and cells tend to travel closer to the center line of the channel. However F_{DEP} is proportional to the third power of radius. Therefore, for smaller cells first peak would be smaller as well. First peak magnitude may vary between 0 to 20 volts. Averaged P_1 values presented in Fig. 4.5 would not be an evidence for a significant change in size. Furthermore, its unlikely to remain sensitive to the small variations in size due to apoptosis by averaging the first peak. Scatter plots of first peak versus Force Index can be more informative.

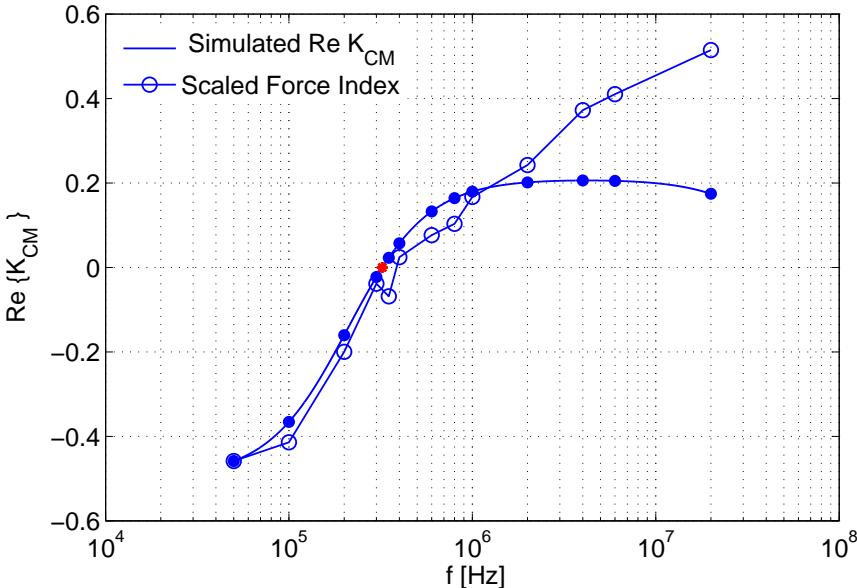


Fig. 4.4: Scaled FI to simulated K_{CM} by double shell model using optimized parameters for MRC5 cells

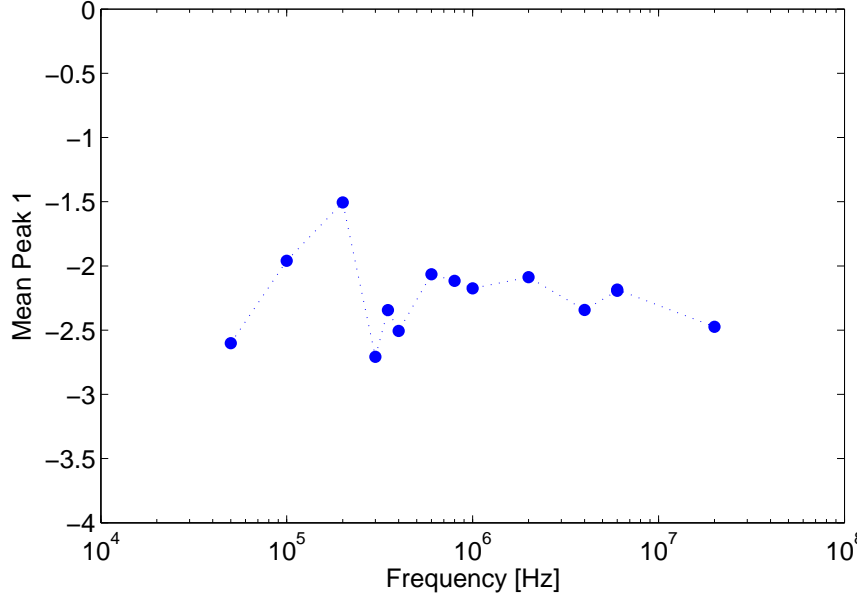


Fig. 4.5: Averaged first peak magnitude for the course of experiment.

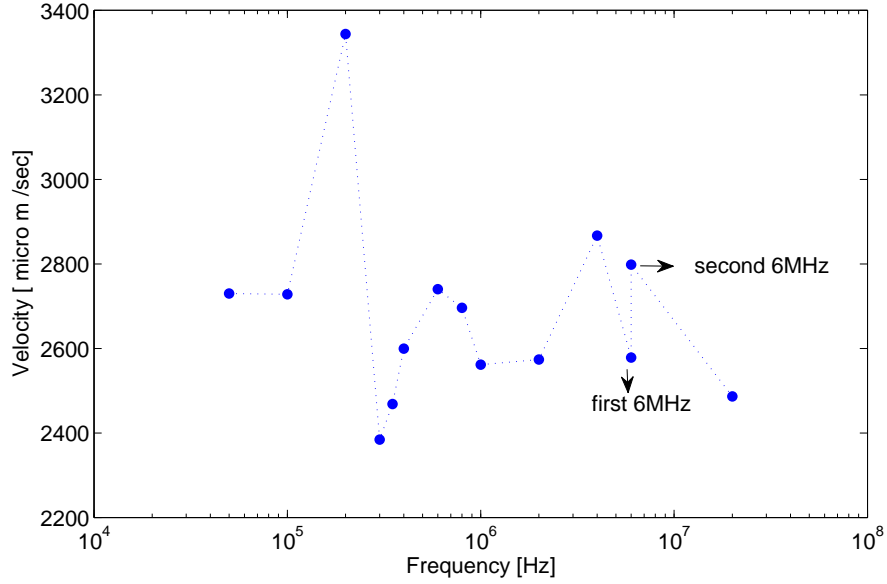


Fig. 4.6: Averaged cell velocity calculated by two peaks.

4.1.4 Force Index correction by particle velocity

Ignoring electric field non-uniformity, size and height variations and by a first order linearization of DEP force and height in the channel we have estimated that particle vertical displacement in the channel is related to velocity as $\Delta z \propto \frac{1}{\text{particle velocity}}$. This results in another rough estimate of Force Index relation to velocity as $FI \propto \frac{1}{\text{particle velocity}}$. Force Index for each single cell has been corrected by its velocity and has been averaged and compared to the original mean Force Index shown in Figure 4.7. Particle Velocity is calculated by dividing the distance between two high density electric field region of detection (210 μm) to the time needed for a cell to travel from first peak to the second peak. 4.7. The corrected mean Force Index and original raw Force Index are not significantly different which is an evident for the nonlinearities and also ignoring cell by cell variations in a population such as size and height entering the channel. Furthermore, the approach used for calculating velocity may not be accurate. When DEP is applied, cell would be attracted or repelled from

the electrodes so it would not travel at the same height as entering the channel. The correct approach through Force Index correction can be obtained by quantifying Force Index versus height, size and velocity by COMSOL simulations [62].

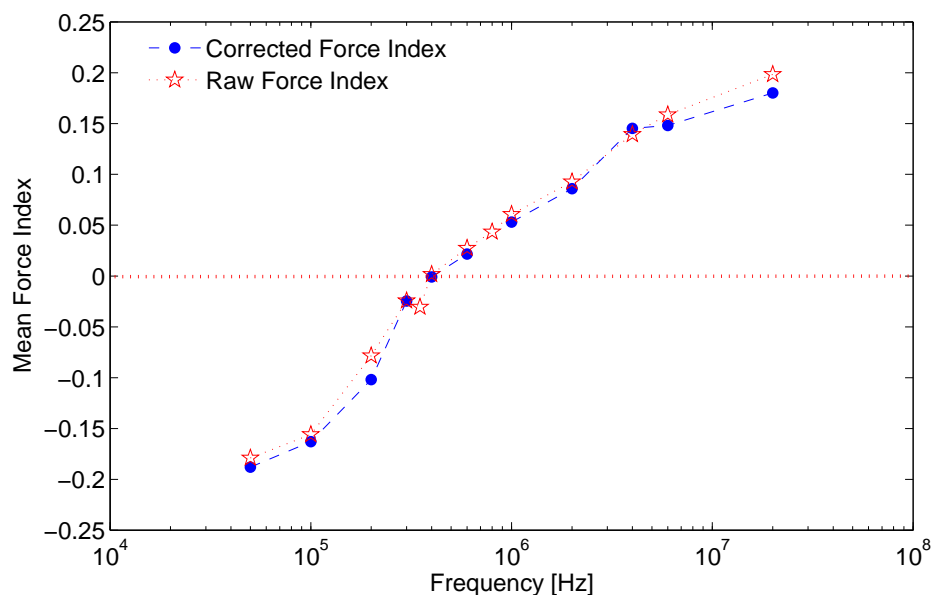


Fig. 4.7: Mean Force Index, FI has been corrected for each cell by velocity.

4.2 DEP response to 5 day starved MRC5 cells

In this section we present the DEP response to MRC5 cells which were starved for 5 days. The expected viability would be less than the healthy nourished culture. At the beginning of the experiment, viability was 91.7 % measured by Trypan Blue assay. The same procedure for Force Index spectrum has been performed here; starting at 50 KHz and finishing with 20 MHz with two 6 MHz measurements at the beginning and at the end. As shown in Fig. 4.8, percentage viability after 5 hours course of experiment (67.7%) is higher than beginning (58.6%). This may be due to higher conductivity of cytoplasm in pre-apoptotic cells.

The cross over frequency for starved cells is higher than non-starved cells, about 1MHz for

starved cells and 400 KHz for non-starved cells obtained from zero crossing of mean Force Index spectrum presented in Fig. 4.9. The Force Index histograms for these cells are shown in Fig. 4.11.

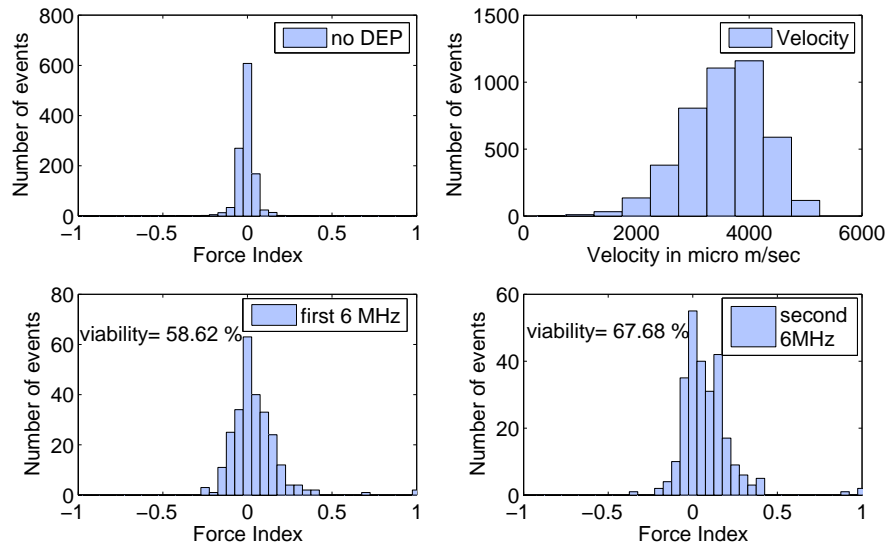


Fig. 4.8: Histograms of no-DEP applied and velocity for the whole course of experiment and 6 MHz measurements at the beginning and end of the experiment.

The increase in the cross over frequency for the starved cells compared to non-starved cells may be due to a decrease in the membrane capacitance for the starved cells. This hypothesis is inferred from the equation for the cross over frequency and the membrane capacitance as explained by Muratore *et al.* (2012) [72].

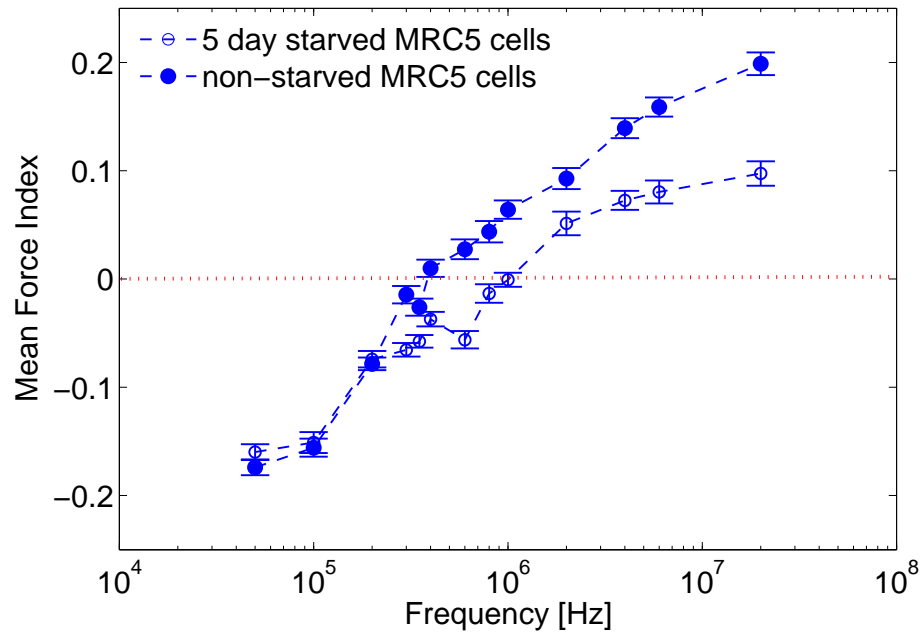


Fig. 4.9: Mean Force Index of starved MRC5 cells compared to non-starved cells.

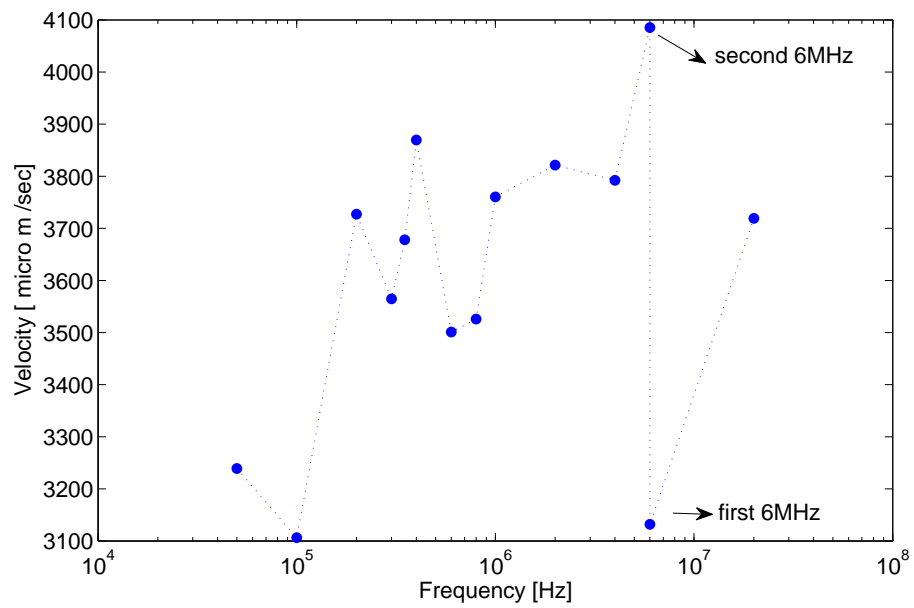


Fig. 4.10: Averaged cell velocity calculated by two peaks.

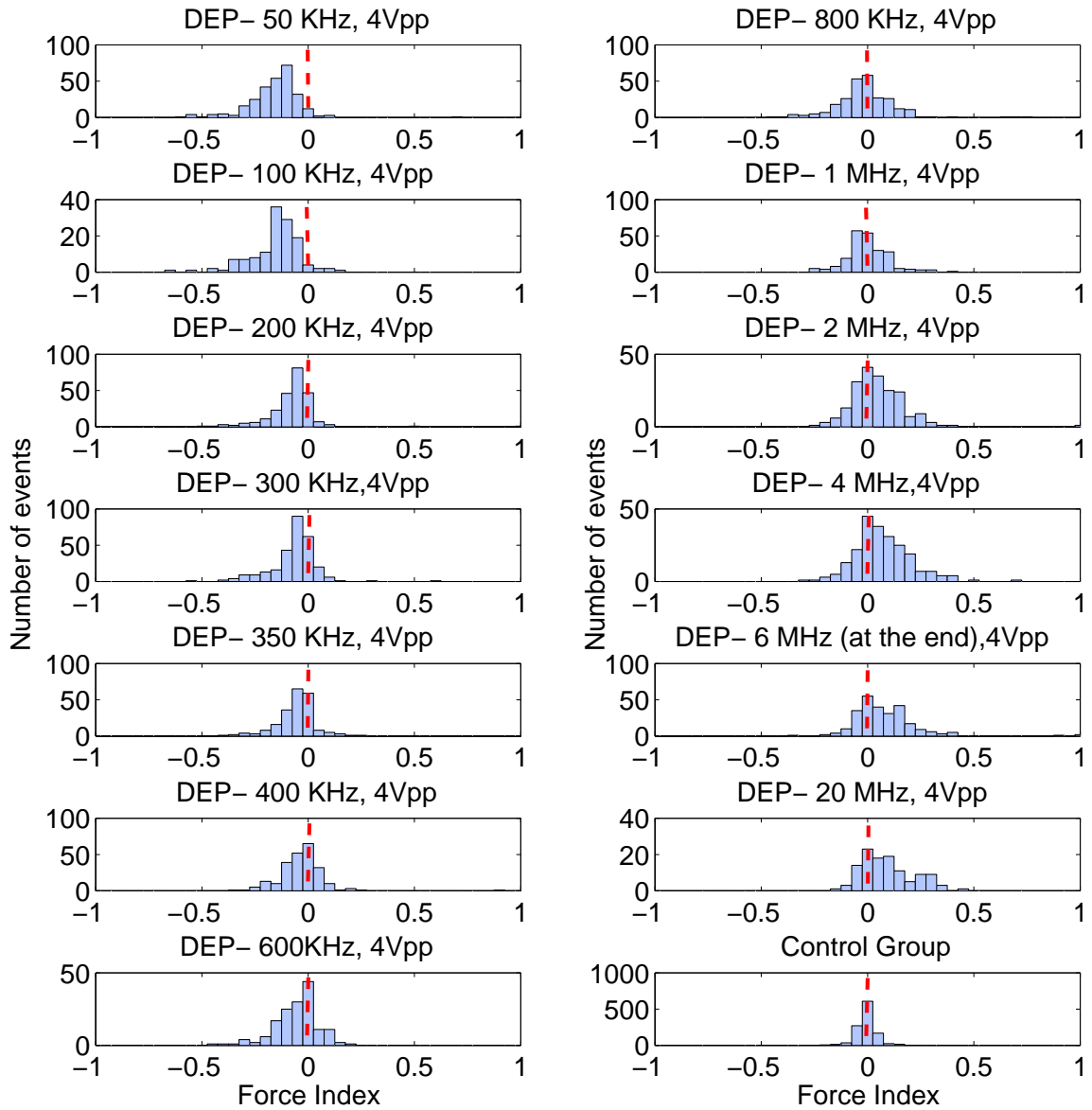


Fig. 4.11: Force Index histogram distribution in different applied DEP voltage frequency.

DEP response to mitochondrial ATP inhibition

As reviewed in Chapter 1, the DEP of cells is influenced by many factors such as membrane capacitance, cytoplasm conductivity and cytoplasm permittivity. Unlike most other dielectric materials, cells adapt to environmental conditions using host of active systems. Some of these active systems have significant impact on the dielectric properties of the cell. For example, the metabolic state is an important factor in controlling ion homeostasis and hence cytoplasm conductivity. Determining the dielectric effects due to perturbations of cell homeostasis is important for many applications of DEP such as separating, sorting and cell manipulation.

In this chapter, we review cell metabolism and its impact on the dielectric response, and we present the DEP response to a perturbation in one of the energy pathways within the cell. We have used Oligomycin to inhibit the mitochondrial ATP production. The DEP response is studied and compared to the mathematical models of cell homeostasis.

5.1 ATP: energy currency of the cell

ATP is the most common form of energy used to drive cellular processes. All organisms use ATP as a means of energy currency. ATP provides its energy by converting to a simpler molecule, ADP which later on is recycled back to ATP via one of the energy conversion pathways within the cell. One of the main uses of ATP in mammalian cells is powering the Na^+/K^+ ATPase pumps used to maintain cell homeostasis. These pumps play a significant role in maintaining ion concentrations in cytoplasm and hence cytoplasm conductivity.

Two major ATP production pathways within the cell are *Glycolysis* within the cytosol (2 ATP per glucose) and *electron transport chain* (34 ATP per glucose) via mitochondria (ETC) [73].

When a cell uptakes glucose from the medium, it is converted to Pyruvate in the cytoplasm by the Glycolysis pathway. Pyruvate molecules can either stay in the cytoplasm or go into the mitochondria electron transport chain. The Pyruvate that has not gone into ETC can be converted into lactate in the cytoplasm by fermentation and diffuses out of the cell. It is crucial to control lactate accumulation in a culture since it increases acidification [74]. Quantifying the dielectric effects of mitochondrial versus Glycolysis ATP production of a cell has application in monitoring bioprocesses especially in biotherapeutic production and in determining the advance of cancer in cells.

5.2 Oligomycin and ATP

Some compounds can be used to control specific aspects of energy production in the cell. Oligomycin is known to inhibit the ATP synthase enzyme and block the proton channel in the mitochondria transmembrane within minutes of treatment [75, 76, 77]. Consequently, the only channel to pump protons inside the mitochondria will be blocked and electron transport will no longer take place. Therefore, Oligomycin inhibits the ATP production pathway through electron transport chain in mitochondria.

Furthermore, Oligomycin is an ATPase enzyme inhibitor. However, it would not result in complete inhibition of the enzyme [78]. Inhibition of the ATPase enzyme results in blockage of ATPase channels in the cytoplasm membrane. These pumps transfer 2 K^+ ions inside and 3 Na^+ ions outside the cell at the expense of one ATP molecule to maintain normal homeostasis as shown in Fig. 5.1 Blocking Na^+/K^+ ATPase pumps impacts the ion concentration inside the cytoplasm and hence cytoplasm conductivity. In this chapter, we have presented the DEP response of the cell following exposure to Oligomycin and we show how cytoplasm conductivity would be affected.

Exposure to Oligomycin will also trigger apoptosis. Decrease of the mitochondria transmembrane potential resulting from lack of ATP to power up channels can initiate permeabilisation of the mitochondrial membrane (MOMP) and *Cytochrome C* release which can trigger apoptosis. TMRE and TMRM assays are normally used for monitoring transmembrane potential and MOMP [79]. Two factors important in apoptosis are Oxygen consumption rate (OCR) and extra cellular acidification (ECAR). Decreased OCR and increased ECAR has been reported following exposure to Oligomycin as well [76]. Abe *et al.* (2010) reported OCR decreased to 40% and ECAR increased to 5 mPH/min in a podocyte cell line after exposure to Oligomycin 1 μ M. Watabe *et al.* (2007) reported apoptosis up to 50% in SH-SY5Y cells with Oligomycin 25 μ M identified by Nexin assay. However, PI assay did not

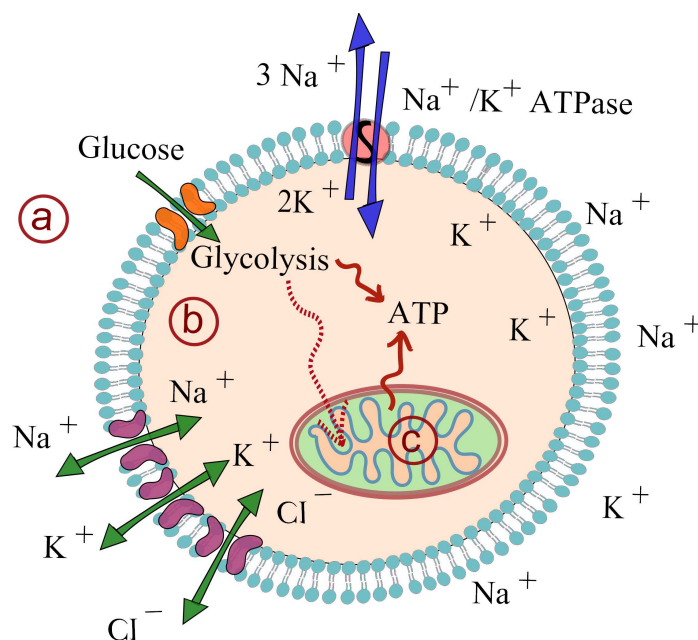


Fig. 5.1: a) medium b) cytoplasm: Glycolysis takes place in cytoplasm. Pyruvate produced in this process can either go into the Glycolysis pathway to produce ATP or into the mitochondria electron transport chain. c) mitochondria produces ATP by electron transport chain. Oligomycin inhibits electron transport chain by blocking proton channels in mitochondria membrane.

detected apoptotic population. In their study, a set of experiments are conducted to clear the fact whether Oligomycin induces apoptosis [80]. Legmann *et al.* (2012) presented decreased OCR and increased ECAR after 10 minutes of treatment by Oligomycin measured by a SeaHorse device [81].

Decrease of ATP levels within the cell by Oligomycin depends critically on factors such as Oligomycin concentration, culture age, and cell line. Sonya *et al.* (1996) reported 69% decrease in ATP concentration in astroglial rat cells after 2 minutes of incubation with Oligomycin 10 $\mu\text{g}/\text{ml}$. Abe *et al.* (2010) reported ATP levels decreased to 60% in a podocyte cell line with Oligomycin 1 μM [82]. Watabe *et al.* reported $\approx 50\%$ decrease in cell ATP levels compared to control after treatment with Oligomycin 25 μM [80]. Jhun *et al.* (2013) reported ATP decrease to $\approx 10\%$ of the control after only 10 minutes of treatment with Oligomycin 10 μM in Insulinoma cell line. ATP levels were relatively constant after 20 more minutes of treatment [75].

5.3 Oligomycin and ions

Since Oligomycin blocks ATPase enzymes, membrane currents and ion concentrations within the cell are expected to be altered after treatment. Oligomycin inhibits ATPase pump activity by decreasing ATP levels. There are other drugs such as Ouabain which directly block these pumps. It has been reported in the literature that adequate concentrations of Oligomycin has the same effect as Ouabain in terms of ATPase activity. Whittam *et al.* (1964) showed that 20 $\mu\text{g/ml}$ Oligomycin results in the same level of ATPase inhibition as 0.1 mM Ouabain [83].

Bricker *et al.* (1966) reported that Oligomycin decreases efflux of Na^+ [84]. Ding *et al.* (2011) have studied Oligomycin impact on membrane currents in the absence of medium K^+ . As mentioned before, ATPase pumps exchange 3Na^+ and 2K^+ at the expense of one ATP molecule. In the absence of K^+ , ATPase pumps are still able to maintain the membrane potential [85]. Cho *et al.* presented increased influx of Ca^{2+} in Jurkat T-cells with different Oligomycin concentrations [77].

In summary, we expect that after treatment with Oligomycin the ATPase pumps would be inhibited. Therefore, K^+ is no longer pumped in and Na^+ would no longer get out at the same rate as before. This will increase internal sodium ion concentration and decrease potassium ion concentration which both impact cytoplasmic conductivity. Monitoring the dielectric response of the cells in time can be a means for monitoring cytoplasmic conductivity, ion concentrations and study metabolic status of the cell.

5.4 Cell preparation and experiment procedure

Chinese Hamster Ovary (CHO) cells expressing a human llama chimeric antibody (EG2) were used for this work. Yves Durocher of the NRC, Canada kindly provided the cell line (CHODG44-EG2-hFc/clone 1A7) [71]. The cells were cultured in 250 mL baffled shaker flasks (VWR International, Radnor, PA) at 120 rpm in an incubator at (37°C) with 10% CO_2 overlay. The cells were grown in BioGro-CHO serum-free medium (BioGro Technologies, Winnipeg, MB) supplemented with 0.5 g/L yeast extract (BD, Sparks, MD), 1 mM glutamine (Sigma, St. Louis, MO), and 4 mM GlutaMax I (Invitrogen, Grand Island, NY).

For the DEP cytometer measurement a sample was taken from the shaker and centrifuged at 377 g for 1 min. After the supernatant was removed the cell pellet was reconstituted in fresh growth medium (37°C and ≈ 1.43 S/m) and low conductivity (≈ 0.067 S/m) medium (37°C) [22.9 mM sucrose (Sigma), 16 mM glucose (Fisher), 1mM CaCl_2 (Fisher), 16mM Na_2HPO_4 (Fisher)] using a ratio of 1:15 (fresh: low conductivity medium) diluting the cell sample to $\approx 2 * 10^5$ cells/mL and until reaching a conductivity of 0.17 S/m as measured by a conductivity meter (Orion 3-Star Plus, Thermo Scientific, Waltham, MA). For the set of experiments with the conductivity of 0.42 S/m, a ratio of 6:17 is used. The Oligomycin treated sample was prepared by adding Oligomycin (Sigma), reconstituted in dimethyl sulfoxide (DMSO), at the desired concentration to the diluted sample. Control samples were prepared by adding the same volume of DMSO without oligomycin to the sample.

Experiments are done in two sets. The first set is performed in a medium with conductivity of 0.17 S/m. Oligomycin concentration used is varied between 0.5, 1, and 2 $\mu\text{g}/\text{ml}$. The results were affected by many undesirable factors such as velocity and size. Therefore, we optimized the DEP cytometer to reduce unwanted effects and came up with the second set of experiments which are done in a medium conductivity of 0.42 S/m. The DEP response (Force Index) is monitored immediately after exposure to the drug.

5.5 Results with medium conductivity of 0.17 S/m

This set of experiments are performed in medium conductivity of 0.17 S/m. Samples are mixed at the beginning of the experiment using a Vortex mixer. Force Index is monitored immediately after exposure to DMSO and/or Oligomycin. It takes about one minute to get the cells from the vial to the volume of analysis in the microfluidic channel. The sample is mixed and purged every 10 minutes to prevent clogging and sedimentation of the cells. Here we present the results of five of these experiments.

The resonance frequency is set to ≈ 1.45 GHz, velocity is adjusted such that the time between peak 1 and peak 2 is 80-90 msec, the average cell diameter is ≈ 12.5 μm , and viabilities are reported at the end of this section. All data collections are performed by *Semi-automated GUI* with window size of 90 msec. The DEP response is obtained by applying a $4V_{P-P}$ sinusoidal voltage to the DEP electrode at 6MHz.

Force Index used in this set is calculated by 5.1:

$$\text{Force Index} = 2 * \frac{P_2 - P_1}{P_2 + P_1} \quad (5.1)$$

In the mean Force Index plots as a function of time, each point is an average of Force Index of cells analyzed in 2 minutes. The purple line is the average of Force Index of the control sample (no Oligomycin added) during the course of measurement. Histograms are plotted with 0.05 width size bins for both the control and the treated sample.

Experiment 1 [19/06/2013]:

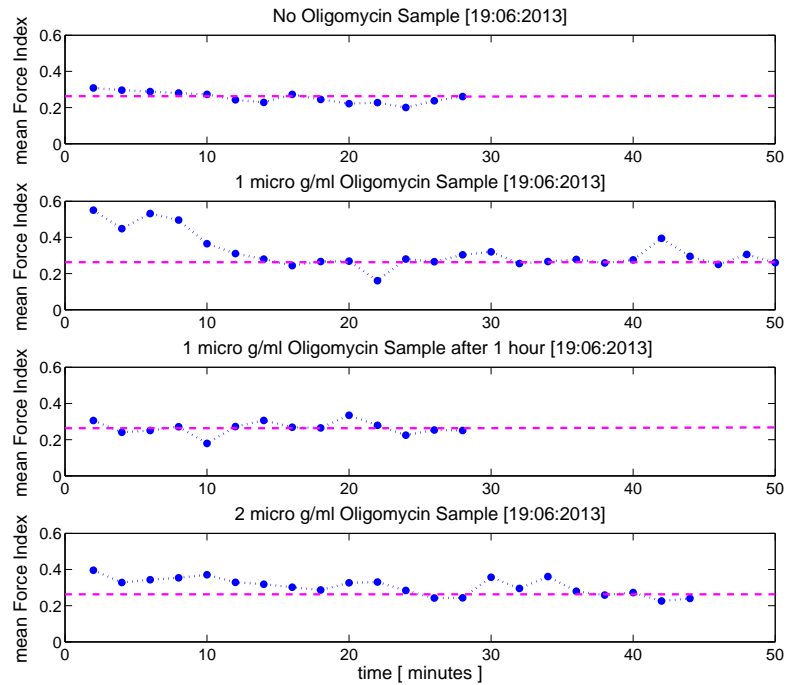


Fig. 5.2: Force Index monitored in time. Purple dashed line represents overall mean FI for the control sample.

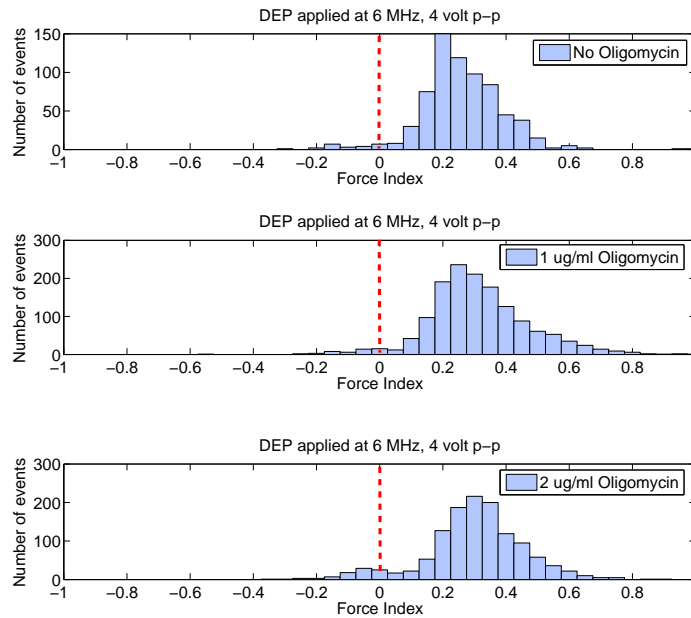


Fig. 5.3: Force Index histograms of control and treated samples.

This experiment was performed to compare different Oligomycin concentrations. As shown in Fig. 5.2, the Force Index of the control sample (no Oligomycin added) is stable around the average. However, Force Index of the treated sample with 1 $\mu\text{g/ml}$ Oligomycin experiences a rise in the first 10 minutes and drops to the control mean Force Index. The sample treated with 1 $\mu\text{g/ml}$ Oligomycin was kept warm for 1 hour and analyzed again. The second measurement after one hour did not show any significant changes in the mean Force Index. Force Index of the sample treated with 2 $\mu\text{g/ml}$ Oligomycin experiences a rise as well but drops faster to the control mean Force Index since the concentration is higher. We hypothesized that the first ten minutes rise was a result of accumulation of protons in the cytoplasm following exposure to Oligomycin. As mentioned before, Oligomycin is the proton pump blocker in the mitochondria membrane. Blocking this pump inhibits protons from returning into the mitochondria in the electron transport chain and they accumulate outside the mitochondria. This hypothesis was rejected after studying the change in pH and ECAR after exposure to Oligomycin. The change in pH would not result in enough H^+ concentration to directly change the conductivity, however, protons scatter very fast.

Histograms of Fig. 5.3 show the change in the Force Index distribution every 10 minutes following exposure to Oligomycin 1 $\mu\text{g/ml}$ and 2 $\mu\text{g/ml}$. As presented in Fig. 5.4, for the 1 $\mu\text{g/ml}$ sample the first rise in the Force Index lingers about 10 minutes, however, it disappears fast in the 2 $\mu\text{g/ml}$ sample histograms. Furthermore, a negative Force Index population arises within the first 10 minutes in the 2 $\mu\text{g/ml}$ Oligomycin sample which indicates the cell going into the apoptotic stage.

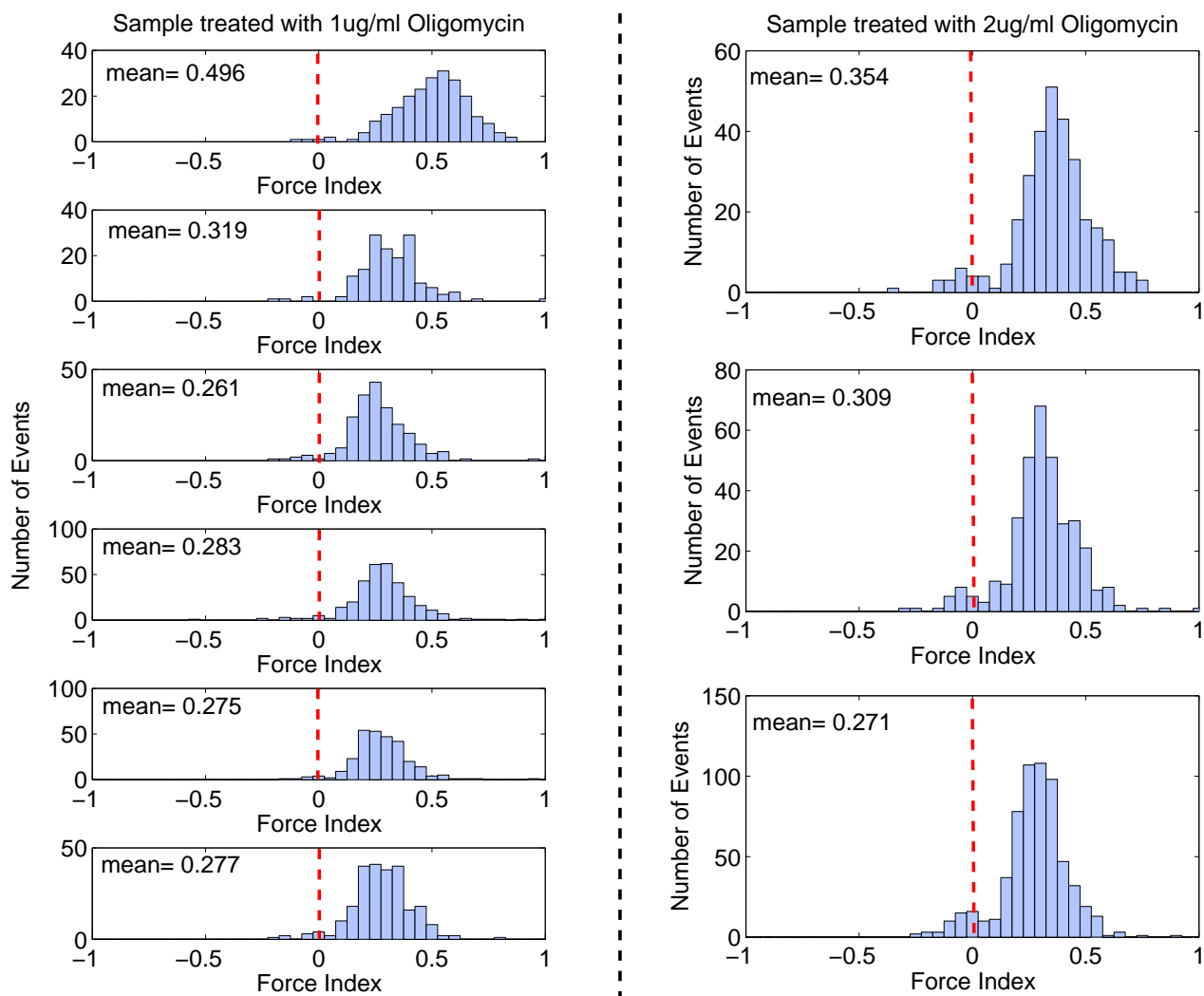


Fig. 5.4: 10 minute histograms of Force Index for different concentrations.

Experiment 2 [16/09/2013]:

In this experiment we studied lower concentrations of Oligomycin.

As presented in Fig. 5.5, mean Force Index of the control sample is stable except a few points that deviate from average due to deviation in velocity. In the 0.5 $\mu\text{g/ml}$ sample no significant change is observed. However, increasing the concentration to 1 $\mu\text{g/ml}$ results in a decrease in mean Force Index. We would expect a decrease in mean Force Index following exposure to Oligomycin but maintaining the velocity during the experiment was hard to achieve since several clogging arise in the system. Besides, the DEP response in 0.17 S/m medium conductivity is very sensitive to size and hence velocity. Consequently, Force Index would not experience a smooth change.

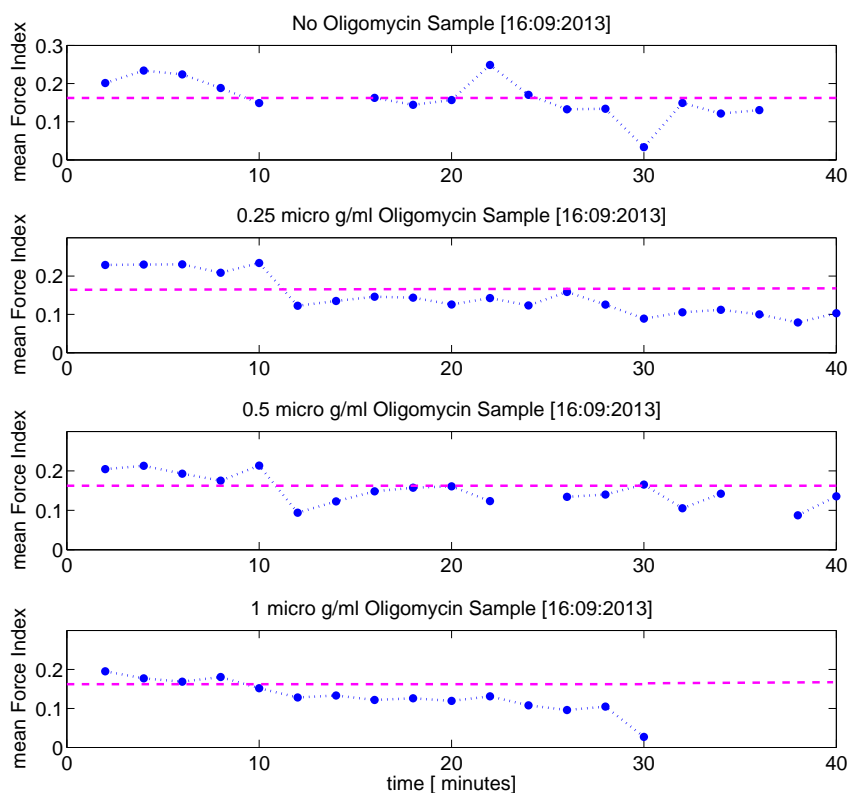


Fig. 5.5: Force Index monitored in time. Purple dashed line represents overall mean FI for the control sample.

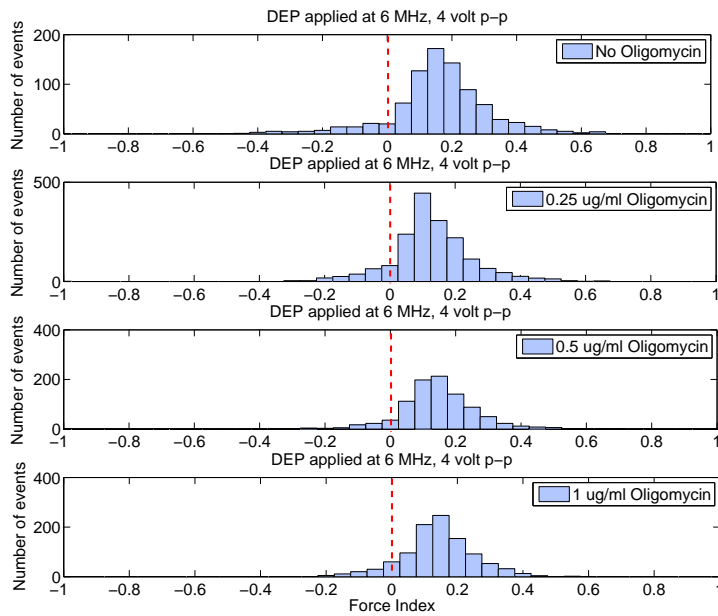


Fig. 5.6: Force Index histograms of control and treated samples.

Experiment 3 [12/11/2013]:

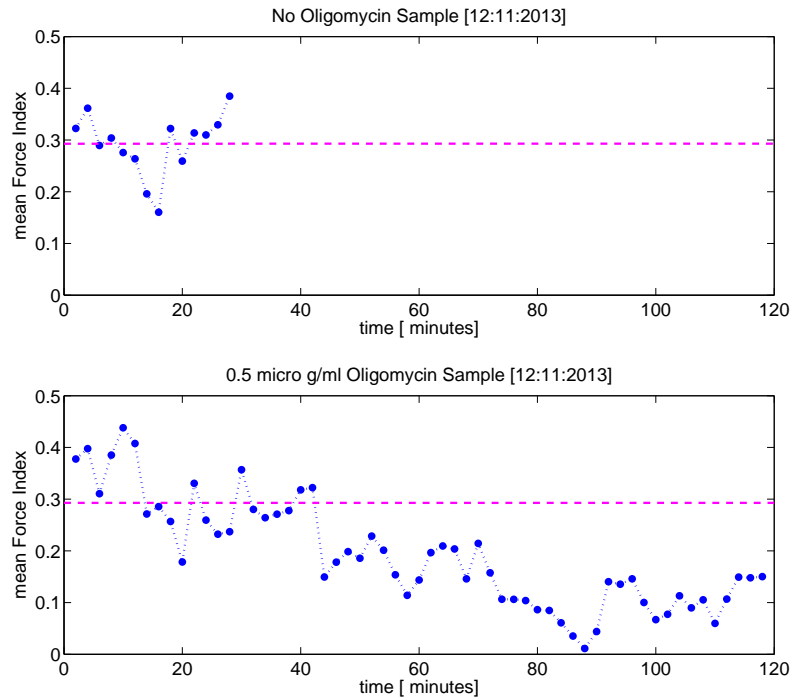


Fig. 5.7: Force Index monitored in time. Purple dashed line represents overall mean FI for the control sample.

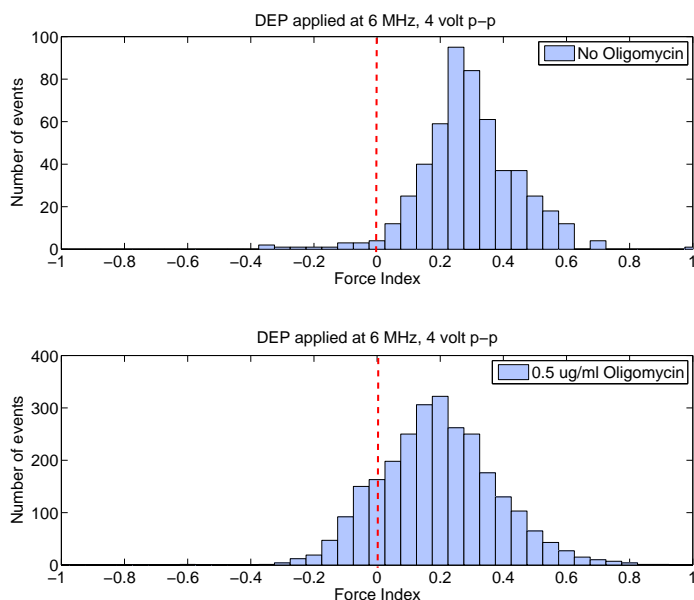


Fig. 5.8: Force Index histograms of control and treated samples.

In this experiment 0.5 $\mu\text{g/ml}$ concentration was repeated again. The experiment with 1 $\mu\text{g/ml}$ Oligomycin encountered clogging and is not reported here. The mean Force Index is decreasing with time. However, control sample mean Force Index is stable during 30 minutes of experiment. The control sample data has been not recorded for more than 30 minutes. In future experiments, with medium conductivity of 0.42 S/m, we have focused just in one concentration and recorded data for the control sample as long as the treated sample.

As shown in histograms of Fig. 5.8, after treatment with Oligomycin 0.5 $\mu\text{g/ml}$ a second population with decreased mean Force Index arises in the Force Index histogram.

Experiment 4 [14/11/2013]: The experiments with 0.5 and 1 $\mu\text{g/ml}$ concentrations have been repeated here. As shown in Fig. 5.9 and 5.10, the mean Force Index has been decreased to ≈ 0.1 below the control mean Force Index (dashed line). The decrease is consistent with these two concentrations.

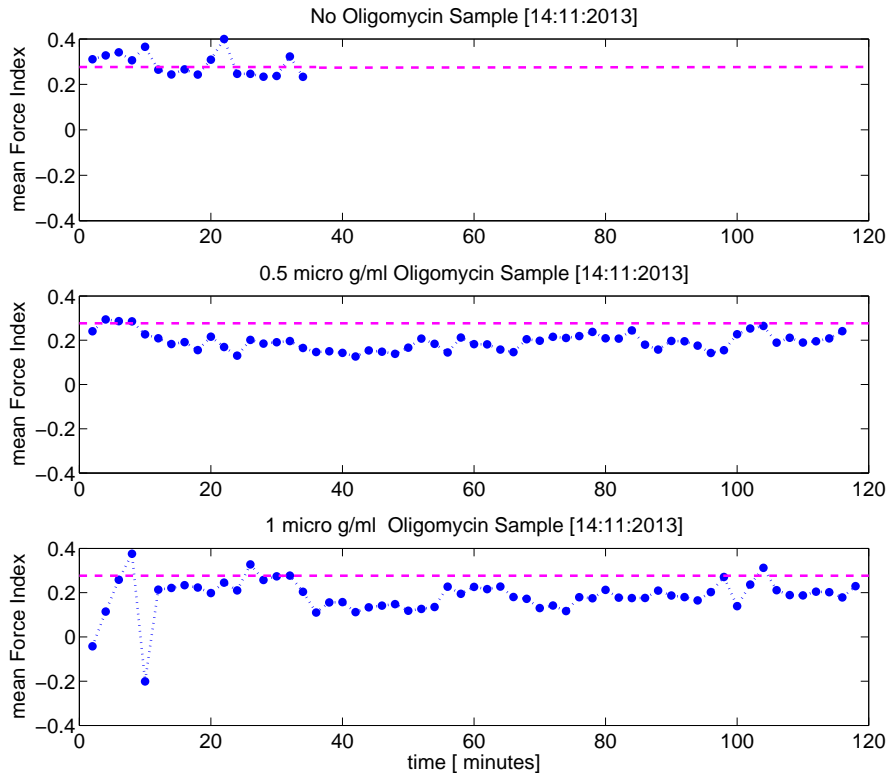


Fig. 5.9: Force Index monitored in time. Purple dashed line represents overall mean FI for the control sample.

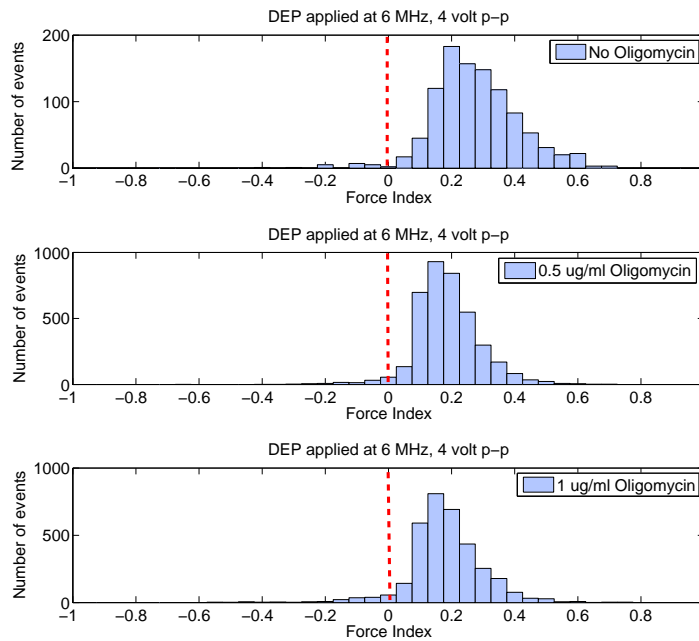


Fig. 5.10: Force Index histograms of control and treated samples.

Experiment 5 [16/01/2014]:

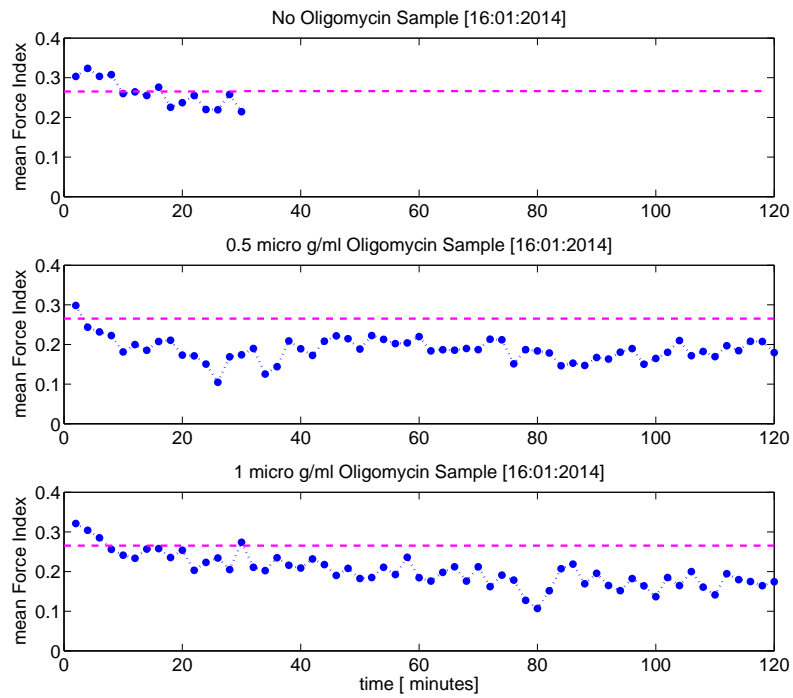


Fig. 5.11: Force Index monitored in time. Purple dashed line represents overall mean FI for the control sample.

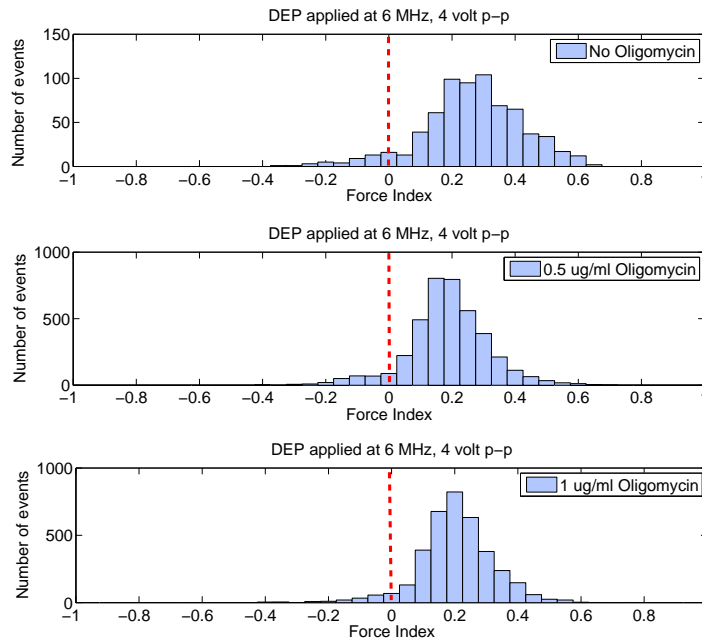


Fig. 5.12: Force Index histograms of control and treated samples.

These experiments (Fig. 5.11) are consistent with the previous experiment in terms of the decrease in mean FI observed in the Oligomycin sample. A slight decrease in the control sample mean Force Index has been observed as well. The mean Force Index in the histograms decreased about ≈ 0.1 after treatment.

To check repeatability, all the experiments are plotted together in Figures 5.13 and 5.14. For both 0.5 and 1 $\mu\text{g/ml}$ Oligomycin concentrations, Force Index decreases ≈ 0.1 below the control mean Force Index except for the first experiment. Viabilities measured by Trypan blue assay and DEP are reported in Table 5.1. Trypan Blue assay has been done at the beginning of the experiment on samples before introducing Oligomycin.

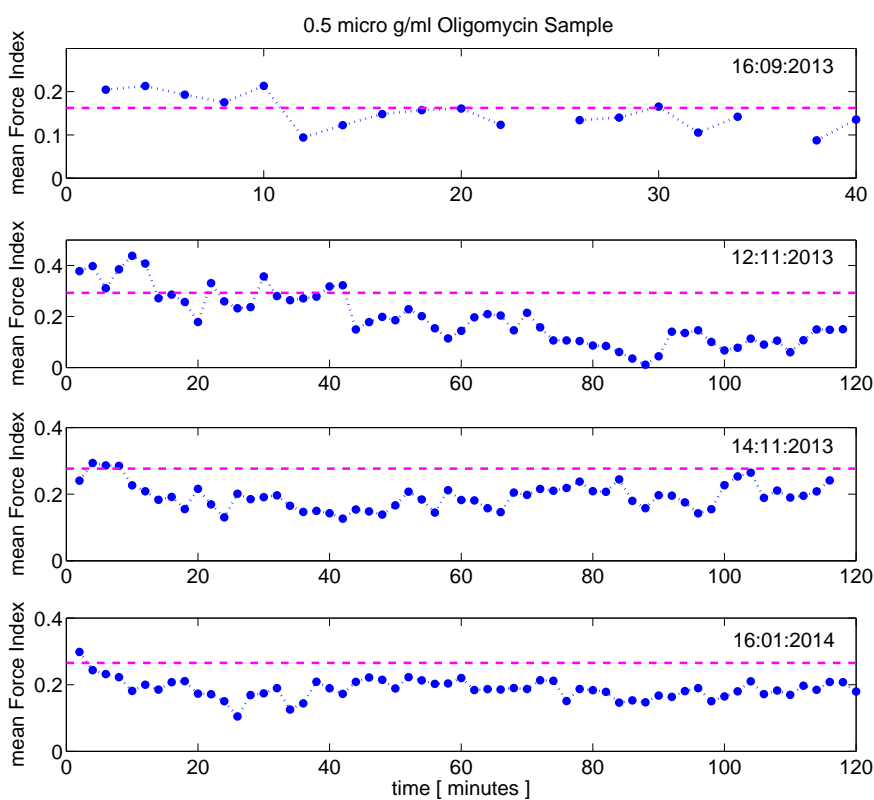


Fig. 5.13: Force Index monitored in time. Purple dashed line represents overall mean FI for the control sample.

Various undesirable factors affected the presented experiments. Firstly, these experiments were done in different days of the culture growth cycle. It has been shown that aging is

important in the ATP to Glycolysis levels within the cell [86]. We will show that we can reduce sensitivity to size by adjusting medium conductivity. In future experiments we tried to prepare the samples within 34-40 passage numbers and 3 day old culture and velocity has been monitored and controlled more carefully.

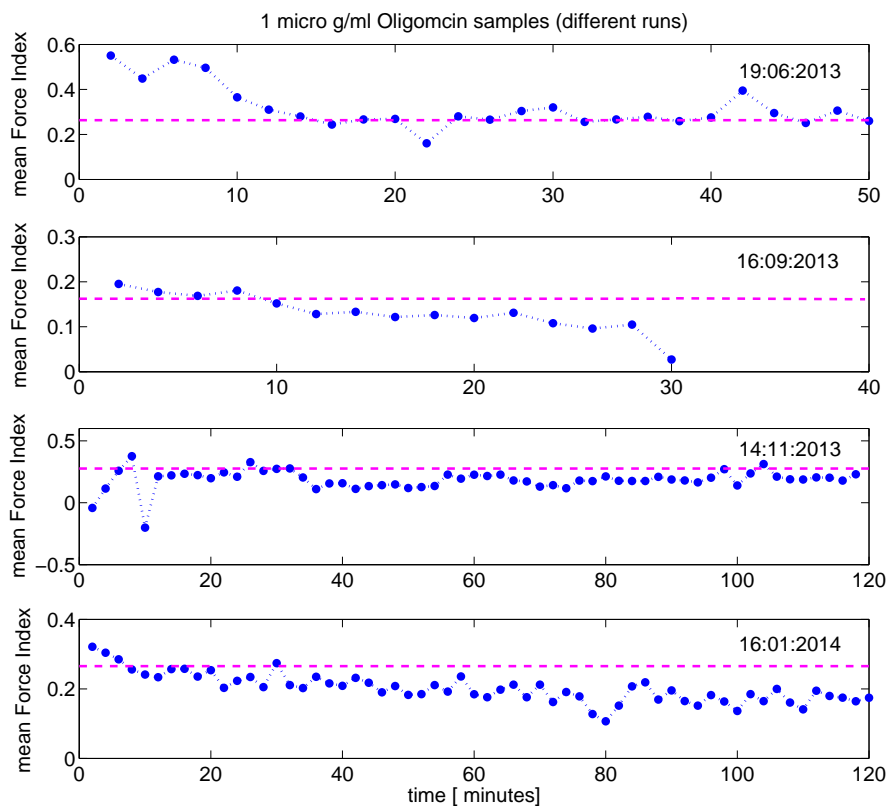


Fig. 5.14: Force Index monitored in time. Purple dashed line represents overall mean FI for the control sample.

Tab. 5.1: Percentage viability: Control compared to Oligomycin 0.5 $\mu\text{g/ml}$

Assays	Exp #1	Exp #2	Exp #3	Exp #4	Exp #5
Trypan Blue	97.1	93.8	91.2	97.1	92.4
DEP on control	96.9	90.1	97.2	98.1	93.7
DEP on Oligomycin 0.5 $\mu\text{g/ml}$	NA	92.1	85.0	97.3	93.3
DEP on Oligomycin 1 $\mu\text{g/ml}$	96.9	91.4	NA	95.6	95.6

5.6 Results with medium conductivity of 0.42 S/m

In order to improve the DEP cytometer sensitivity to the changes in the cytoplasm conductivity and decrease the size and velocity variability effects, medium conductivity has been chosen such that the mean Force Index is zero for the untreated cells. This was done by measuring the dielectric response (Force Index) for medium conductivities from 0.17 S/m to 0.45 S/m and finding the conductivity where the mean Force Index was zero. At each conductivity the mean was measured for $N \approx 500$ cells. Cells with no DEP voltage applied are expected to have a near zero Force Index, but a measurable off set is evident, shown in Fig. 5.16. This may be due to asymmetries in the electrodes or signal path yielding slightly larger signals from one pair of detection electrodes [69].

The histograms for these experiments are shown in Fig. 5.15. By a linear fit to the mean Force Index versus medium conductivity (shown in Fig. 5.16), a medium conductivity of 0.42 has been calculated as the medium conductivity resulting in zero DEP force and hence zero mean Force Index. This medium conductivity was used for the remainder of the tests. The uncertainty estimate was found by standard error of the mean (SEM) or standard deviation divided by square root of the sample size .

All samples were more than 96 % viable in Trypan blue assay with $\approx 12.5 \mu\text{m}$ averaged diameter. The conductivity was set by using low conductivity ($\approx 0.067 \text{ S/m}$) medium (37°C) [22.9 mM sucrose (Sigma), 16 mM glucose (Fisher), 1mM CaCl_2 (Fisher), 16mM Na_2HPO_4 (Fisher)] (Polevaya et al., 1999) and then adding the appropriate volume of growth media required (for example 17:6 for 0.42 S/m) to reach the chosen cell density and conductivity, as measured by a conductivity meter (Orion 3-Star Plus, Thermo Scientific, Waltham, MA).

Medium conductivity adjustment reduces unwanted sensitivities due to size, as shown in the simulation of Fig. 5.17. However, the sensitivity to the cytoplasm conductivity for both 0.17 S/m and 0.42 S/m medium conductivities are not significantly different, shown in Fig. 5.18. This zero dielectrophoresis force conductivity can be used to estimate the cytoplasm conductivity. Using a double shell model, for a null in the dielectrophoresis force at 6 MHz the estimated cytoplasm conductivity is 0.42 S/m. The fact that the cytoplasm and zero mean Force Index conductivity are the same is a coincidence and is not significant. Any other choice in DEP frequency would have yielded a different zero mean Force Index medium conductivity. Substituting the cytoplasm conductivity of 0.42 in the double shell model, the mean Force Index curve versus K_{CM} experimentally which is presented in Fig. 5.19. The fact that cytoplasm conductivity is fixed to 0.42 S/m might not be realistic since in different medium conductivities cells adapt to the new environment. Therefore, cytoplasm conductivity is a dynamic parameter rather than fixed [86].

In this section we have used the following definition for Force Index:

$$\text{Force Index} = \frac{P_2 - P_1}{P_2 + P_1} \quad (5.2)$$

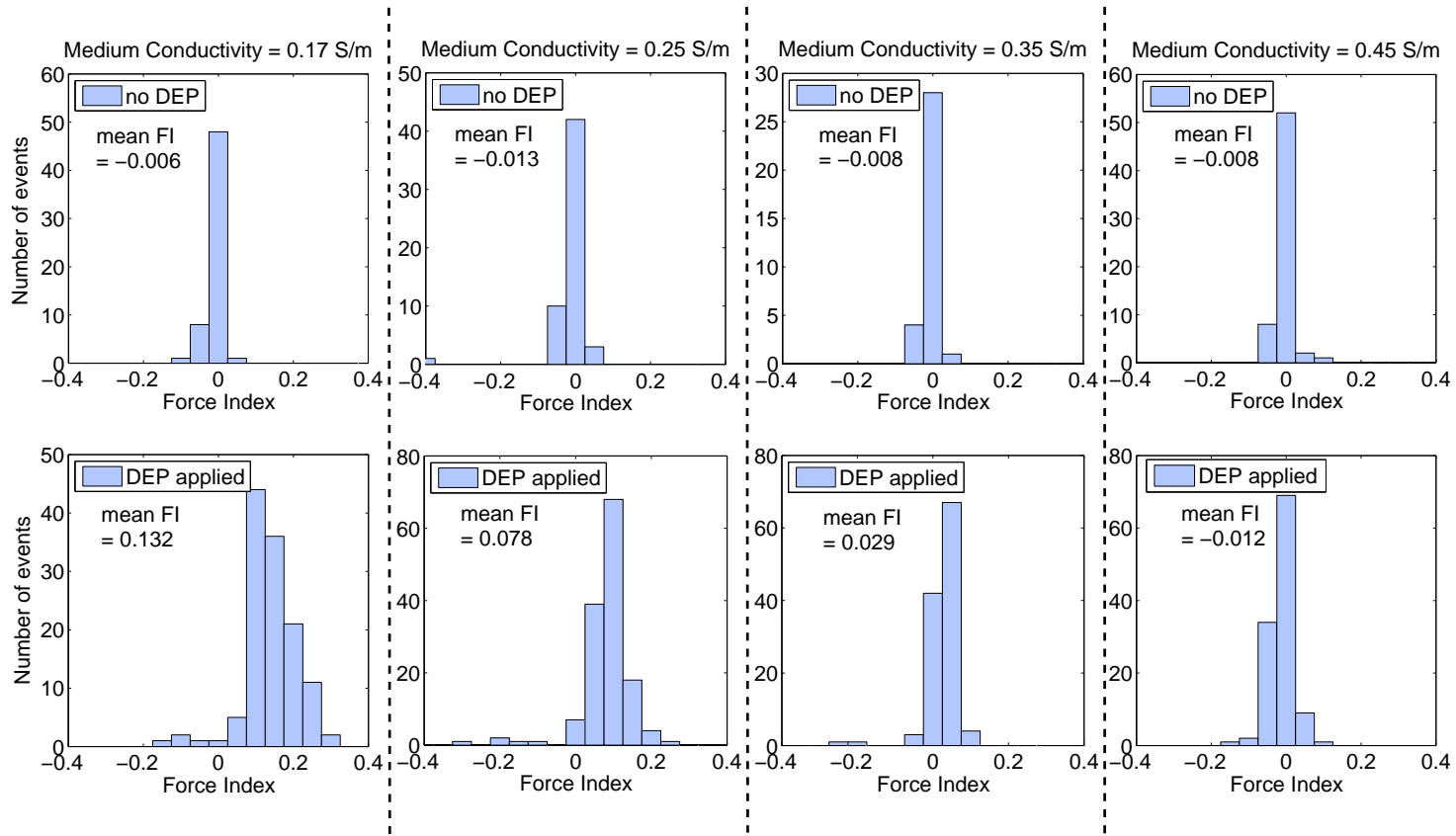


Fig. 5.15: Force Index histograms for different medium conductivities.

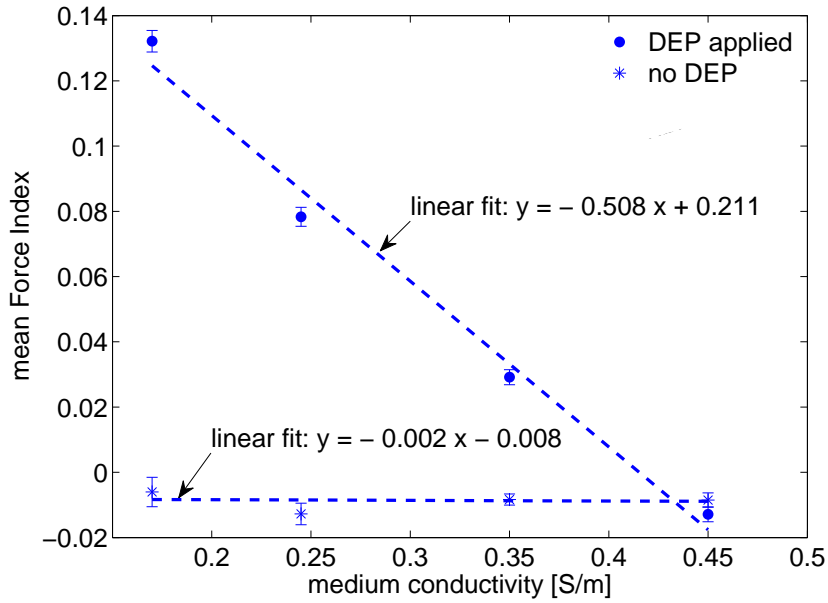


Fig. 5.16: Mean Force Index for 0.17-0.45 S/m medium conductivities. Solid circles stand for the case in which DEP is applied. Hollow circles stand for the case in which DEP is not applied.

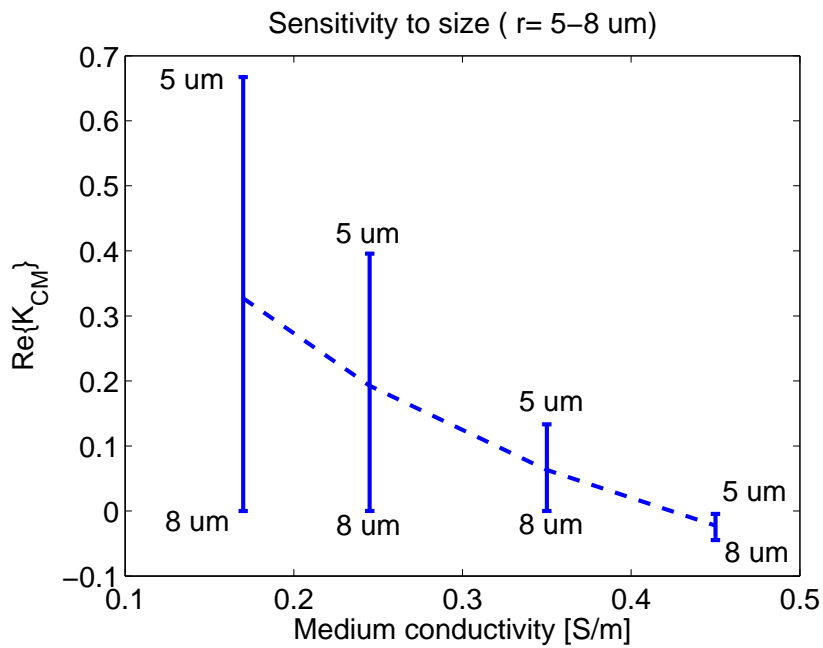


Fig. 5.17: K_{CM} sensitivity to cell radius in different medium conductivities simulated by a double shell model with a σ_{cyl} of 0.42 S/m.

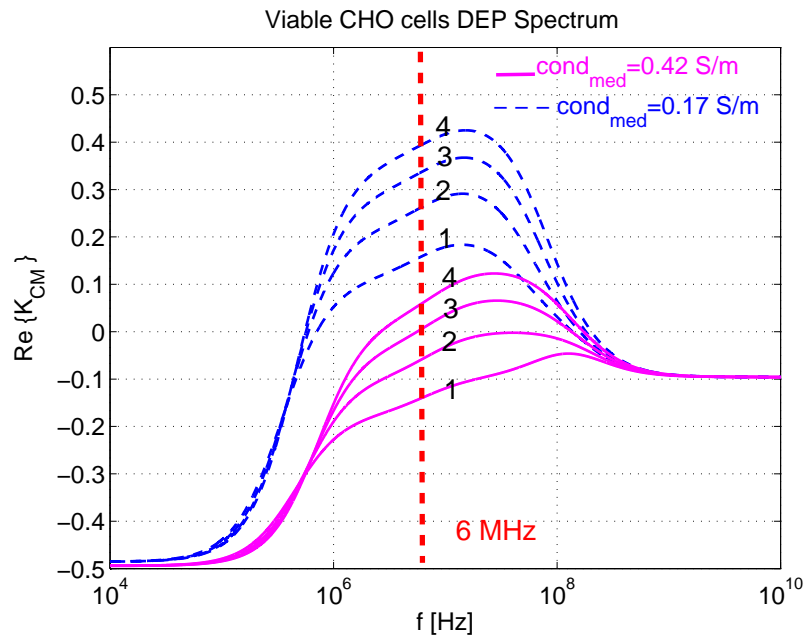


Fig. 5.18: K_{CM} sensitivity to cytoplasm conductivity in medium conductivity of 0.17 S/m and 0.42 S/m. For 1-4 σ_{cyt} is varying from 0.22-0.52 S/m in steps of 0.1 S/m.

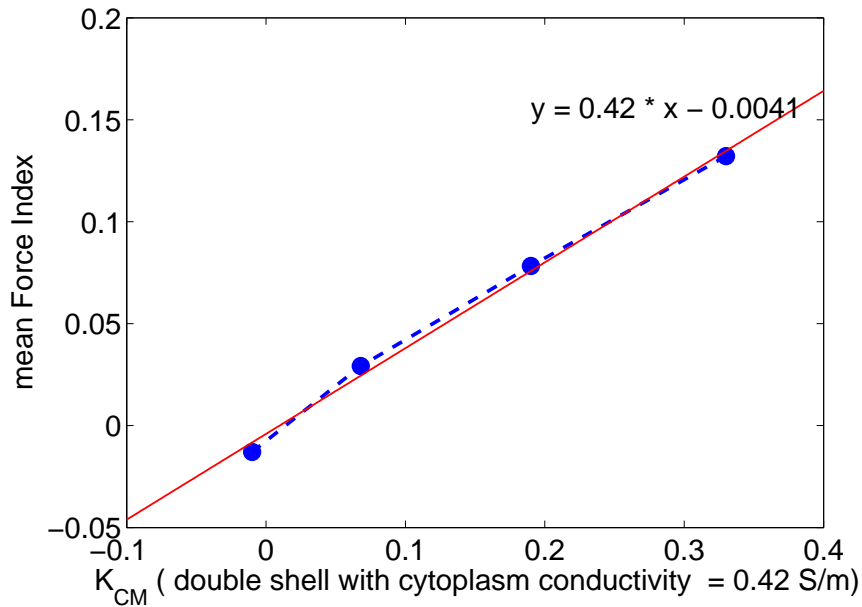


Fig. 5.19: Simulated K_{CM} using double shell model. $\sigma_{cyt} = 0.42$ S/m, other parameters are set as defined in Chapter 1.

5.6.1 Results with optimized medium conductivity of 0.42 S/m

The resonance frequency is set to ≈ 1.45 GHz, velocity is adjusted such that the time between peak 1 and peak 2 is 100 msec, the average cell diameter is ≈ 12.5 μm , and viabilities are reported at the end of this section. All data collection is performed by *Semi-automated GUI* with window size of 100 msec. The DEP response is obtained by applying a $4V_{P-P}$ sinusoidal voltage to the DEP electrode at 6MHz. Samples are mixed by Vortex immediately after addition of Oligomycin/DMSO and purged for one minute. Peak values were recorded for two hours for the control and the Oligomycin sample.

The Oligomycin treated sample was prepared by adding Oligomycin (Sigma), reconstituted in dimethyl sulfoxide (DMSO), at the concentration of 8 $\mu\text{g}/\text{ml}$ to the diluted sample. Control samples were prepared by adding the same volume of DMSO without oligomycin to the sample. For each test run the cells were in passages 35 – 40 and came from a 3 day old culture. This consistency is important as the age of a cell is known to affect the ratio of mitochondrial to glycolysis ATP production [87].

Experiment 1 [17/03/2014]:

As shown in Fig. 5.20, the control sample Force Index is stable around its average over 120 minutes. However, a decrease of about 0.1 in the Force Index is observed in the Oligomycin treated sample. The majority of the change occurs within the first 60 minutes. As shown in histograms of Fig. 5.21 and 5.22, Force Index histograms of the Oligomycin sample shifts to negative values which is evidence for the decreased cytoplasm conductivity.

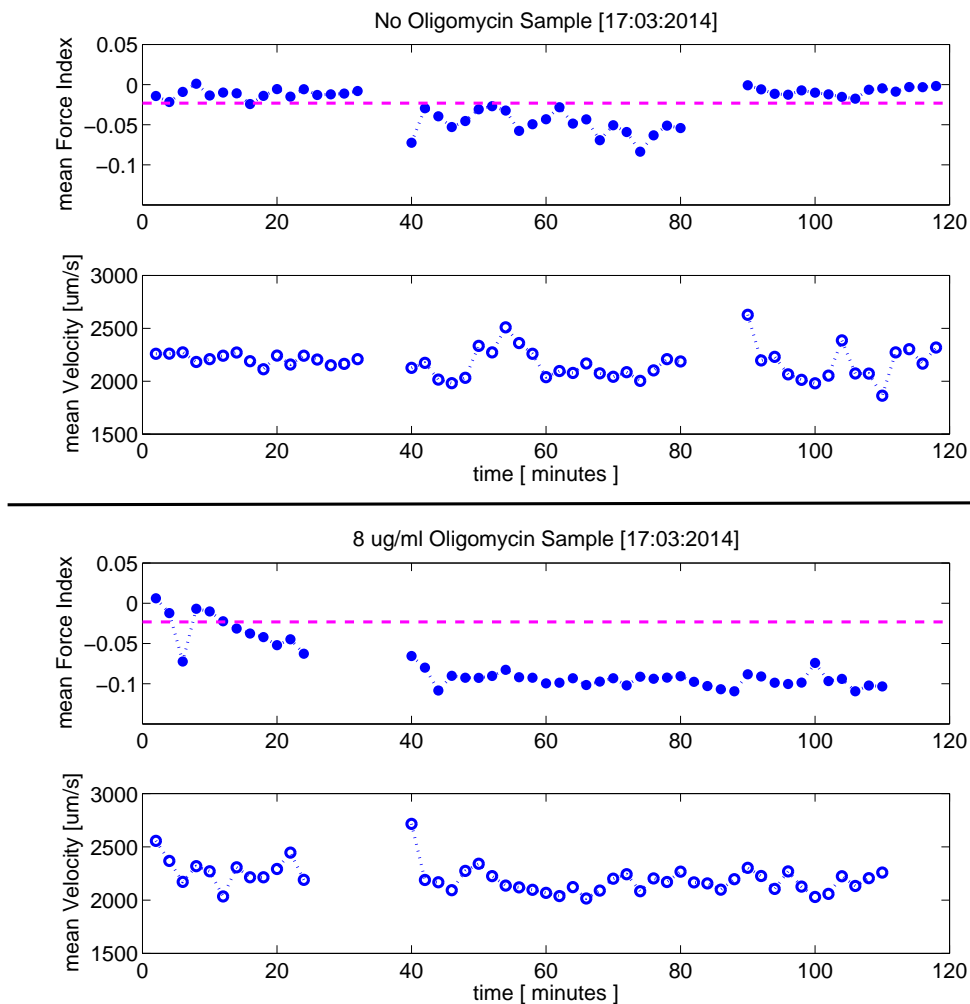


Fig. 5.20: Force Index and velocity monitored in time. Purple dashed line represents overall mean FI for the control sample.

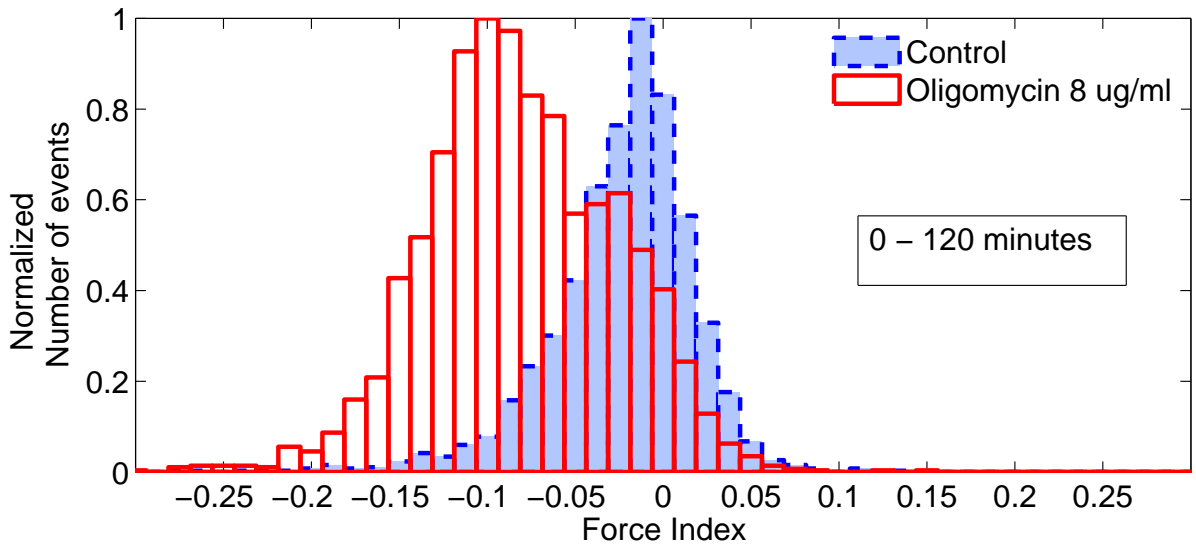


Fig. 5.21: Force Index histogram over 120 minutes of experiment.

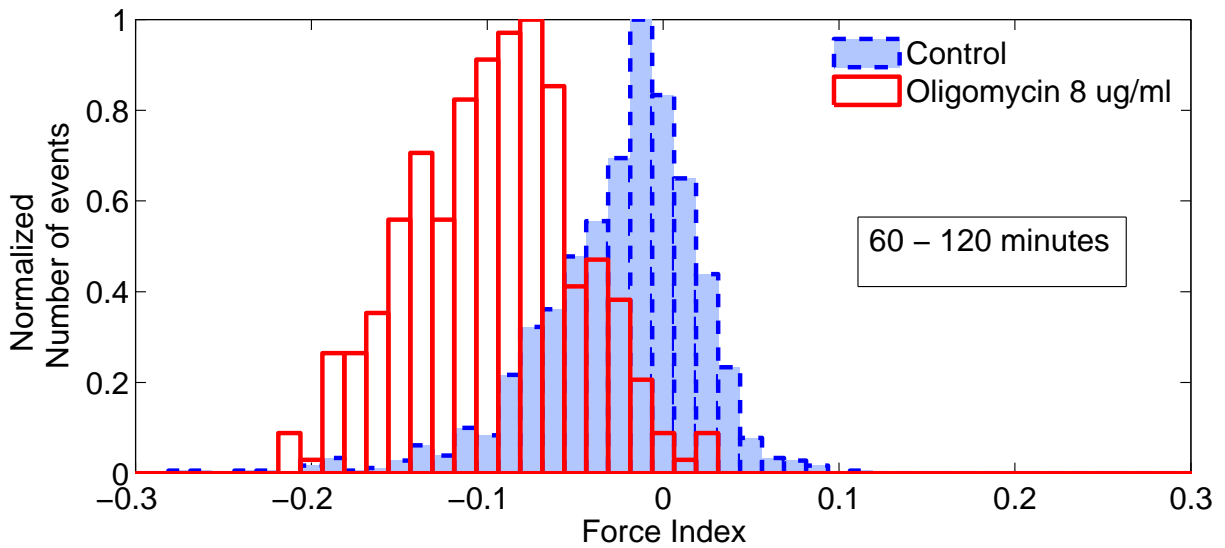


Fig. 5.22: Force Index histogram after 60 minutes of experiment.

Experiment 2 [20/03/2014]: As shown in Fig. 5.23, the control sample Force Index is stable around its average over 70 minutes and changes less than 0.01. However, a decrease of about 0.05 in the Force Index is observed in the Oligomycin treated sample. The majority of the change is occurring within the first 60 minutes. As shown in histograms of Fig. 5.24 and 5.25, the mean FI of the treated sample decreases to negative values which is evidence for the decreased cytoplasm conductivity. The Force Index distribution does not experience further change after 60 minutes of treatment.

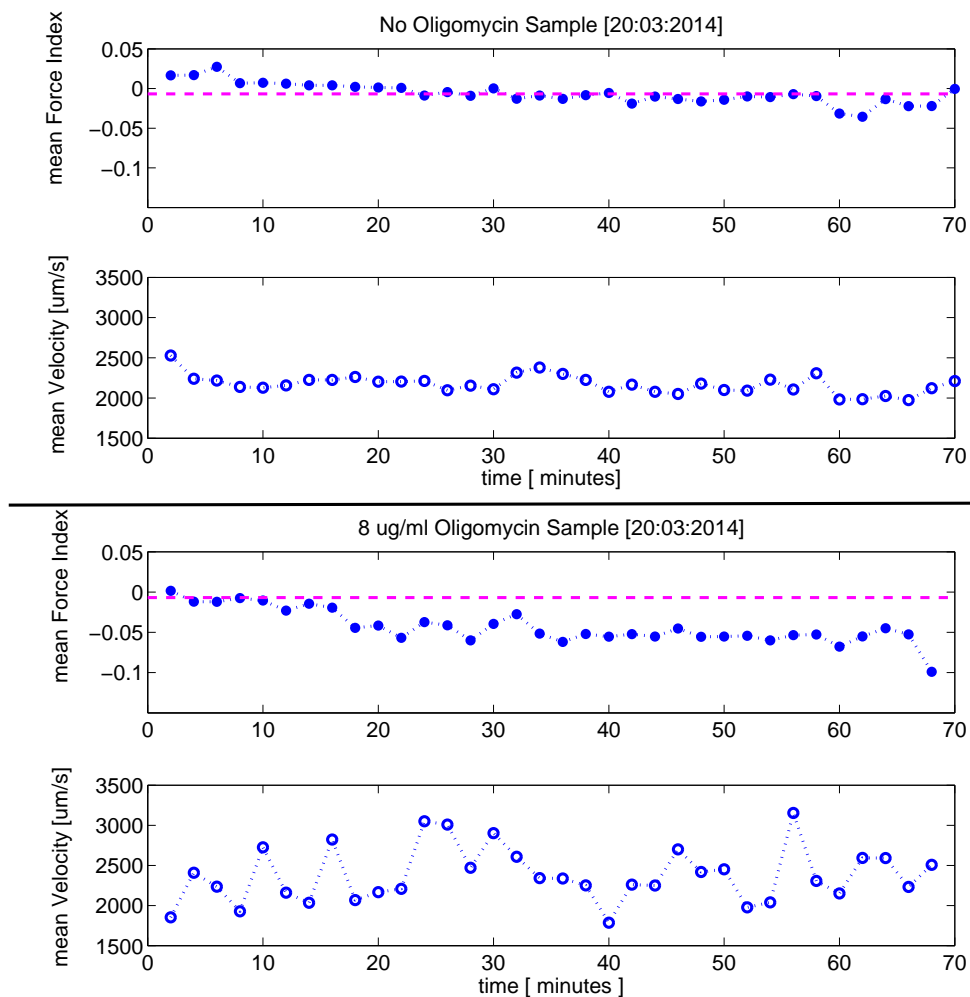


Fig. 5.23: Force Index and velocity monitored in time. Purple dashed line represents overall mean FI for the control sample.

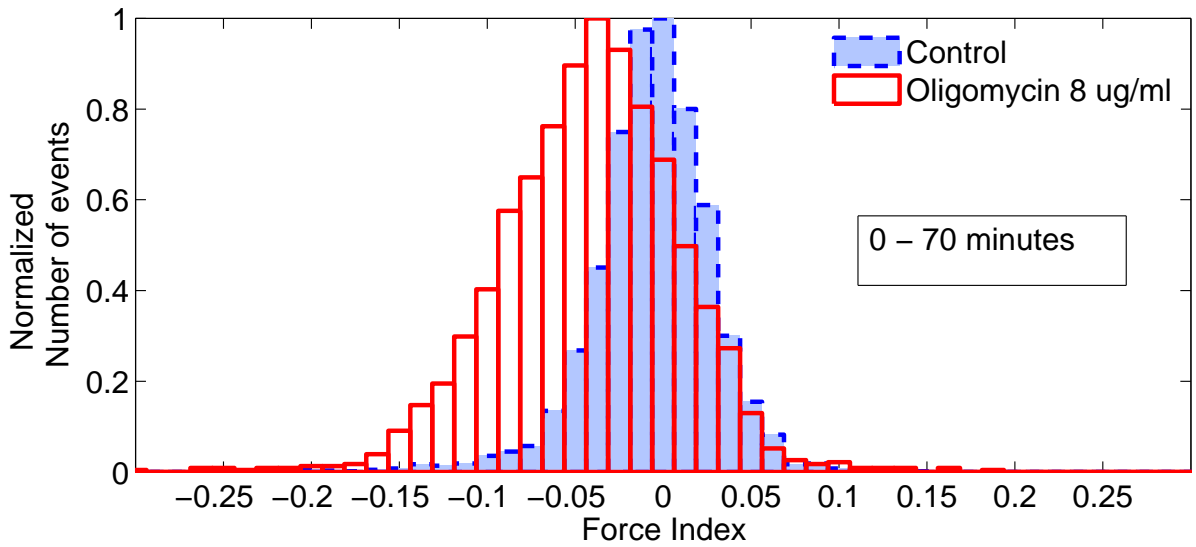


Fig. 5.24: Force Index histogram over 120 minutes of experiment.

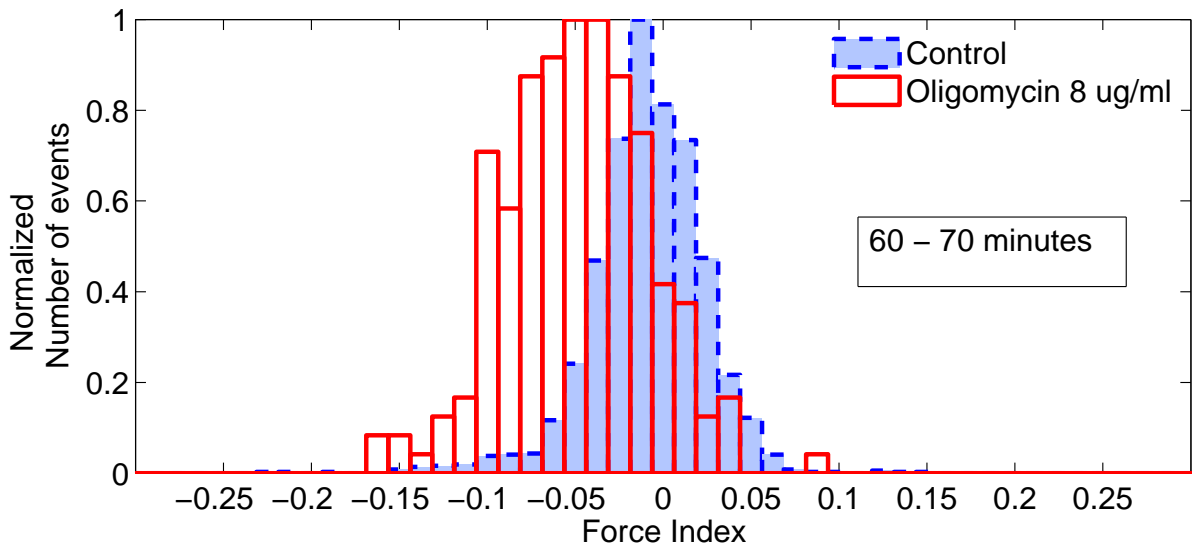


Fig. 5.25: Force Index histogram after 60 minutes of experiment.

Experiment 3 [10/04/2014]: In this experiment Force Index of the treated sample experiences a decrease of about 0.05. However, Force Index for the control sample remains stable. Force Index distribution after 60 minutes of treatment does not experience further decrease; meaning the majority of change takes place within the first 60 minutes of exposure to Oligomycin..

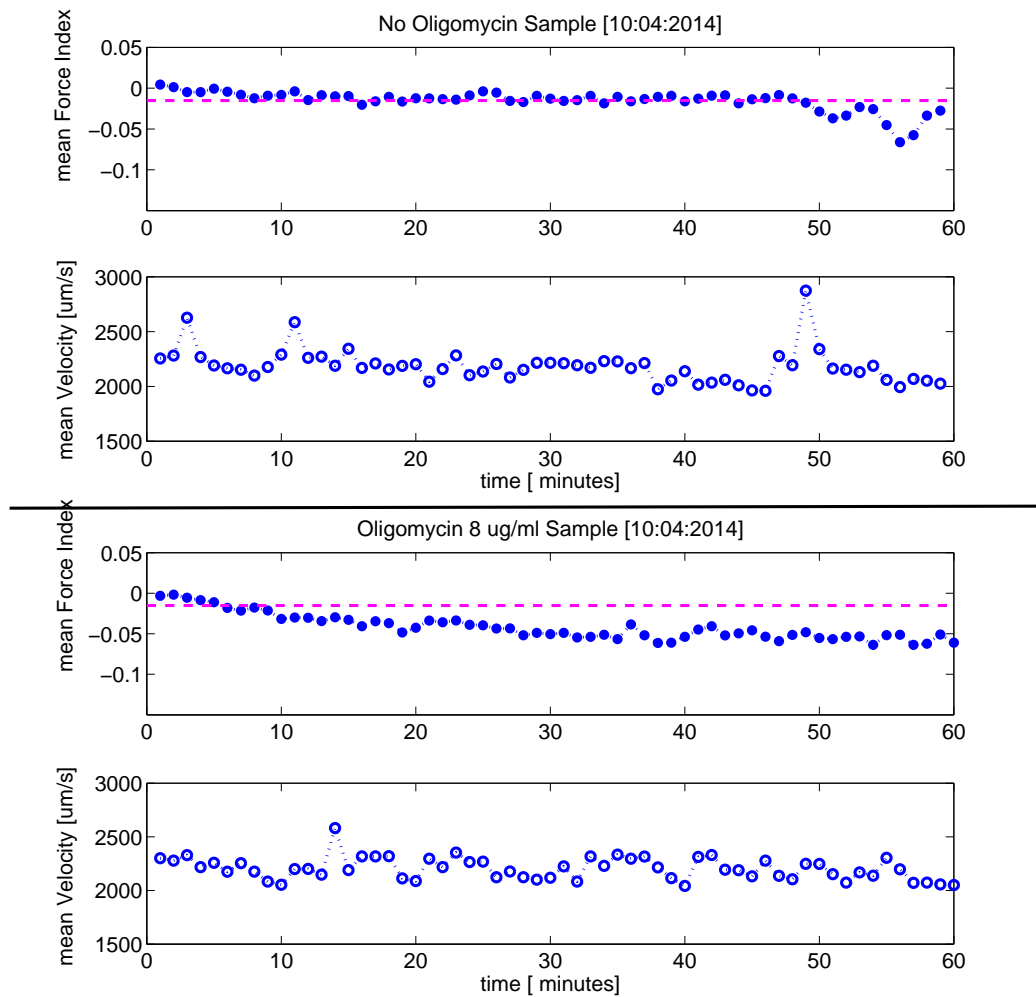


Fig. 5.26: Force Index and velocity monitored in time. Purple dashed line represents overall mean FI for the control sample.

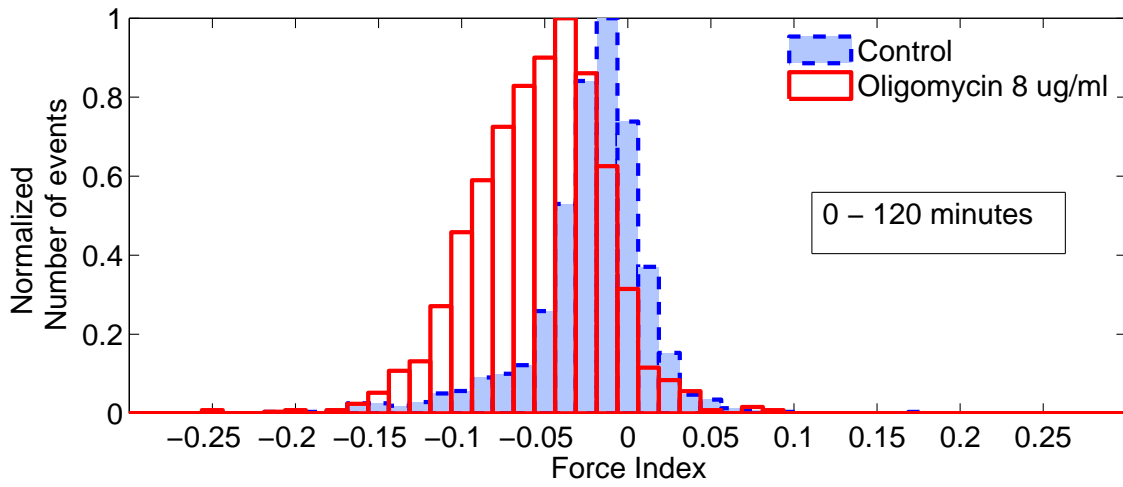


Fig. 5.27: Force Index histogram after 120 minutes of experiment.

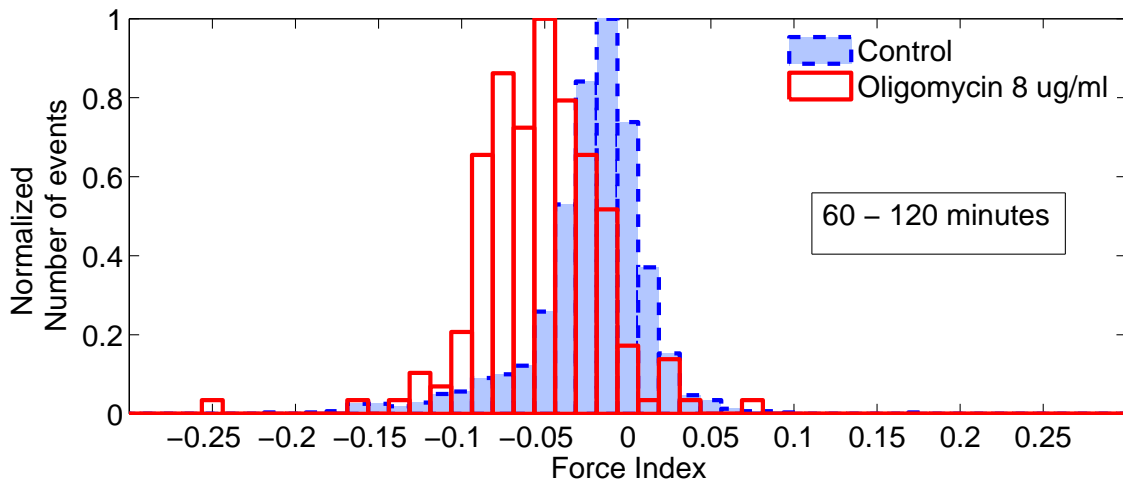


Fig. 5.28: Force Index histogram over 60 minutes of experiment.

Tab. 5.2: Percentage viability of the control samples.

Assays	Exp #1	Exp #2	Exp #3
Trypan Blue	99.0	98.7	95.6
Nexin	96.6	93.9	93.2
Via count	97.8	97.8	97.0

Percentage viability for these three experiments before treatment are reported in Table 5.2.

5.7 Estimating cytoplasm conductivity

In section 5.6, we have calculated K_{CM} for the mean Force Index of different medium conductivities. In this calculation, it is assumed that cytoplasm conductivity is fixed to 0.42 S/m and does not vary dynamically with medium conductivity. Using the mean Force Index plot versus K_{CM} (Fig. 5.19), we can estimated the drop in the cytoplasm conductivity under the assumption of linearity of K_{CM} with negative values of Force Index.

If the Force Index value drops by 0.05 following one hour of exposure to Oligomycin, this decrease corresponds to a decrease of 0.11 in K_{CM} value obtained from Fig. 5.19. The K_{CM} variations with cytoplasm conductivity in a medium conductivity of 0.42 S/m is simulated and shown in Fig. 5.29 which indicates a cytoplasm conductivity of 0.255 S/m after treatment with Oligomycin.

The decrease in the mean Force Index of the control sample within the first 10 minutes might be due to adaptation of the cells to the medium conductivity of 0.42 S/m after re-suspension from the growth medium (conductivity of ≈ 1.4 S/m).

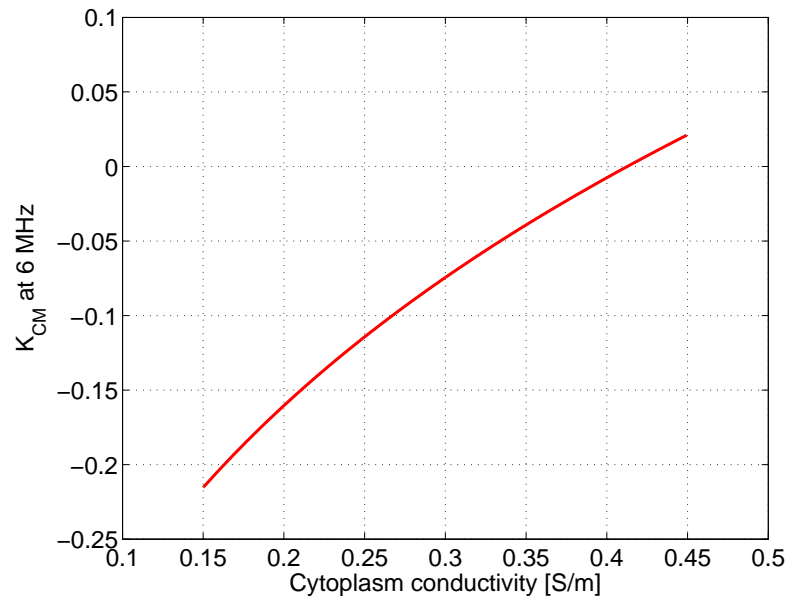


Fig. 5.29: K_{CM} calculated by the double shell model versus cytoplasm conductivity with medium conductivity of 0.42 S/m, other parameters are fixed as presented in Chapter 1.

5.8 Chapter conclusion

Metabolism plays a critical role in determining the overall dielectric response of cells in either analysis or manipulation of cells by DEP. In this work, we demonstrated that perturbations to the dielectric response of cells due to loss of mitochondrial ATP can be detected. This detection was possible by optimizing the choice of DEP signal frequency and medium conductivity.

Following one hour of exposure to Oligomycin the Force Index reaches a steady state and does not experience a further decrease. The Oligomycin concentration used in this study is high enough to assure the ATP synthase inhibition in the mitochondria following 10 minutes of exposure [75]. The stabilized mean Force Index is an evidence for other energy production pathways within the cell; i.e. Glycolysis in cytoplasm. If all the ATP were produced through the mitochondrial pathway the Force Index would be expected to drop more significantly.

These results are in agreement with computational models of ion homeostasis presented in Chapter 1. The next generation of the Hodgkin Huxley model for non-excitabile cells, predicts that after 30-60 minute inhibition of the ATPase pumps the, cell dynamically reaches equilibrium [32, 7, 6]. This time constant depends on the numbers of pores and pumps on the membrane and the initial state compared to the medium. During this time, the cell experiences a decrease in the K^+ concentration (efflux) and an increase in the Na^+ ion concentration inside the cytoplasm (influx). Since K^+ is the dominant contributor to the cytoplasm conductivity, the decrease in the internal K^+ concentration is mostly responsible for the decrease in the cytoplasm conductivity and hence the decrease in the Force Index.

Conclusion and future work

DEP of cells is influenced by many factors such as membrane capacitance, cytoplasm conductivity and cytoplasm permittivity. In Chapter 1, many examples of physiological events within the cell which impact these dielectric properties were presented. Apoptosis was presented as one of the major processes in which cytoplasm and membrane properties undergo a significant change. We have employed a DEP cytometers as a reliable means to detect the onset of the apoptosis.

We have studied dielectric response of two different cell lines; Chinese hamster ovary cells and MRC5 cells. Furthermore, we showed that starved and fresh cultures of MRC5 cells have a different dielectric response in a frequency range of 50 KHz to 6 MHz. Dielectric properties of MRC5 cells were optimized to match the experimental and simulated cross over frequency by a double shell model. This estimation has not been reported previously in the literature.

Oligomycin was used to inhibit mitochondrial ATP production which has an impact on the ATPase pumps in the membrane and hence ion homeostasis, ion concentrations, and cyto-

plasm conductivity. One can imagine using this approach to quantify mitochondrial versus Glycolysis ATP production by measuring dielectric responses with and without Oligomycin treatment. Oxygen consumption rate and metabolism bi-products evaluation offer a method to estimate mitochondrial versus Glycolysis ATP production however these methods are not applicable at the single cell level. Hence, this quantification has the application in the monitoring of bioprocesses, especially in therapeutic production and in determining the advance of cancer in cells [88, 85, 89, 90]. It is known that cancerous cells have higher Glycolysis level compared to the normal cells [91]. It is observed that cancer cells produce majority of their energy by high levels of Glycolysis known as *Warburg* effect.

In terms of future work, to quantify mitochondrial versus Glycolysis ATP production we suggest to inhibit Glycolysis and study the DEP response in time. Furthermore, it is possible to trap one single treated cell in the analysis volume and monitor the DEP response in time. In this manner, we would be able to eliminate differences in a cell population and controlling velocity would be easier.

Oligomycin is in fact an inhibitor of the ATPase enzyme which eventually inhibits APT dependent pumps such as Na^+/K^+ ATPase pumps. On the other hand, Ouabain is known to inhibit Na^+/K^+ ATPase pumps directly. Monitoring the dielectric response following inhibition of the pumps by Ouabain and comparing it with the equivalent Oligomycin concentration in terms of the ATPase activity would be beneficial as a future study.

Bibliography

- [1] R. Phillips, J. Kondev, J. Theriot, and H. Garcia, *physical biology of the cell*, 1st ed. Garland Science, 2008.
- [2] R. G. Mortimer, *Physical Chemistry*. Academic Press Elsevier, 2008.
- [3] K. Asami, Y. Takahashi, and S. Takashima, "Dielectric properties of mouse lymphocytes and erythrocytes," *Biochim Biophys Acta*, vol. 1010, no. 1, p. 49, January 1989.
- [4] Y. Plevaya, I. Ermolina, M. Schlesinger, B.-Z. Ginzburg, and Y. Feldman, "Time domain dielectric spectroscopy study of human cells normal and malignant white blood cells," *Biochim Biophys Acta*, vol. 1419, p. 257, 1999.
- [5] T. Kotnik, D. Miklavcic, and T. Slivnik, "Time course of transmembrane voltage induced by time-varying electric fields - a method for theoretical analysis and its application," *Bioelectrochemistry and Bioenergetics*, vol. 45, no. 1, pp. 3–16, MAR 1998.
- [6] E. Jakobsson, "Interactions of cell volume, membrane potential and membrane transport parameters," *American Journal of Physiology*, vol. 238, 1980.
- [7] C. M. Armstrong, "The Na⁺ K⁺ pump, Cl⁻ ion, and osmotic stabilization of cells," *Proceedings of the National Academy of Sciences*, vol. 100, no. 10, 2003.
- [8] T. B. Jones, *Electromechanics of Particles*. Cambridge University Press, 1995.
- [9] R. Pethig, "Dielectrophoresis: Status of the theory, technology, and applications," *Biomicrofluidics*, vol. 4, no. 2, p. 022811, jun 2010.
- [10] A. W. Griffith and J. M. Cooper, "Single-cell measurements of human neutrophil activation using electrorotation," *Anal. Chem*, vol. 70, p. 2607, 1998.
- [11] J. Voldman, *Biomolecular sensing, preprocess and analysis*. Springer, 2007.

- [12] M. Nikolic-Jaric, T. Cabel, E. Salimi, A. Bhide, K. Braasch, M. Butler, G. E. Bridges, and D. J. Thomson, "Differential electronic detector to monitor apoptosis using dielectrophoresis-induced translation of flowing cells (dielectrophoresis cytometry)," *Biomicrofluidics*, vol. 7, no. 2, MAR 2013.
- [13] F. F. Becker, X. B. Wang, Y. Huang, R. Pethig, J. Vykoukal, and P. R. Gascoyne, "Separation of human breast cancer cells from blood by differential dielectric affinity," *Proceedings of the National Academy of Sciences of the United States of America*, vol. 92, no. 3, pp. 860–864, JAN 31 1995.
- [14] M. Stephens, M. Talary, R. Pethig, A. Burnett, and K. Mills, "The dielectrophoresis enrichment of CD34(+) cells from peripheral blood stem cell harvests," *Bone Marrow Transplantation*, vol. 18, no. 4, pp. 777–782, OCT 1996.
- [15] Y. Huang, X. Wang, F. Becker, and P. Gascoyne, "Introducing dielectrophoresis as a new force field for field-flow fractionation," *Biophysical Journal*, vol. 73, no. 2, pp. 1118–1129, AUG 1997.
- [16] X. Wang, J. Yang, Y. Huang, J. Vykoukal, F. Becker, and P. Gascoyne, "Cell separation by dielectrophoretic field-flow-fractionation," *Analytical Chemistry*, vol. 72, no. 4, pp. 832–839, FEB 15 2000.
- [17] J. Yang, Y. Huang, X. Wang, X.-B. Wang, F. F. Becker, and P. R. C. Gascoyne, "Dielectric properties of human leukocyte subpopulations determined by electrorotation as a cell separation criterion," *Biophysical Journal*, vol. 76, p. 3307, 1999.
- [18] C. Reichle, T. Schnelle, T. Muller, T. Leya, and G. Fuhr, "A new microsystem for automated electrorotation measurements using laser tweezers," *Biochimica et Biophysica Acta*, vol. 1459, no. 1, pp. 218–229, JUL 20 2000.
- [19] J. Gimsa, P. Marszalek, U. Loewe, and T. Y. Tsong, "Dielectrophoresis and electrorotation of neurospora slime and murine myeloma cells," *Biophysical Journal*, vol. 60, no. 4, pp. 749–760, OCT 1991.
- [20] R. Hagedorn, G. Fuhr, T. Muller, and J. Gimsa, "Traveling-wave dielectrophoresis of microparticles," *Electrophoresis*, vol. 13, no. 1-2, pp. 49–54, JAN-FEB 1992.
- [21] H. Morgan, N. Green, M. Hughes, W. Monaghan, and T. Tan, "Large-area travelling-wave dielectrophoresis particle separator," *Journal of micromechanics and microengineering*, vol. 7, no. 2, pp. 65–70, JUN 1997.
- [22] X. B. Wang, Y. Huang, F. F. Becker, and P. R. C. Gascoyne, "A unified theory of dielectrophoresis and travelling wave dielectrophoresis," *Journal of physics: Applied physics*, vol. 27, no. 7, pp. 1571–1574, JUL 14 1994.
- [23] X.-B. Wang, Y. Huang, P. R. Gascoyne, F. F. Becker, R. Holzel, and R. Pethig, "Changes in friend murine erythroleukaemia cell membranes during induced differentiation determined by electrorotation," *Biochim Biophys Acta*, vol. 1193, p. 330, 1994.

- [24] K. Chan, H. Morgan, E. Morgan, I. Cameron, and M. Thomas, "Measurements of the dielectric properties of peripheral blood mononuclear cells and trophoblast cells using ac electrokinetic techniques," *Biochim Biophys Acta*, vol. 1500, p. 313, 2000.
- [25] H. Ziervogel, R. Glaser, D. Schadow, and S. Heymann, "Electrorotation of lymphocytes: the influence of membrane events and nucleus," *Bioscience Reports*, vol. 6, no. 11, 1986.
- [26] Y. Huang, X. Wang, P. Gascoyne, and F. Becker, "Membrane dielectric responses of human T lymphocytes following mitogenic stimulation," *Biochim Biophys Acta*, vol. 1417, p. 51, 1999.
- [27] R. Pethig, L. Jakubek, S. R.H., E. Heart, E. Corson, and P. Smith, "Electrokinetic measurements of membrane capacitance and conductance for pancreatic β -cells," *IEE Proc.-Nanobiotechnol*, vol. 152, 2005.
- [28] T. D. Pollard, W. C. Earnshaw, and J. Lippincott-Schwartz, *Cell biology*, 2nd ed. Elsevier Inc, 208.
- [29] F. L. Ginn, J. D. Shelbume, and B. F. Trump, "Disorders of cell volume regulation," *The American journal of pathology*, vol. 53, p. 1041, 1968.
- [30] S. P. Yu, " Na^+ / K^+ atpase the new face of an old player in pathogenesis and apoptotic/hybrid cell death," *Biochemical Pharmacology*, vol. 66, 2003.
- [31] B. Hille, *Ion Channels of Excitable Membranes*. Sinauer Associates Inc., 2001.
- [32] J. A. Hernandez and E. Cristina, "Modeling cell volume regulation in nonexcitable cells: the roles of the Na^+ pump and of cotransport systems," *Am J Physiol*, vol. 275, pp. 1067–80, 1998.
- [33] D. C. Tosteson and J. F. Hoffman, "Regulation of cell volume by active cation transport in high and low potassium sheep red cells," *The Journal of General Physiology*, vol. 44, 1960.
- [34] A. M. Weinstein, "Dynamics of cellular homeostasis: recovery time for a perturbation from equilibrium." *Bulletin of Mathematical Biology*, vol. 59, no. 3, pp. 451–481, 1997.
- [35] C. Poignard, A. Silve, F. Campion, L. M. Mir, O. Saut, and L. Schwartz, "Ion fluxes, transmembrane potential, and osmotic stabilization: a new dynamic electrophysiological model for eukaryotic cells," *European Biophysics Journal*, vol. 40, no. 3, pp. 235–236, 2011.
- [36] J. A. Fraser and C. L.-H. Huang, "A quantitative analysis of cell volume and resting potential determination and regulation in excitable cells," *The Journal of Physiology*, vol. 509, pp. 459–478, 2004.

- [37] A. Takeuchi, S. Tatsumi, N. Sarai, K. Terashima, S. Matsuoka, and A. Noma, "Ionic mechanisms of cardiac cell swelling induced by blocking Na^+/K^+ pump as revealed by experiments and simulation," *The Journal of General Physiology*, vol. 128, no. 5, pp. 495–507, 2006.
- [38] T. W. Smith, R. L. Rasmusson, L. A. Lobaugh, and M. Lieberman, " Na^+/K^+ pump inhibition induces cell shrinkage in cultured chick cardiac myocytes," *Basic Research in Cardiology*, vol. 88, pp. 411–420, 1993.
- [39] R. Ellis, "Macromolecular crowding: obvious but underappreciated," *Trends in Biochemical Sciences*, vol. 26, no. 10, pp. 597–604, OCT 2001.
- [40] Y. Huang, W. B. Wang, R. Holzel, F. F. Becker, and P. R. C. Gascoyne, "Electrorotational studies of the cytoplasmic dielectric properties of friend murine erythroleukaemia cells," *Physics in Medicine and Biology*, vol. 40, no. 11, pp. 1789–1806, NOV 1995.
- [41] J. Gimsa, T. Muller, T. Schnelle, and G. Fuhr, "Dielectric spectroscopy of single human erythrocytes at physiological ionic strength: Dispersion of the cytoplasm," *Biophysical Journal*, vol. 71, no. 1, pp. 495–506, JUL 1996.
- [42] J. F. Kerr, A. H. Wyllie, and A. R. Currie, "Apoptosis: a basic biological phenomenon with wide-ranging implications in tissue kinetics," *British Journal of Cancer*, vol. 26, no. 4, pp. 239–257, 1972.
- [43] S. Elmore, "Apoptosis: A review of programmed cell death," *Toxicologic Pathology*, vol. 35, pp. 495–516, 2007.
- [44] F. M. Hughes and J. A. Cidlowski, "Potassium is critical regulator of apoptotic enzymes in vitro and in vivo," *Advan. Enzyme Regul*, vol. 39, 1999.
- [45] D. Kanduc, A. Mittelman, R. Serpico, E. Sinigaglia, A. A. Sinha, C. Natale, R. Santacroce, M. G. D. Corcia, A. Lucchese, L. Dini, P. Pani, S. Santacroce, S. Simone, R. Bucci, and E. Farber, "Cell death: Apoptosis versus necrosis," *International Journal of Oncology*, vol. 21, no. 1, pp. 165–170, 2002.
- [46] S. L. Spencer and P. K. Sorger, "Measuring and Modeling Apoptosis in Single Cells," *Cell*, vol. 144, no. 6, pp. 926–939, MAR 18 2011.
- [47] P. Patel and G. H. Markx, "Dielectric measurement of cell death," *Enzyme and Microbial Technology*, vol. 43, no. 7, pp. 463 – 470, 2008. [Online]. Available: <http://www.sciencedirect.com/science/article/pii/S0141022908002457>
- [48] F. H. Labeed, H. M. Coley, and M. P. Hughes, "Differences in the biophysical properties of membrane and cytoplasm of apoptotic cells revealed using dielectrophoresis," *Biochimica et Biophysica Acta (BBA) - General Subjects*, vol. 1760, no. 6, pp. 922 – 929, 2006.

- [49] S. Yu, L. Canzoniero, and D. Choi, "Ion homeostasis and apoptosis," *Current Opinion in Cell Biology*, vol. 13, no. 4, pp. 405–411, AUG 2001.
- [50] I. L. Cameron, N. K. R. Smith, T. B. Pool, and R. L. Sparks, "Intracellular concentration of sodium and other elements as related to mitogenesis and oncogenesis in vivo," *American Association for Cancer*, 1980.
- [51] F. H. Labeed, H. M. Coley, H. Thomas, and M. P. Hughes, "Assessment of multidrug resistance reversal using dielectrophoresis and flow cytometry," *Biophysical Journal*, vol. 85, no. 3, pp. 2028–34, 2003.
- [52] R. Pethig and M. S. Talary, "Dielectrophoretic detection of membrane morphology changes in Jurkat T-cells undergoing etoposide-induced apoptosis," *IET Nanobiotechnology*, vol. 1, no. 1, pp. 2–9, FEB 2007.
- [53] X. Wang, F. Becker, and P. Gascoyne, "Membrane dielectric changes indicate induced apoptosis in HL-60 cells more sensitively than surface phosphatidylserine expression or DNA fragmentation," *Biochimica et Biophysica Acta*, vol. 1564, no. 2, pp. 412–420, AUG 31 2002.
- [54] K. Ratanachoo, P. Gascoyne, and M. Ruchirawat, "Detection of cellular responses to toxicants by dielectrophoresis," *Biochimica et Biophysica Acta*, vol. 1564, no. 2, pp. 449–458, AUG 31 2002.
- [55] Y. Lv, L. Zeng, G. Zhang, Y. Xu, Y. Lu, K. Mitchelson, J. Cheng, and W. Xing, "Systematic dielectrophoretic analysis of the Ara-C-induced NB4 cell apoptosis combined with gene expression profiling," *International Journal of Nanomedicine*, vol. 8, pp. 2333–2350, 2013.
- [56] B. Klein, K. Woerndl, U. Luetz-Meindl, and H. H. Kerschbaum, "Perturbation of intracellular K⁺ homeostasis with valinomycin promotes cell death by mitochondrial swelling and autophagic processes," *Apoptosis*, vol. 16, no. 11, pp. 1101–1117, NOV 2011.
- [57] S. Yu, "Regulation and critical role of potassium homeostasis in apoptosis," *Progress in Neurobiology*, vol. 70, no. 4, pp. 363–386, JUL 2003.
- [58] F. Hughes, C. Bortner, G. Purdy, and J. Cidlowski, "Intracellular K⁺ suppresses the activation of apoptosis in lymphocytes," *Journal of Biological Chemistry*, vol. 272, no. 48, pp. 30 567–30 576, NOV 28 1997.
- [59] J. McCarthy and T. Cotter, "Cell shrinkage and apoptosis: a role for potassium and sodium ion efflux," *Cell Death and Differentiation*, vol. 4, no. 8, pp. 756–770, DEC 1997.
- [60] A. Xiao, L. Wei, S. Xia, S. Rothman, and S. Yu, "Ionic mechanism of ouabain-induced concurrent apoptosis and necrosis in individual cultured cortical neurons," *Journal of Neuroscience*, vol. 22, no. 4, pp. 1350–1362, FEB 15 2002.

- [61] G. Barbiero, F. Duranti, G. Bonelli, J. Amenta, and F. Baccino, "Intracellular ionic variations in the apoptotic death of l cells by inhibitors of cell cycle progression," *Experimental Cell Research*, vol. 217, no. 2, pp. 410–418, APR 1995.
- [62] T. I. Cabel, "Dielectrophoretic analysis of polystyrene spheres in fluidic suspens," Master's thesis, Department of Electrical and Computer Engineering University of Manitoba Winnipeg, MB, Canada, 2013.
- [63] J. Voldman, R. Braff, M. Toner, M. Gray, and M. Schmidt, "Holding forces of single-particle dielectrophoretic traps," *Biophysical Journal*, vol. 80, no. 1, pp. 531–541, JAN 2001.
- [64] J.-S. Park, S.-H. Song, and H.-I. Jung, "Continuous focusing of microparticles using inertial lift force and vorticity via multi-orifice microfluidic channels," *Lab on a Chip*, vol. 9, no. 7, pp. 939–948, 2009.
- [65] P. Williams, T. Koch, , and J. Giddings, "Characterization of near-wall hydrodynamic lift forces using sedimentation field flow fractionation," *Chemical Engineering Communications*, vol. 111, pp. 121–147, 1992.
- [66] *Sensonit glass-based microfluidic technology with metallization: Design rules and process steps*, CMC Microsystems, Kingston, ON, September 2009.
- [67] G. A. Ferrier, "Electrical detection and actuation of single biological cells with application to deformability cytometry for markerless diagnostics," Ph.D. dissertation, Department of Electrical and Computer Engineering University of Manitoba Winnipeg, MB, Canada, 2011.
- [68] A. Bhide, "An artificial neural network-based signal classifier for automated identification of detection signals from a dielectrophoretic cytometer," Master's thesis, Department of Electrical and Computer Engineering, University of Manitoba, Winnipeg, 2013.
- [69] M. Nikolic-Jaric, G. A. Ferrier, D. J. Thomson, G. E. Bridges, and M. R. Freeman, "Dielectric response of particles in flowing media: The effect of shear-induced rotation on the variation in particle polarizability," *Physical Review*, vol. 84, no. 1, 1, JUL 25 2011.
- [70] K. Braasch, M. Nikolic-Jaric, T. Cabel, E. Salimi, G. E. Bridges, D. J. Thomson, and M. Butler, "The Changing Dielectric Properties of CHO Cells Can Be Used to Determine Early Apoptotic Events in a Bioprocess," *Biotechnology and Bioengineering*, vol. 110, no. 11, pp. 2902–2914, NOV 2013.
- [71] A. Bell, Z. J. Wang, M. Arbabi-Ghahroudi, T. A. Chang, Y. Durocher, U. Trojahn, J. Baardsnes, M. L. Jaramillo, S. Li, T. N. Baral, M. O'Connor-McCourt, R. MacKenzie, and J. Zhang, "Differential tumor-targeting abilities of three single-domain antibody formats," *Cancer Letters*, vol. 289, no. 1, pp. 81–90, MAR 1 2010.

- [72] M. Muratore, V. Srsen, M. Waterfall, A. Downes, and R. Pethig, "Biomarker-free dielectrophoretic sorting of differentiating myoblast multipotent progenitor cells and their membrane analysis by Raman spectroscopy," *Biomicrofluidics*, vol. 6, no. 3, SEP 2012.
- [73] B. G. Meisenberg and W. H. Simmons, *Principles of Medical Biochemistry*, 3rd ed. Saunders, 2012.
- [74] Y. Tsao, A. Cardoso, R. Condon, M. Voloch, P. Lio, J. Lagos, B. Kearns, and Z. Liu, "Monitoring Chinese hamster ovary cell culture by the analysis of glucose and lactate metabolism," *Journal of Biotechnology*, vol. 118, no. 3, pp. 316–327, AUG 22 2005.
- [75] B. S. Jhun, H. Lee, Z.-G. Jin, and Y. Yoon, "Glucose Stimulation Induces Dynamic Change of Mitochondrial Morphology to Promote Insulin Secretion in the Insulinoma Cell Line INS-1E," *PLOS ONE*, vol. 8, no. 4, APR 2 2013.
- [76] Y. Abe, T. Sakairi, H. Kajiyama, S. Shrivastav, C. Beeson, and J. B. Kopp, "Bioenergetic characterization of mouse podocytes," *American Journal of Physiology- Cell Physiology*, vol. 299, no. 2, pp. C464–C476, AUG 2010.
- [77] J. Cho, M. Balasubramanyam, G. Chernaya, J. Gardner, A. Aviv, J. Reeves, P. Dargis, and E. Christian, "Oligomycin inhibits store-operated channels by a mechanism independent of its effects on mitochondrial ATP," *Biochemical Journal*, vol. 324, no. 3, pp. 971–980, JUN 15 1997.
- [78] J. Skou and M. Esmann, "The na^+/k^+ atpase," *Journal of Bioenergetics and Biomembranes*, vol. 24, no. 3, pp. 249–261, Jun 1992.
- [79] R. Chalmers-Redman, A. Fraser, G. Carlile, A. Pong, and W. Tatton, "Glucose protection from MPP⁺-induced apoptosis depends on mitochondrial membrane potential and ATP synthase," *Biochemical and Biophysical Research Communications*, vol. 257, no. 2, pp. 440–447, APR 13 1999.
- [80] M. Watabe and T. Nakaki, "Atp depletion does not account for apoptosis induced by inhibition of mitochondrial electron transport chain in human dopaminergic cells," *Neuropharmacology*, vol. 52, pp. 536–541, 2007.
- [81] R. Legmann, J. Melito, D. Ferrick, and S. Bioscience, "Antioxidant enhances spare respiratory capacity in cardiomyocytes as a protective response to oxidative stress induced by hypoxia and redox cycling agent," *Experimental biology*, 2012.
- [82] Y. Abe, T. Sakairi, H. Kajiyama, S. Shrivastav, C. Beeson, and J. B. Kopp, "Bioenergetic characterization of mouse podocytes," *American Journal of Physiology- Cell Physiology*, vol. 299, no. 2, pp. C464–C476, AUG 2010.
- [83] R. Whittam, K. Wheeler, and A. Blake, "Oligomycin and active transport reactions in cell membranes," *Nature*, vol. 203, no. 494, pp. 720–&, 1964.

- [84] N. S. Bricker and S. Klahr, "Effects of dinitrophenol and oligomycin on the coupling between anaerobic metabolism and anaerobic sodium transport by the isolated turtle bladder," *General Physiology*, 1966.
- [85] Y. Ding, J. Hao, and R. F. Rakowski, "Effects of Oligomycin on Transient Currents Carried by Na⁺ Translocation of Bufo Na⁺/K⁺-ATPase Expressed in Xenopus Oocytes," *Journal of Membrane Biology*, vol. 243, no. 1-3, pp. 35–46, OCT 2011.
- [86] P. Gascoyne, R. Pethig, J. Burt, and F. Becker, "Membrane changes accompanying the induced differentiation of friend murine erythroleukemia cells studied by dielectrophoresis," *Biochimica et Biophysica Acta*, vol. 1149, no. 1, pp. 119–126, JUN 18 1993.
- [87] K. C. Das and H. Muniyappa, "Age-dependent mitochondrial energy dynamics in the mice heart: Role of superoxide dismutase-2," *Experimental Gerontology*, vol. 48, no. 9, pp. 947–959, SEP 2013.
- [88] W. Hao, C.-P. B. Chang, C.-C. Tsao, and J. Xu, "Oligomycin-induced Bioenergetic Adaptation in Cancer Cells with Heterogeneous Bioenergetic Organization," *Journal of Biological Chemistry*, vol. 285, no. 17, pp. 12 647–12 654, APR 23 2010.
- [89] F. Meuwly, F. Papp, P. Ruffieux, A. Bernard, A. Kadouri, and U. von Stockar, "Use of glucose consumption rate (GCR) as a tool to monitor and control animal cell production processes in packed-bed bioreactors," *Journal of Biotechnology*, vol. 122, no. 1, pp. 122–129, MAR 9 2006.
- [90] J. Schmidt, U. Mueller, C. Wallimann, S. Mathes, C. Probst, S. Siegrist, C. Andretta, C. Leist, and U. Graf-Hausner, "Monitoring atp status in the metabolism of production cell lines," *Bioprocess International*, 2008.
- [91] H. Pelicano, D. S. Martin, R. H. Xu, and P. Huang, "Glycolysis inhibition for anticancer treatment," *Oncogene*, vol. 25, no. 34, pp. 4633–4646, AUG 2006.